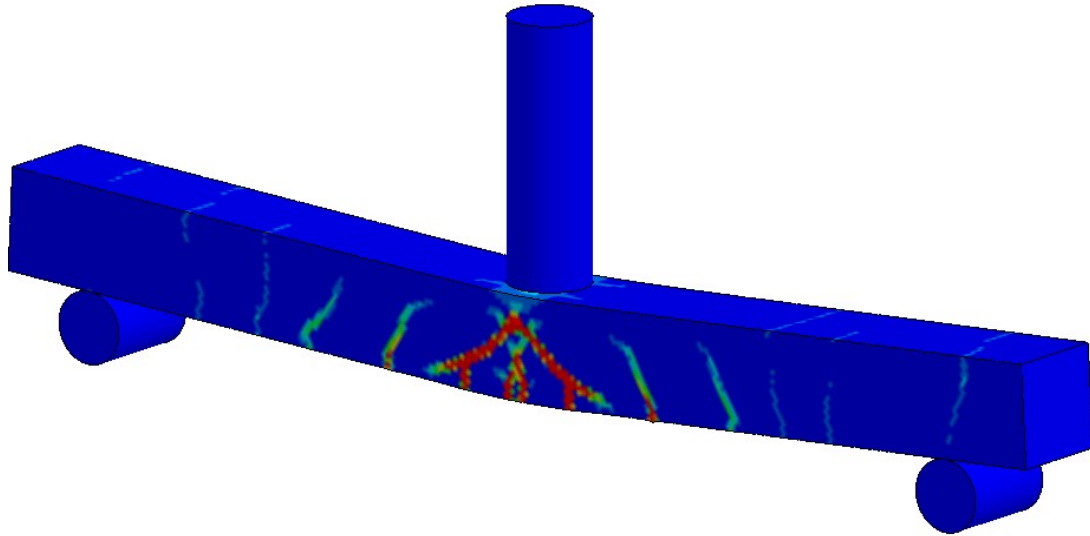![Chalmers University of Technology logo]

Structural Response of Concrete Beams Subjected to Drop Weight Impact

A parametric study using numerical modelling

Master's Thesis in the Master's Programme Structural Engineering and Building Technology

MICHAELA MUNTHER

JOSEFINE RUNEBRANT

Structural Response of Concrete Beams Subjected to Drop Weight Impact

A parametric study using numerical modelling

Master's Thesis in the Master's Programme Structural Engineering and Building Technology

MICHAELA MUNTHER

JOSEFINE RUNEBRANT

Department of Architecture and Civil Engineering

Division of Structural Engineering

Concrete structures

CHALMERS UNIVERSITY OF TECHNOLOGY

Göteborg, Sweden 2018

Structural Response of Concrete Beams Subjected to Drop Weight Impact
A parametric study using numerical modelling

Master's Thesis in the Master's Programme Structural Engineering and Building Technology

MICHAELA MUNTHER

JOSEFINE RUNEBRANT

Department of Architecture and Civil Engineering
Division of Structural Engineering
Concrete Structures
Chalmers University of Technology
SE-412 96 Göteborg
Sweden
Telephone: + 46 (0)31-772 1000

Cover:
Visualisation of the structural response at the time of maximum displacement of a concrete beam subjected to drop weight impact from LS-DYNA

Structural Response of Concrete Beams Subjected to Drop Weight Impact

A parametric study using numerical modelling

Master's Thesis in the Master Programme Structural Engineering and Building Technology

MICHAELA MUNTHER

JOSEFINE RUNEBRANT

Department of Architecture and Civil Engineering

Division of Structural Engineering

Concrete Structures

Chalmers University of Technology

ABSTRACT

A structure subjected to an impact load will respond differently compared to when subjected to static loading. Finite element modelling of dynamically loaded structures has not been practiced to the same extent as of statically loaded ones, and consequently the results are not as reliable. Modelling choices in nonlinear finite element analyses of dynamically loaded structures are important to the resulting response of the model. In this thesis different levels of numerical modelling are used to describe the structural behaviour of reinforced concrete beams subjected to drop weight impact.

An aim of this project was to develop an already existing 3D solid finite element (FE) model in LS-DYNA. Another objective was to evaluate when simplified models, such as a 2D FE model using beam elements in Abaqus and a two-degrees-of-freedom (2DOF) system, are applicable. Another aim was to investigate the sensitivity of these models as well as the 3D FE model through parametric studies.

Based on an existing 3D solid FE model, a more refined model was created by comparing different modelling techniques regarding e.g. structural behaviour of the reinforcement, and interaction between concrete and reinforcement. The 2DOF model, the Abaqus model and the LS-DYNA model were validated by comparison to test results. Using these validated models, parametric studies were performed varying the dynamic load and the beam geometry as well as the amount of reinforcement.

The further development of the LS-DYNA model by including a bond-slip relation and a non-linear structural behaviour of the reinforcement gave satisfying results. For the 2DOF model used in this thesis it was found to be necessary that the model is calibrated for each separate case and that the correspondence with the Abaqus model was less accurate when the mass of the drop weight was small in relation to the beam. This indicated that the time dependency of the response of the beam is captured in the Abaqus model, but not in the 2DOF model. To conclude, it is believed that time dependent transformation factors in the 2DOF model would make it possible to capture a behaviour like that in Abaqus and achieve a model that is applicable in all load cases.

Key words: Reinforced concrete beam, impact load, numerical modelling, FE modelling, bond-slip, LS-DYNA, CDPM2, Abaqus, 2DOF model

Strukturell respons hos betongbalkar utsatta för fallviktsbelastning
En parameterstudie utförd genom numerisk modellering

Examensarbete inom mastersprogrammet Konstruktionsteknik och Byggnadsteknologi

MICHAELA MUNTHER

JOSEFINE RUNEBRANT

Institutionen för Arkitektur och Samhällsbyggnadsteknik
Avdelningen för Konstruktionsteknik
Betongbyggnad
Chalmers Tekniska Högskola

SAMMANFATTNING

En konstruktion utsatt för stötbelastning reagerar annorlunda jämfört med en statiskt belastad. Finita elementmodellering av dynamiskt belastade konstruktioner har inte studerats i samma utsträckning som statiskt belastade och följaktligen är resultaten inte lika tillförlitliga. Modelleringsval i ickelinjär finit elementanalys av dynamiskt belastade konstruktioner är avgörande för den resulterande responsen hos modellen. I detta arbete används olika nivåer av numerisk modellering för att beskriva strukturresponsen hos en betongbalk utsatt för en fallviktsbelastning.

Ett syfte med detta projekt var att utveckla en befintlig finita elementmodell med 3D solida element i LS-DYNA. En annan avsikt var att utvärdera när förenklade modeller som en finita elementmodell med 2D balkelement i Abaqus och ett tvåfrihetsgraderssystem (2DOF) är tillämpbara. Ett annat syfte var att undersöka känsligheten hos dessa modeller och LS-DYNA-modellen genom en parameterstudie.

Baserat på den befintliga 3D solida finita elementmodellen skapades en förfinad modell genom att jämföra olika modelleringsval så som strukturresponsen hos armeringen och interaktionen mellan betong och armering. 2DOF-modellen, Abaqus-modellen och LS-DYNA-modellen validerades genom att jämföra dem med testresultat. Vidare genomfördes en parametersstudie med dessa tre validerade modeller då den dynamiska lasten samt balkens geometri och armeringsmängd varierades.

Utvecklingen av LS-DYNA-modellen, då vidhäftning-glidningssambandet mellan betong och armering samt en ickelinjär strukturrespons hos armeringen inkluderades, gav tillfredställande resultat. För 2DOF-modellen upptäcktes det nödvändigt att kalibrera modellen för varje separat fall och att överensstämmelsen med Abaqus-modellen var sämre när fallviktens massa var liten i förhållande till balkens. Detta indikerade att tidsberoendet hos balkens respons fångas i Abaqus-modellen men inte i 2DOF-modellen. En slutsats är att tidsberoende transformationsfaktorer i 2DOF-modellen förmodligen skulle göra det möjligt att fånga detta beteende och få en modell som kan användas för alla lastfall.

Nyckelord: Armerad betongbalk, stötbelastning, numerisk modellering, FE-modellering, vidhäftning-glidningssamband, LS-DYNA, CDPM2, Abaqus, 2DOF-modell

Contents

Preface

In this project different levels of numerical modelling of reinforced concrete beams subjected to drop weight impact have been studied. This project is a continuation of previous master theses, within a research project financed by the Swedish Civil Contingencies Agency, at the division of Structural Engineering, Chalmers. It is carried out as a co-operation between Norconsult and Chalmers during a period from January to June 2018.

We would like to start to thank our supervisor Morgan Johansson for his devoted and thorough guidance through the entire project and sharing of his expertise on the subject. We would also like to thank our examiner Joosef Leppänen for his thorough and considerate support with anything from practicalities to theoretical advice. Additionally, thanks to Fabio Lozano, who has shared his knowledge about Finite Element Modelling and helped us forward in our work.

We would also like to thank Norconsult and the team *Bro och Analys* for the pleasant time spent together during the spring.

Finally, we are proud of what we have accomplished together, with good cooperation and many laughter, during this final semester of our education.

Gothenburg, June 2018

Michaela Munther and Josefine Runebrant

Notations

Abbreviations

2DOF	Two Degrees of Freedom
CDM	Central Difference Method
CDPM2	Concrete Damage Plasticity Model 2
DIF	Dynamic Increase Factor
FE	Finite Element
SDOF	Single Degree of Freedom

Greek lower-case letters

γ_I	Reduction factor
δ	Deformation of impact zone
ε	Strain
η_u	Quota of displacements
η_{w_y}	Quota of transferred energy
κ_F	Transformation factor for the force
κ_k	Transformation factor for the stiffness
κ_m	Transformation factor for the mass
κ_{mF}	Transformation factor on the ratio between the mass and force
ρ	Density
σ	Stress
τ_b	Bond stress
ϕ	Diameter of reinforcement
ω	Angular eigenfrequency
ω_{max}	Highest angular eigenfrequency

Roman upper-case letters

E	Young's modulus
E_{eq}	Equivalent young's modulus
E_k	Kinetic energy
F	Force
F_k	Characteristic pressure load
I	Impulse

I_0	Impulse equal to the momentum of body 1 immediately before impact
I_I	Moment of inertia, state I
I_{II}	Moment of inertia, state II
I_k	Characteristic impulse
L	Length
M_{Rd}	Moment capacity
Q	Equivalent static load
R	Resistance of structure
R_m	Resistance limit
W_e	External work on a system
W_i	Internal work in a system
W_{el}	Section modulus for elastic response
W_{pl}	Section modulus for plastic response

Roman lower-case letters

a	Timestep scaling factor in LS-DYNA
c	Wave propagation speed, cover thickness
b	Width
f_c	Concrete compressive strength
f_t	Concrete tensile strength
f_u	Ultimate strength of reinforcement
f_y	Yield strength
g_b	Self-weight of beam
h	Height
k	Stiffness of a structure
k_s	Secant stiffness of a structure
l_{el}	Element length
m	Mass
p	Momentum
s	Relative displacement (slip)
t	Time
t_1	Load duration
u	Displacement
$\dot{u}$	Velocity

$\ddot{u}$	Acceleration
u_{el}	Reversible displacement of a structure
$u_{el-pl.el}$	Reversible displacement of a structure with elasto-plastic response
$u_{el-pl.pl}$	Irreversible displacement of a structure with elasto-plastic response
u_{pl}	Irreversible displacement of a structure
u_{ref}	Displacement of reference point
u_{tot}	Total displacement of a structure
v	Velocity
w	Crack width
w_f	Ultimate crack width

1 Introduction

1.1 Background

Protective structures need to have the ability to withstand impulse loading like explosions and collisions. A suitable material for this kind of structures is reinforced concrete. However, it is of importance to have the knowledge about failure modes that may occur in concrete structures subjected to dynamic loads since they can be different from failure modes occurring in statically loaded structures.

Excessive finite element modelling has been performed on statically loaded structures and can be considered to give rather accurate results. Finite element modelling of dynamically loaded structures has not been practiced to the same extent, and consequently the results are not as reliable. The modelling choices in nonlinear finite element analyses of dynamically loaded structures have shown to be of high importance to the resulting response of the model. Consequently, parametric studies can improve the accuracy of future analyses.

There is an ongoing research project, financed by the Swedish Civil Contingencies Agency, at the division of Structural Engineering, Chalmers, of which this master's thesis was a part. Previous work within this part of the research project are the PhD project Ekstöm (2017) and the master thesis projects Lovén and Svavarsdóttir (2016) and Lozano and Makdesi (2017). This thesis was carried out as a co-operation between Norconsult and Chalmers.

1.2 Aim

The aim of this project was to increase the understanding of how dynamic loading affects the structural behaviour of reinforced concrete beams by using finite element (FE) analyses in 2D and 3D as well as analyses using two-degrees-of-freedom (2DOF) models.

A specific question that was investigated in this thesis was how impact loaded structures can be modelled efficiently using the simplified methods of 2DOF systems and 2D FE models with beam elements. To further develop already existing 3D solid FE models in LS-DYNA used in previous work was another purpose of the project. Furthermore, one objective was to increase the understanding of how the structural response of the models is affected by the modelling choices by conducting parametric studies varying different parameters in the models.

The thesis project was as a part of an ongoing research project a continuation of previous MSc theses as well as a preparation for future master's thesis projects.

1.3 Method

In this project, a simply supported beam subjected to an impact load represented by a drop-weight was studied and is demonstrated in Figure 1.1.
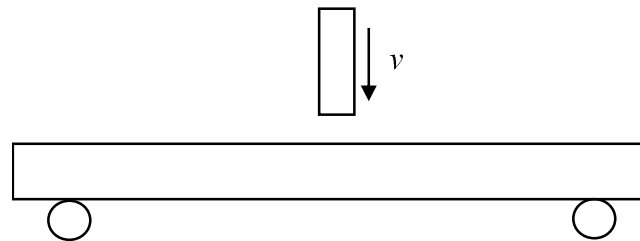
Figure 1.1   The structure studied in this project.

The first part of the project consisted of a literature review covering the basics of structural dynamics. The simplified methods using single-degree-of-freedom (SDOF) and 2DOF systems were investigated to understand how and when they can be used. Furthermore, previous MSc thesis projects regarding concrete structures subjected to impact loading were studied.

A 2DOF system was adopted to analyse the structural response of the beam in a simplified way. This was done using a numerical explicit time stepping method, Central Difference Method (CDM). FE analyses in 2D were performed using plastic beam elements in Abaqus.

Finite element analyses using 3D solid elements in LS-DYNA were carried out. Based on existing models, a more refined model was created by comparing different modelling techniques regarding e.g. choice of material parameters, structural behaviour of the reinforcement, and interaction between concrete and reinforcement.

The 2DOF model, the Abaqus model and the LS-DYNA model were validated by comparison to tests carried out previously within the research project. In the analyses using these models, parametric studies were performed. In the simplified models, parameters related to the mass of the drop weight, the drop height of the weight, the beam geometry, and the reinforcement amount were varied. Due to the more extensive computational time in the LS-DYNA model, the parametric study in 3D was limited to the parameters regarding the drop weight and the reinforcement amount.

1.4 Limitations

In this project, the studied beam is simply supported and made of reinforced normal concrete. No experiments were conducted in this project, but results from the analyses were compared with tests in previous master's thesis within the research project.

The elements which were used in the 3D analyses of this project were tetrahedral and the only material model for concrete that was used is Concrete Damage Plasticity Model 2 (CDPM2) which is developed by Peter Grassl *et al.* (2013) in a project with Chalmers.

No damping factors were included in the FE-analyses or in the simplified analyses since it was deemed they would have a negligible effect in the case of short load duration.

1.5 Thesis outline

In this thesis chapter 2-4 presents the theory which this project is built on. The following two chapters, 5-6, describes the method and how the modelling of the different models are done. In chapter 7-8 the results are presented and discussed. Lastly, the conclusion and references are covered in chapter 9-10.

Chapter 2: The structural behaviour of the relevant materials as well as their simplified response used in mathematical models are treated in this chapter. Furthermore, some basic theory behind effects of fast loading is introduced.

Chapter 3: To analyse impulse loaded structures, it is important to have the knowledge about the fundamentals in dynamics, which is briefly treated in this chapter.

Chapter 4: In this chapter a simplified way to describe an impulse loaded beam using an equivalent 2DOF system is introduced.

Chapter 5: In this project, two simplified methods are used to predict the behaviour of a simply supported reinforced concrete beam subjected to impact loading: the 2DOF system and 2D FE model using beam elements in Abaqus. These two methods are presented in this chapter.

Chapter 6: The theory behind the more detailed 3D FE model using solid elements in LS-DYNA are described in this chapter.

Chapter 7: The modelling choices in the simplified as well as the more advanced methods are evaluated and improved in this chapter, and then the final models are validated.

Chapter 8: Parametric studies are presented in this chapter performed in all three models.

Chapter 9: In this chapter the conclusion of this thesis is presented as well as suggestions for future studies.

Chapter 10: The references used in this thesis are presented in this chapter.

2 Material and Structural Response

2.1 Introduction

To understand the limitations of models used in calculations, it is of importance to understand the actual structural behaviour of the studied structure. The relevant materials in this project are concrete, reinforcing steel and the composite material reinforced concrete; these will be briefly treated in the following sections. Furthermore, the response of these materials is influenced when a load is applied fast, as in this project. Some basic theory behind this effect will be introduced. In the mathematical models used, the response of the material is often simplified into elastic, plastic, or elasto-plastic response, which are also covered in this chapter.

2.2 Concrete

2.2.1 Structural response

High compressive strength is characteristic for plain concrete. However, the tensile strength is much lower. Both the tensile and compressive stress-strain relations are non-linear which can be seen in Figure 2.1.
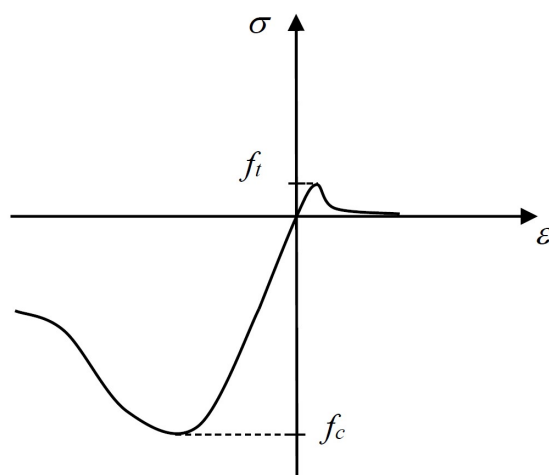
Figure 2.1   Schematic illustration of the stress-strain relationship for concrete subjected to uniaxial loading, from Lovén and Svavarsdóttir (2016).

2.2.2 Fracture energy

To describe the post-peak behaviour of concrete in tension, fracture mechanics can be used. As described by Plos (2000), the fracture energy, G_F, is a material parameter that describes how much energy that is consumed or dissipates when a crack develops fully through a specimen. The use of fracture energy as a parameter is convenient for transferring experimental data to input parameters in e.g. a finite element model. The stress-displacement graph from a test can be divided into an elastic stress-strain relation together with a stress-crack opening curve, see Figure 2.2. The area under the stress-crack opening curve defines the fracture energy.
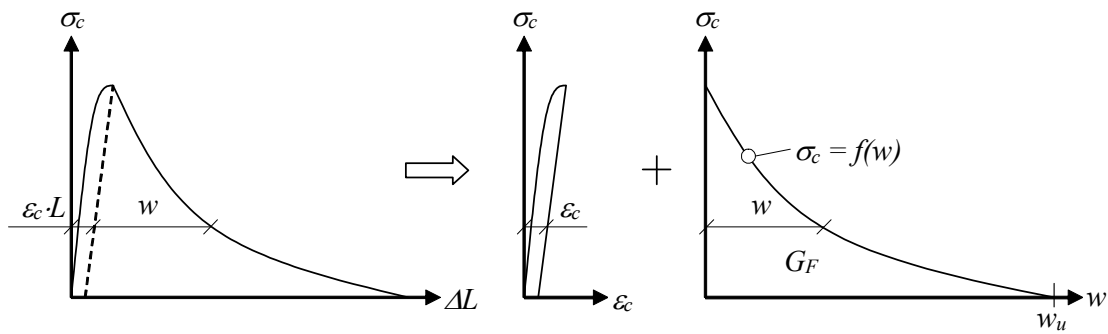
Figure 2.2   Schematic picture of how the pre- and post-peak behaviour of concrete is described, from Johansson (2000).

This partition is done since the crack will localize into a fracture zone whose size is independent of specimen size. If the stress-displacement graph was to be transferred into a stress-strain relation only, it would give different curves for different specimen sizes and thereby not be able to represent the material itself.

2.3 Reinforcing steel

Reinforcing steel has different structural behaviour depending on if the steel is cold worked or hot rolled, this is described by e.g. Engström (2015). If the steel is hot rolled it demonstrates a more ductile response with a characteristic yield behaviour and large strain hardening effect, see Figure 2.3(a). The cold worked steel does not have the same yield behaviour as the hot rolled, this is demonstrated in Figure 2.3(b). Instead, the 0.2 % proof-stress is used here to represent the yield strength. This stress is defined as the stress of which the plastic strain after unloading is 0.2 %. The strain hardening effects of cold worked steel is normally significantly smaller than for hot rolled.

(a)   (b)
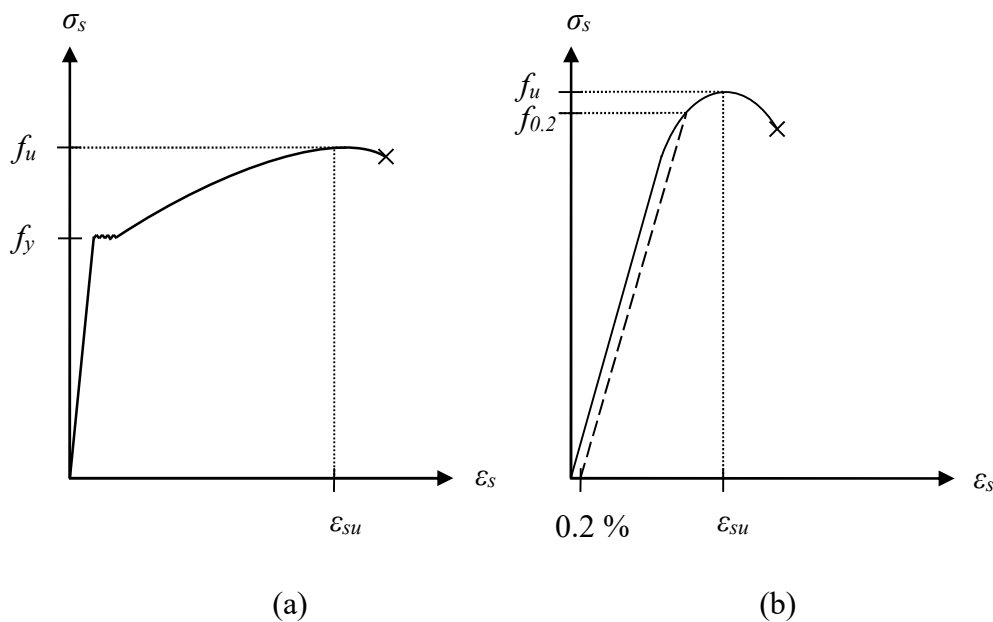
Figure 2.3   Structural behaviour of reinforcing steel, a) hot rolled and b) cold worked.

2.4 Reinforced concrete

Reinforced concrete is a composite material where the high compressive strength of concrete and the high tensile strength of reinforcing steel are united. The structural behaviour of reinforced concrete is described by Engström (2015) and is schematically shown in Figure 2.4. The response can be divided into four stages; uncracked, cracked, yielding of the reinforcement and failure.
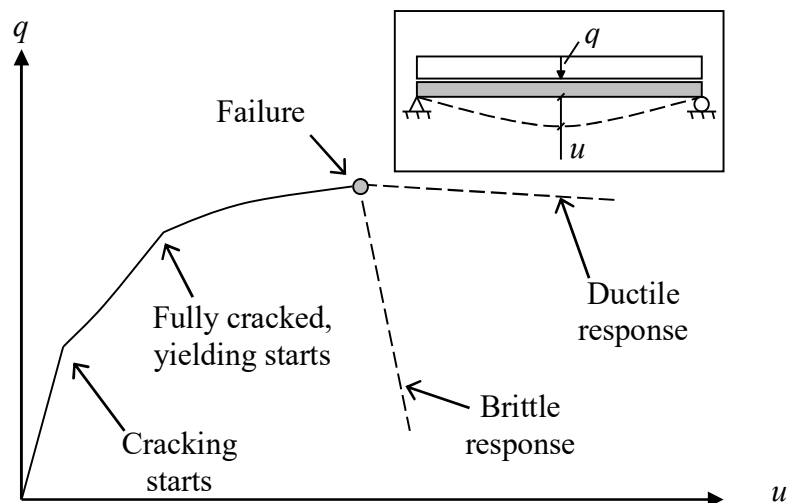
Figure 2.4   The structural behaviour of reinforced concrete, modified from Johansson (2012).

In the uncracked stage the reinforcement has small influence and the flexural rigidity is mostly governed by the concrete. The response is relatively stiff and linear in this stage. This is referred to as state I.

When the tensile strength of the concrete is reached in a section, a crack is formed. In the early stages of cracking the concrete between the cracks has a large contribution to the stiffness, this is called tension stiffening. When the cracks propagate in the structure the stiffness decreases until the structure can be regarded as fully cracked and the stiffness is to a high degree governed by the reinforcement. The stiffness of the fully cracked section is referred to as state II stiffness.

In the third stage the reinforcement will start to yield and the response of the structure changes drastically. The strain hardening of the steel allows the load on the structure to be increased beyond the yield strength of the steel.

The failure of the structure can be brittle or ductile depending on the properties of the section, e.g. the amount and the ductility properties of the reinforcement. A formation of a plastic hinge will develop if the response of the reinforcement is ductile and a suitable reinforcement configuration, with regard to cross-section and concrete strength, is present.

2.5 Strain rate effects

The rate of which a strain is applied to a structure affects the response of the materials, this is described by e.g. Johansson (2000). When a strain is applied fast, materials tend to be stiffer and stronger. According to Johansson, the strain rate effect on concrete can be explained by viscous and structural effects, see Figure 2.5.
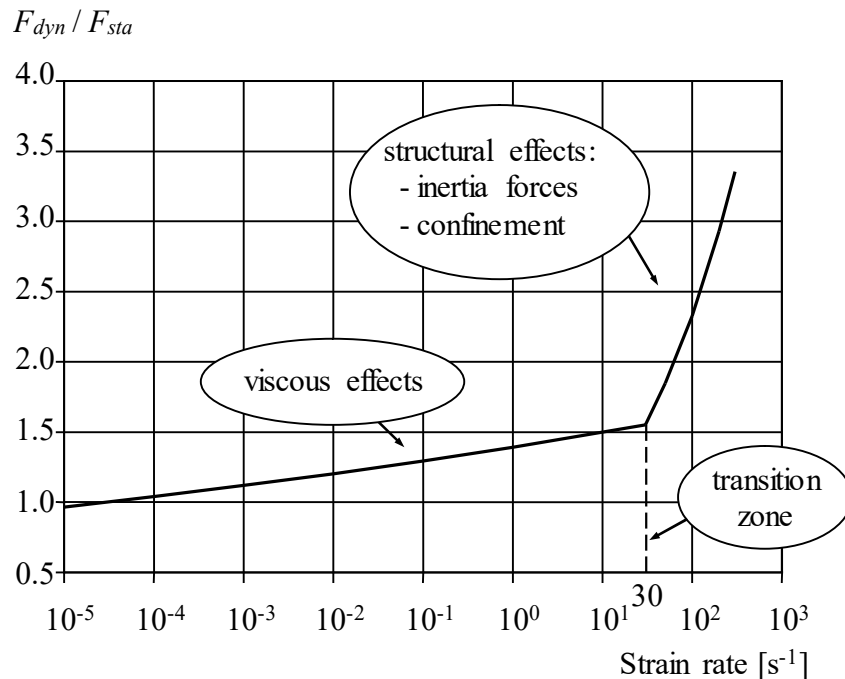
Figure 2.5   Strain rates for which viscous and structural effects are influencing concrete in compression, modified from Johansson (2000).

The viscous effects have an impact on the formation of cracks in the material. During static loading, the crack propagates through the material slower and has time to find the weaker path. At high strain rates on the other hand, the crack propagates without having time to make use of the same weaknesses within the material. This gives rise to a stiffer and stronger response.

At higher strain rates, the structural effects are influencing the strength. This is mainly due to inertia forces that develops at the tip of the crack. When concrete is subjected to compression, faster than it responds, a confinement effect will arise. This leads to a stress state close to plain strain which increases the strength of the concrete.

The strain rate effects are usually treated by the Dynamic Increase Factor (DIF) which is calculated as the ratio between the dynamic and static strength:

$$DIF = \frac{F_{dyn}}{F_{sta}} \tag{2.1}$$

The DIF for concrete in tension according to different theories can be seen in Figure 2.6.
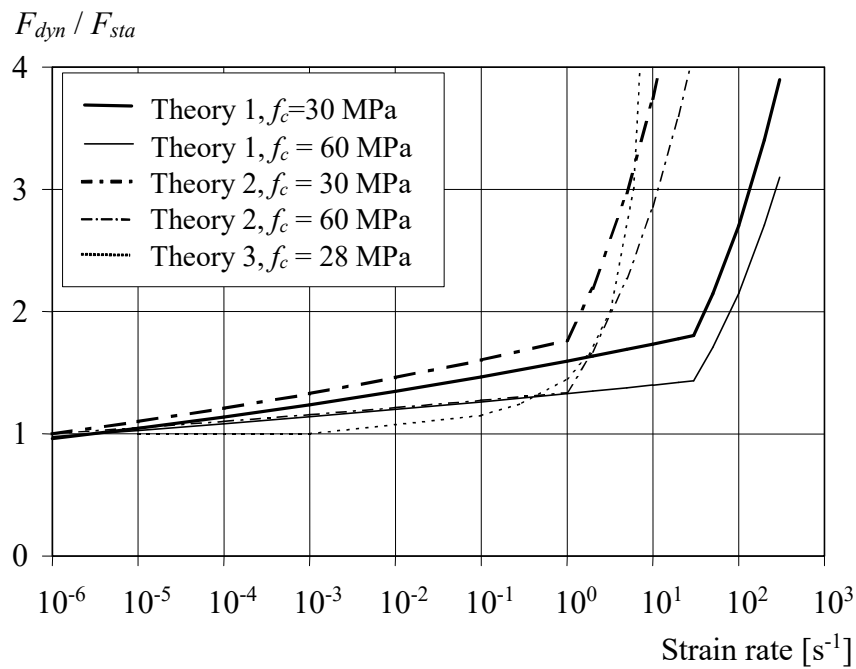
Figure 2.6   DIF for concrete in tension from different theories with regard to the strain rate, modified from Johansson (2000).

Regarding the reinforcement, strain rate effects lead to increased yield and ultimate strength. The Young's modulus however, is not affected. The DIF for reinforcement according to different theories is shown in Figure 2.7.
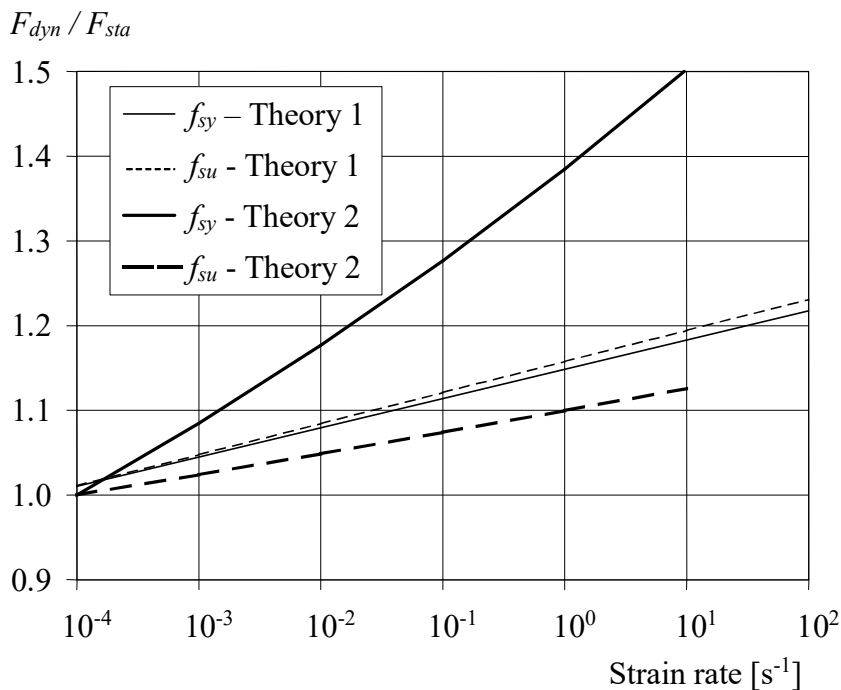
Figure 2.7   DIF for reinforcement from different theories with regard to strain rate, modified from Johansson (2000).

In this project, an impact load which results in a strain rate of approximately 10^0 - 10^1 s^{-1} will be analysed. This can be placed in relation to a static load where the strain rate is in a range around 10^{-5} and a blast between 10^2 - 10^3, see Figure 2.8.
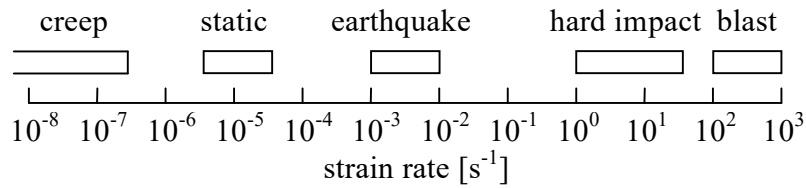
Figure 2.8   Strain rates for different kind of loading, from Johansson (2000).

2.6 Simplified models of structural response

2.6.1 Linear elastic behaviour

Deformations of a structure with elastic response are reversible and the stiffness, k, of the structure is constant. The resistance, R, varies linearly with the displacement, u. The relation can be described by:

$$R(u) = k \cdot u \tag{2.2}$$

The elastic structural response is illustrated in Figure 2.9.
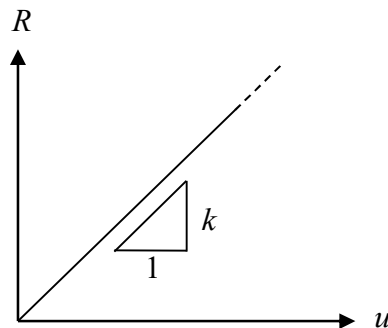
Figure 2.9   Linear elastic structural behaviour.

2.6.2 Ideally plastic behaviour

The resistance in an ideally plastic case is equal to the applied load, F, until the capacity of the structure is reached. Until this point no deformation is developed. When the capacity is reached, the resistance is constant and the displacement, u, is irreversible and infinite.

The resistance of the material can be given as:

$$R(u) = \begin{cases} F & u = 0 \\ R_m & u > 0 \end{cases} \tag{2.3}$$

The relation between the resistance and the displacement is shown in Figure 2.10.
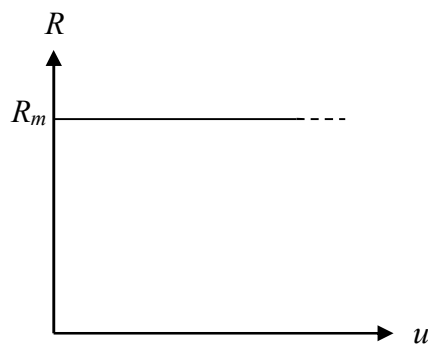
Figure 2.10   Ideally plastic structural behaviour.

2.6.3 Elasto-plastic behaviour

In the elasto-plastic case, the response is a combination between the linear elastic and the ideally plastic case. The resistance develops linearly until an upper limit and then remains constant. If the resistance limit is reached, there will be an irreversible plastic displacement, $u_{el-pl.pl}$.

$$R(u) = \begin{cases} k \cdot u & u < u_{el-pl.el} \\ R_m & u \geq u_{el-pl.el} \end{cases} \tag{2.4}$$

The total displacement will be:

$$u_{tot} = u_{el-pl.el} + u_{el-pl.pl} \tag{2.5}$$

In Figure 2.11, the response of an elasto-plastic structure is illustrated. As shown in the figure, the unloading of an elasto-plastic structure is similar to that of an elastic one.
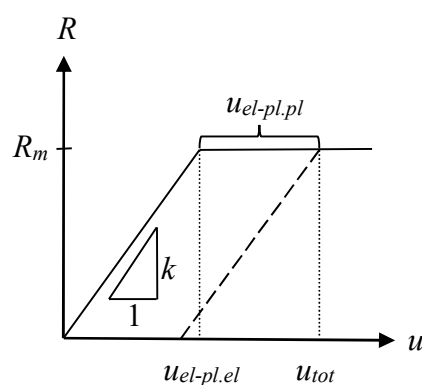
Figure 2.11   Elasto-plastic structural response.

3 Basics of Structural Dynamics

3.1 Introduction

To analyse impulse loaded structures, it is important to have the knowledge about the fundamentals in dynamics. This starts with basic concepts as energy and work, that are briefly treated in this chapter. Furthermore, these concepts help to understand the interaction between two bodies and the characteristics of an impact, which are covered in this chapter as well. This chapter is based on the theory described by Johansson and Laine (2012).

3.2 Energy, momentum, impulse, and work

The kinetic energy, E_k, for a body with mass m and velocity v, is defined as:

$$E_k = \frac{mv^2}{2} \tag{3.1}$$

The momentum, p, of the body is defined as:

$$p = mv \tag{3.2}$$

When an external force, $F(t)$, acts on a body from time $t = 0$ to $t = t_1$, there will be a change in momentum, defined as an impulse, I.

$$I = p - p_0 = m\,v - mv_0 = \int_0^{t_1} F(t)dt \tag{3.3}$$

If the body is initially at rest ($v_0 = 0$) this can be written as:

$$I = mv \tag{3.4}$$

Using equations (3.1) and (3.4), the change in kinetic energy can be expressed as:

$$E_k = \frac{I^2}{2m} \tag{3.5}$$

When the force acts on the body, it gives rise to a change in velocity and consequently a change in kinetic energy. This change is equal to the external work that the force has performed on the body. In this case, where the body is initially at rest, the external work on the body can be expressed as in equation (3.6).

$$W_e = \frac{mv^2}{2} = E_k \tag{3.6}$$

When the external force causes a displacement, u, the work can also be calculated using the component of the force acting in the direction of the displacement, see equation (3.7). The work is calculated assuming a displacement along the x-axis and the integral describes the area under the force-displacement curve.

$$W_e = \int_0^u F(x)dx \tag{3.7}$$

The body subjected to an external work will respond with an internal work, W_i. The maximum displacement is reached when the internal work is of equal magnitude as the external work.

$$W_i = W_e \tag{3.8}$$

This can be visualized using the areas under the force-displacement curve for the external work and resistance-displacement curve for the internal work. The structural response, as described in Section 2.6, is simplified to elastic, plastic or elastoplastic and the graph of the internal work is described accordingly. Equilibrium is reached when the areas are of equal size and then the final displacement is reached. In Figure 3.1, the equilibrium for an elastic, plastic and elasto-plastic structure, respectively, are shown.
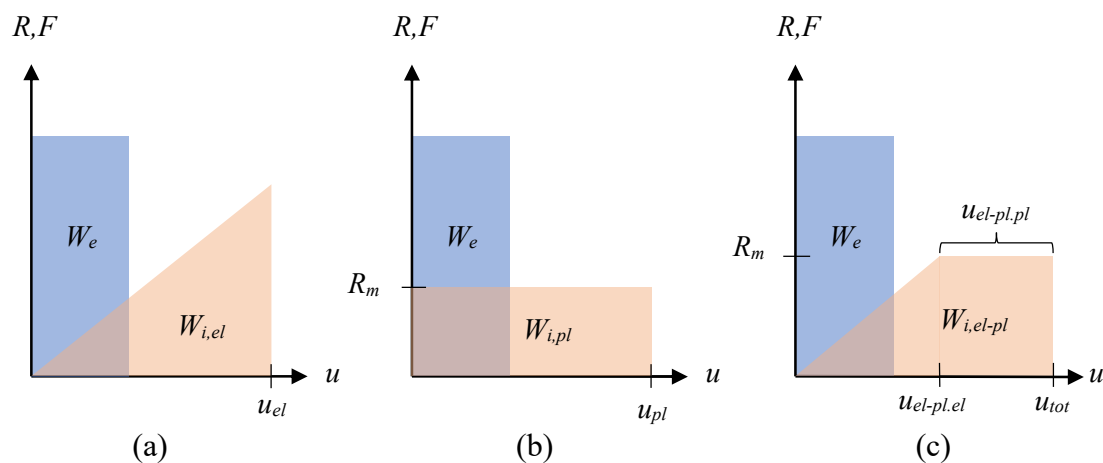
Figure 3.1   Equilibrium between external and internal work for: a) elastic, b) plastic, and c) elasto-plastic response.

3.3 Dynamic load cases

There are two ideal cases of dynamic loading: characteristic impulse and characteristic pressure load, see Figure 3.2. In both cases, the maximum force is reached instantaneously. The characteristic impulse has an infinitely high pressure and an infinitely short duration, but an impulse content of I_k. On the contrary, a characteristic pressure load defined by the characteristic pressure F_k, has an infinite duration, see Figure 3.2. In reality, the loading will be somewhere in between these two cases.

(a)   (b)
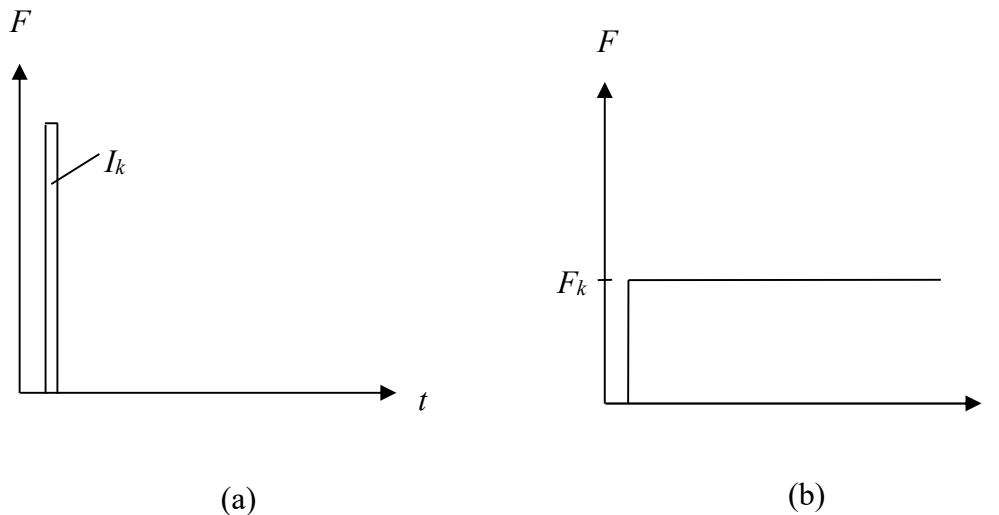
Figure 3.2   The two ideal cases of dynamic loading, (a) characteristic impulse and (b) characteristic pressure load.

In this project, the impact will be assumed to be an impulse. The reason is that the main part of the load will be transferred during a short time in relation to the time it takes for the whole structure to respond. The impulse load in this project is an impact, which by definition is a high-velocity collision. Based on Chen and May (2009), and experience within the research project, e.g. Jönsson and Stenseke (2018), the load in this project is expected to have the shape illustrated in Figure 3.3.
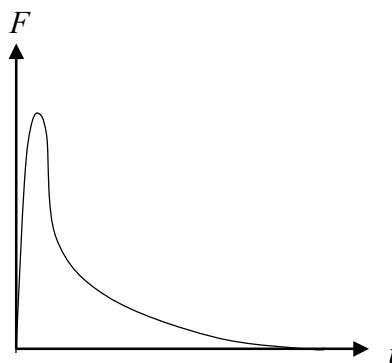
Figure 3.3   Simplification of the expected shape of the dynamic load in this project.

An illustration of an impact between the two arbitrary bodies: body 1, with mass m_1 and body 2, with mass, m_2, can be seen in Figure 3.4. Body 1 has an initial velocity before impact, while body 2 is at rest.
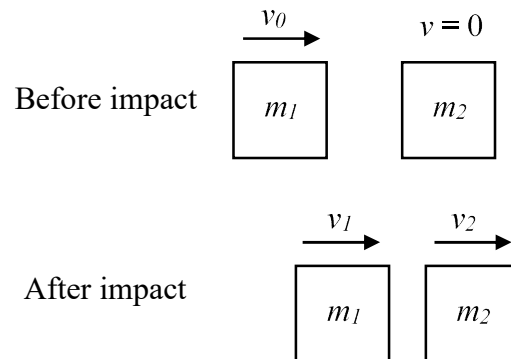
Figure 3.4   Impact between two arbitrary bodies.

If body 1 has velocity v_0 and body 2 is at rest, the kinetic energy before impact can be written as:

$$E_{k,0} = \frac{m_1 v_0^2}{2}$$

(3.9)

The momentum of the system before impact is:

$$p_0 = m_1 v_0 = I_0$$

(3.10)

The impact can be elastic or plastic and the momentum is conserved in the system regardless of which. If it is elastic, the kinetic energy is preserved as well. In the plastic case, a plastic work is performed, transforming a part of the kinetic energy into potential energy in body 1 and/or in the contact surface between the two bodies.

3.4 Elastic response of an impact

After an impact, where the response of body 1 is elastic, the velocity of the two bodies can be derived from the conservation of momentum and kinetic energy. The velocity for body 1 after impact will then be:

$$v_1 = \frac{m_1 - m_2}{m_1 + m_2} v_0$$

(3.11)

and the velocity for body 2 will be:

$$v_2 = \frac{2m_1}{m_1 + m_2} v_0$$

(3.12)

The kinetic energy for the two bodies is then:

$$E_{k,1} = \left(\frac{m_1 - m_2}{m_1 + m_2}\right)^2 E_{k,0} \tag{3.13}$$

$$E_{k,2} = \frac{4m_1 m_2}{(m_1 + m_2)^2} E_{k,0} \tag{3.14}$$

3.5 Plastic response of an impact

After a plastic impact, the two bodies move with the same velocity. With regard to the conservation of momentum, the velocity of the two bodies after impact can be derived to:

$$v_1 = v_2 = \frac{m_1}{m_1 + m_2} v_0 \tag{3.15}$$

and the kinetic energy for the two bodies is then:

$$E_{k,12} = \frac{m_1}{m_1 + m_2} E_{k,0} \tag{3.16}$$

4 Discrete Systems

4.1 Introduction

A common simplified way to describe an impulse loaded structure is to use a single-degree-of-freedom (SDOF) system. To include a falling object in the analysis, the system can be expanded to an equivalent two-degree-of-freedom (2DOF) system. The extension of the system from one to two degrees of freedom increases the complexity of the system substantially.

To analyse a system using the simplified method of transferring it into a discrete system involves simplifications and can lead to less accurate results. However, since the calculations are simple and fast, the simplified method is in many cases a good alternative.

4.2 SDOF system

4.2.1 Equation of motion for SDOF system

A SDOF system consists of a mass, m, a resistance, $R(u)$, and a damper, $c(\dot{u})$, see Figure 4.1. In this project, though, the effect of the damping is neglected due to the nature of the impulse loading. When a force, $F(t)$, acts on the system, it gives rise to a displacement, u. The first derivative of the displacement with respect to time defines the velocity, $\dot{u}$. The acceleration, $\ddot{u}$, is defined by the second derivative.
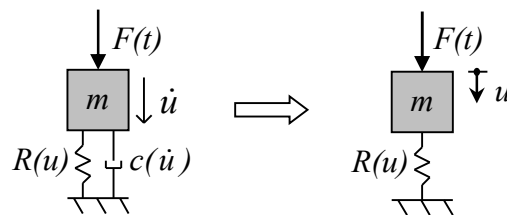
Figure 4.1   Single degree of freedom system, from Johansson (2012).

Using Newton's second law, the differential equation of motion for the SDOF system is defined as:

$$m\ddot{u} + R(u) = F(t) \tag{4.1}$$

The resistance of the spring varies depending on its mechanical properties, as described in Section 2.6.

4.2.2 Response of a SDOF system subjected to an impulse

When SDOF system is subjected to an impulse, the displacement can be calculated from the energy balance described in Figure 3.1. According to Johansson *et al.* (2014), the expression for the external work on the system, derived in Section 3.2, is only valid for a characteristic impulse load:

$$W_e = \frac{I_k{}^2}{2m} \tag{4.2}$$

The corresponding internal work in an elastic system is defined as:

$$W_{i,el} = \frac{R(u_{el})u_{el}}{2} = \frac{ku_{el}^2}{2} \tag{4.3}$$

Using equations (3.8), (4.2), and (4.3) the displacement for a system with an elastic response can be expressed as:

$$u_{el} = \frac{I_k}{m\omega} \tag{4.4}$$

where ω is the eigenfrequency defined as:

$$\omega = \sqrt{\frac{k}{m}} \tag{4.5}$$

If the response of the system is plastic instead, the internal work is defined as:

$$W_{i,pl} = R_m u_{pl} \tag{4.6}$$

Using equations (3.8), (4.2) and (4.6) the plastic displacement can be expressed as:

$$u_{pl} = \frac{I_k^{\ 2}}{2mR_m} \tag{4.7}$$

The internal work for an elasto-plastic response of a spring can be calculated as:

$$W_{i,ep} = \frac{R_m u_{el-pl.el}}{2} + R_m u_{el-pl.pl} = \frac{R_m}{2}\left(u_{el-pl.el} + 2u_{el-pl.pl}\right) \tag{4.8}$$

Using equations (3.8), (4.2) and (4.8) the plastic part of the displacement can be expressed as:

$$u_{el-pl.pl} = \frac{I_k^{\ 2}}{2mR_m} - \frac{u_{el-pl.el}}{2} \tag{4.9}$$

From equation (2.4), the elastic part of the elasto-plastic displacement can be calculated as:

$$u_{el-pl.el} = \frac{R_m}{k} \tag{4.10}$$

By inserting equation (4.10) in equation (4.9), the plastic displacement can be rewritten as:

$$u_{el-pl.pl} = \frac{I_k^2}{2mR_m} - \frac{R_m}{2k} \tag{4.11}$$

The total displacement for a system with an elasto-plastic response can then be calculated according to:

$$u_{tot} = u_{el-pl.el} + u_{el-pl.pl} = \frac{R_m}{2k} + \frac{I_k^2}{2mR_m} \tag{4.12}$$

4.2.3 Equivalent static load

To analyse a structure with respect to dynamic loading, it can be convenient to transform the dynamic load into an equivalent static load. The equivalent static load is defined as the static load that generates an external work of the same magnitude as the dynamic load:

$$W_{e,sta} = W_{e,dyn} \tag{4.13}$$

For the elastic response, the external work caused by a static load, Q, can be calculated as:

$$W_{e,sta} = \frac{Qu_{el}}{2} \tag{4.14}$$

From equations (4.13), (4.14) and (4.2), the equivalent static load, Q_{eq}, for an elastic system can be calculated as:

$$Q_{eq,el} = \frac{I_k^2}{mu_{el}} \tag{4.15}$$

Using equation (4.4), this can be expressed as:

$$Q_{eq,el} = I_k \omega \tag{4.16}$$

For the plastic response, the external work caused by a static load, Q, can be calculated as:

$$W_{e,sta} = Qu_{pl} \tag{4.17}$$

Using equations (4.2) and (4.13) together with (4.17) the equivalent static load can be expressed by:

$$Q_{eq,pl} = \frac{{I_k}^2}{2mu_{pl}} \tag{4.18}$$

Using equation (4.7), the equivalent static load is calculated as:

$$Q_{eq,pl} = R_m \tag{4.19}$$

The external work in an elasto-plastic case caused by a static load, Q, can be expressed as:

$$W_{e,sta} = \frac{Qu_{el-pl.el}}{2} + Qu_{el-pl.pl} = \frac{Q}{2}\left(u_{el-pl.el} + 2u_{el-pl.pl}\right) \tag{4.20}$$

Equations (4.2) and (4.13) together with (4.20) gives the following expression for the equivalent static load:

$$Q_{eq,el-} = \frac{{I_k}^2}{m\left(u_{el-pl.el} + 2u_{el-pl.pl}\right)} \tag{4.21}$$

Using equations (4.10) and (4.11), the equivalent static load can be written as:

$$Q_{eq,el-pl} = R_m \tag{4.22}$$

4.2.4 The influence of the shape of the impulse

The external work on a system is influenced by the resistance, this is explained in Johansson (2014) and Johansson *et al.* (2014). In previous sections, the impulse was assumed to correspond to a characteristic impulse. This is the case e.g. in a system with no resistance ($R = 0$) and the external work can then be calculated according to equation (4.2).

For a system with a resistance, where the load does not correspond to a characteristic impulse, there will be a reduction of the external work done on the system resulting in a smaller displacement. Consequently, for such a case, a higher impulse is needed to cause the same response to the structure as a so called characteristic impulse would do. This can be explained by that the shape of the impulse is altered, it is more spread over time and the maximum value of the force is lower, and hence, this kind of impulse is gentler on the structure.

The system can be evaluated using pressure-impulse diagrams, see Figure 4.2. The diagram is based on that different combinations of the dynamic load, $F(t)$, causes the same critical displacement, $u_{1,crit}$, on a system. For a known dynamic load, the pressure-impulse diagrams can be used to determine if the load causes a displacement larger than the allowed.
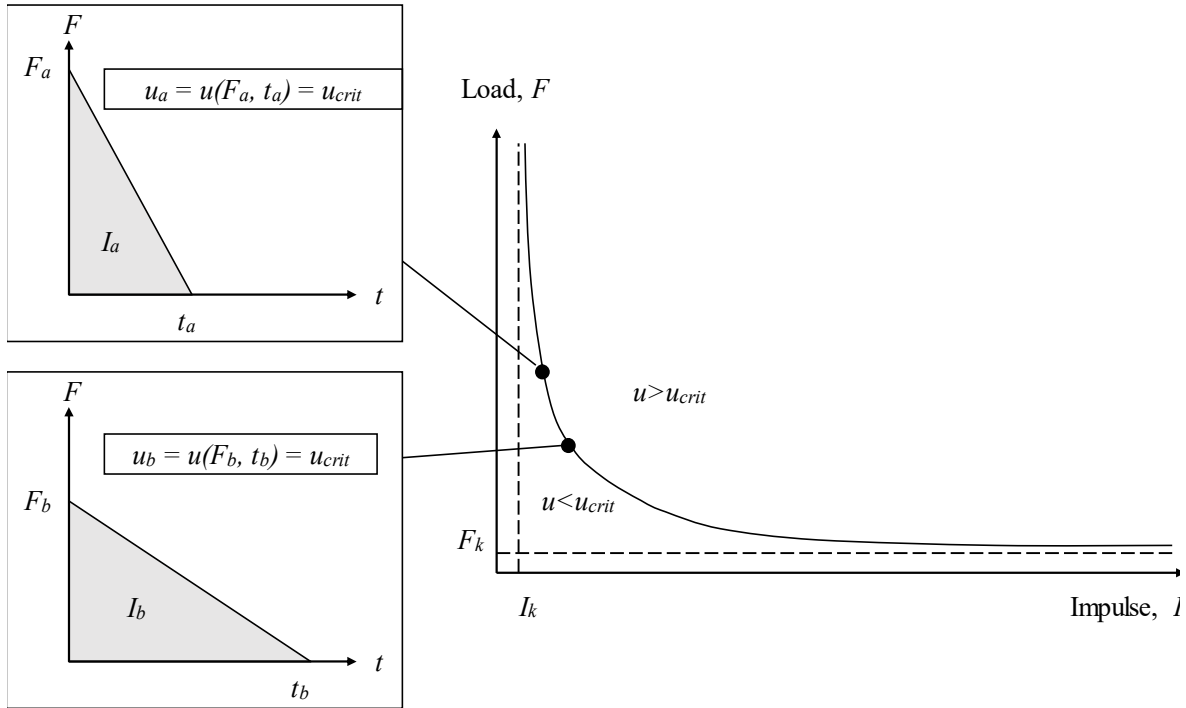
Figure 4.2   Illustration of a pressure-impulse diagram, modified from Johansson (2012).

Johansson (2012) treats the effects of an impulse different from the characteristic by defining a reduction factor $\gamma_I \geq 1$, which is used to reduce the external work as:

$$W_e = \frac{(I/\gamma_I)^2}{2m}$$

(4.23)

Here, γ_I describes how close to a characteristic impulse the actual impulse is where $\gamma_I = 1.0$ indicates a characteristic impulse. The value of γ_I depends on several factors such as the duration of the load, the resistance of the system and the shape of the load.

4.3 2DOF system

4.3.1 Equation of motion for the 2DOF system

A 2DOF system is similar to a SDOF system, but with two masses, and two resistances, see Figure 4.3, where the interaction between the bodies is represented by R_1. To derive the equation of motion for the system, a free body diagram is used, see Figure 4.4.
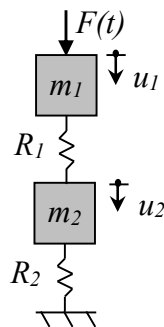
Figure 4.3   2DOF system without dampers, modified from Johansson (2014).
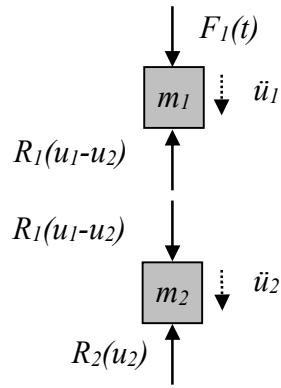
Figure 4.4   Free body diagram of the two degree of freedom system.

For body 1 and 2, Newton´s second law gives:

$$\downarrow: \quad F_1(t) - R_1(u_1 - u_2) = m_1 \ddot{u}_1$$

$$\downarrow: \quad R_1(u_1 - u_2) - R_2(u_2) = m_2 \ddot{u}_2$$

(4.24)

In the next step, the parameters that are dependent on the displacement or the derivatives of the displacement are moved to the left-hand side and the force to the right hand-side.

$$m_1 \ddot{u}_1 + R_1(u_1 - u_2) = F_1(t)$$

$$m_2 \ddot{u}_2 - R_1(u_1 - u_2) + R_2(u_2) = 0$$

(4.25)

On matrix form the equation system can be written as:

$$\begin{bmatrix} m_1 & 0 \\ 0 & m_2 \end{bmatrix} \begin{bmatrix} \ddot{u}_1 \\ \ddot{u}_2 \end{bmatrix} + \begin{bmatrix} R_1(\Delta u) \\ -R_1(\Delta u) + R_2(u_2) \end{bmatrix} = \begin{bmatrix} F_1(t) \\ 0 \end{bmatrix}$$

(4.26)

Where:

$$\Delta u = u_1 - u_2$$

(4.27)

and the response, R_i, can be e.g. elastic, plastic or elasto-plastic as described in equations (2.2), (2.3) or (2.4). The equation of motion for the 2DOF system is then expressed as:

$$\boldsymbol{M}\ddot{\boldsymbol{u}} + \boldsymbol{R}(\Delta u, u_2) = \boldsymbol{F}(t)$$

(4.28)

In the linear elastic case, the resistance depending on the difference between the displacements can be separated and the matrix written as:

$$\begin{bmatrix} m_1 & 0 \\ 0 & m_2 \end{bmatrix} \begin{bmatrix} \ddot{u}_1 \\ \ddot{u}_2 \end{bmatrix} + \begin{bmatrix} k_1 & -k_1 \\ -k_1 & k_1 + k_2 \end{bmatrix} \begin{bmatrix} u_1 \\ u_2 \end{bmatrix} = \begin{bmatrix} F_1(t) \\ 0 \end{bmatrix} \tag{4.29}$$

The equation of motion can then be written as:

$$\boldsymbol{M\ddot{u} + Ku = F}(t) \tag{4.30}$$

A convenient way to handle the elasto-plastic case is to use the secant stiffness, $k_{s,1}$ and $k_{s,2}$, so that the equation of motion can be written in the same way as the linear elastic case.

$$\begin{bmatrix} m_1 & 0 \\ 0 & m_2 \end{bmatrix} \begin{bmatrix} \ddot{u}_1 \\ \ddot{u}_2 \end{bmatrix} + \begin{bmatrix} k_{s,1} & -k_{s,1} \\ -k_{s,1} & k_{s,1} + k_{s,2} \end{bmatrix} \begin{bmatrix} u_1 \\ u_2 \end{bmatrix} = \begin{bmatrix} F_1(t) \\ 0 \end{bmatrix} \tag{4.31}$$

The secant stiffness is used for the plastic branch of the resistance-displacement curve and during unloading. The principle of the secant stiffness is illustrated in Figure 4.5.
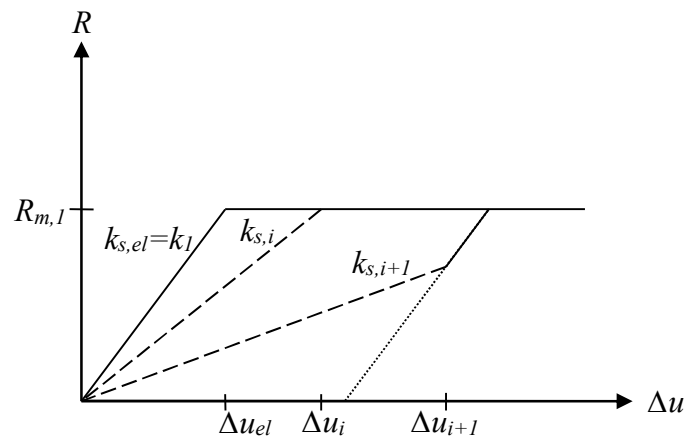
Figure 4.5   Schematic illustration of the secant stiffness for the elasto-plastic case.

4.3.2 Influence of the response of body 1

Depending on whether the response of the spring in body 1 is elastic, plastic or elasto-plastic the impulse, and therefore also the energy, transferred to body 2 will be affected, this is explained in Johansson (2014). When body 2 can be regarded as totally stiff, the impulse will have the following character for the different cases.

If the response of body 1 is elastic, the transferred impulse to body 2 is illustrated in Figure 4.6
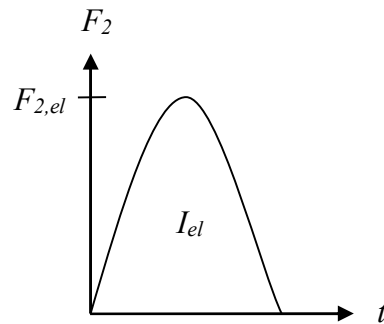
Figure 4.6   Shape of the impulse in case of elastic response, modified from Johansson (2014).

The transferred force, $F_{2,el}$, corresponds to half a sinus wave and is equal to the resistance of body 1, R_1. The force will increase until the maximum value of the elastic displacement of body 1 is reached, corresponding to the maximum force. The maximum value, $F_{2,el}$, can be calculated according to equation (4.32) and is derived in Johansson (2014).

$$F_{2,el} = v_0\sqrt{k_1 m_1} \tag{4.32}$$

At this point, the transferred impulse is equal to the momentum, I_0, of body 1 before impact is calculated as in equation (4.33). Compare with equation (3.4).

$$I_0 = m_1 v_0 \tag{4.33}$$

The force and the displacement will decrease in the same manner as it appeared and during this time, energy will continue to be transferred. The final value of the impulse will hence be twice the size of I_0:

$$I_{el} = 2I_0 \tag{4.34}$$

For the plastic case, the impulse is illustrated in Figure 4.7. The maximum value of the force is reached instantaneously and then remain constant until unloading.
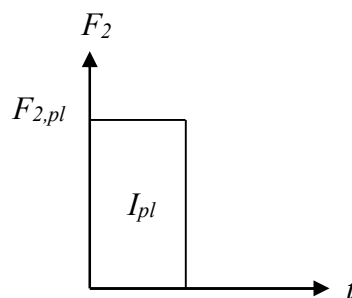
Figure 4.7   Shape of the impulse in case of plastic response, modified from Johansson (2014).

In the plastic case the impulse is of the same magnitude as I_0:

$$I_{pl} = I_0 \qquad (4.35)$$

If the resistance of body 1 is elasto-plastic the response will be a combination of the elastic and plastic case, see Figure 4.8. The loading is elastic until the resistance limit, then the force is constant until the maximum deformation is reached. During unloading, it shows elastic behaviour again, but this time from a limit according to the plastic resistance limit, as schematically shown in Figure 4.8.
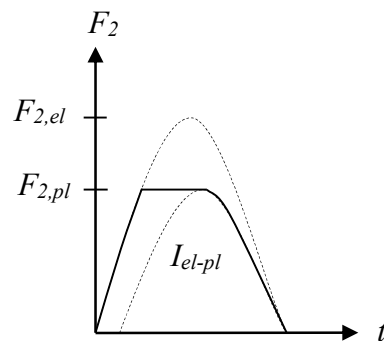
Figure 4.8   *Shape of the impulse in case of elasto-plastic response, modified from Johansson (2014).*

The size of the impulse in this case is somewhere in between the elastic and plastic case:

$$I_0 < I_{el-pl} < 2I_0 \qquad (4.36)$$

If body 2 cannot be considered totally stiff, the maximum value of the contact force will decrease but the impulse will be of the same magnitude; i.e. the duration of the impact load will increase.

The impulses discussed in this section will give rise to a response in body 2, R_2. This response is complex and can be very different depending on how the two bodies interact with each other. The ratio between the frequencies and masses of the two bodies are parameters that affect the response.

4.4 Transformation into discrete systems

4.4.1 Beam into SDOF system

To transform the beam into an equivalent SDOF system, transformations factors can be used according to Johansson (2012). The transformation is illustrated in Figure 4.9.
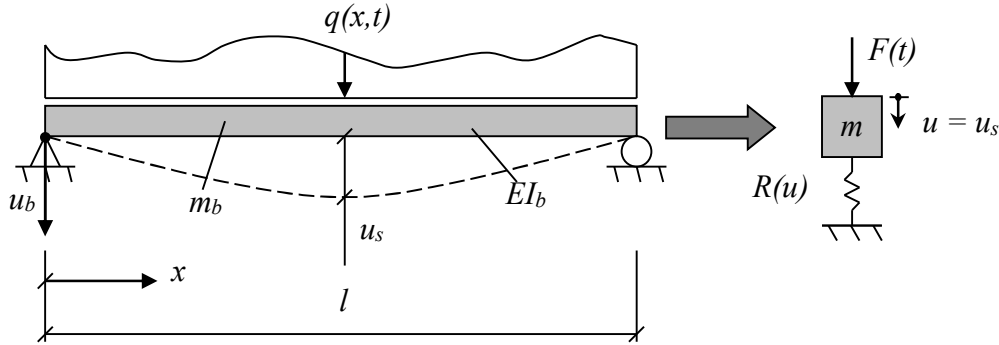
Figure 4.9   *The beam transformed into the 2DOF system, modified from Johansson and Laine (2012).*

To do this transformation, a system point along the x-axis is used. Since the shape of the deformed beam can be considered known, the displacement in all other points along the beam can be expressed in relation to the system point:

$$u_b(x) = \alpha(x) \cdot u_s \tag{4.37}$$

The point with maximum displacement is often suitable to use as the system point, and in this project, it is also the largest displacement that is of interest. The transformed system is to be described as:

$$m\ddot{u} + R(u) = F(t) \tag{4.38}$$

where m, $R(u)$ and $F(t)$ are the components in the SDOF system. To transform the beam into this SDOF system, the mass of the beam is multiplied with the transformation factor κ_m, the resistance with κ_k and the force with κ_f. The equivalent equation of motion representing the beam can then be written as:

$$\kappa_m m_b \ddot{u} + \kappa_k R_b(u) = \kappa_F F_b(t) \tag{4.39}$$

Biggs (1964) has stated that κ_F is equal to κ_k, which leads to that equation (4.39) can be written as:

$$\kappa_{mF} m_b \ddot{u} + R_b(u) = F_b(t) \tag{4.40}$$

Where:

$$\kappa_{mF} = \frac{\kappa_m}{\kappa_F} \tag{4.41}$$

The transformation factors are derived by conservation of kinetic energy as well as internal and external work. For the entire derivation, refer to e.g. Johansson and Laine (2012). In Table 4.1, the transformation factors are summarized for a simply supported beam subjected to a point load in the middle of the span with the system point localized directly under the point load. Depending on if the response is elastic or plastic, the deformed shape of the beam will be different, resulting in different transformation factors.

Table 4.1   Summary of transformation factors for a simply supported beam subjected to a point load, from Johansson and Laine (2012).

Transformation factor	Elastic response	Plastic response
κ_m	0.486	0.333
κ_F	1.000	1.000
κ_{mF}	0.486	0.333

4.4.2 Drop weight into SDOF system

The drop weight can be transformed into a SDOF system in a similar way as the beam, and described as:

$$\kappa_{mF} m_w \ddot{u} + R_w(u) = F_w(t) \tag{4.42}$$

Considering that the drop weight is deformed in the axial direction, the transformation factors are somewhat different. The derivations of the transformation factors, see Lovén and Svavarsdóttir (2016), are based on the same principles as for the beam, using conservation of energy. The displacement shape of the weight depends on the stiffness of the beam as well as on how the load is assumed to be applied. The ideal displacement shape is triangular if the load is assumed to be evenly distributed along the length and the beam considered stiff, but rectangular if the weight is considered much stiffer than the beam or the load assumed to be a point load, see Figure 4.10.
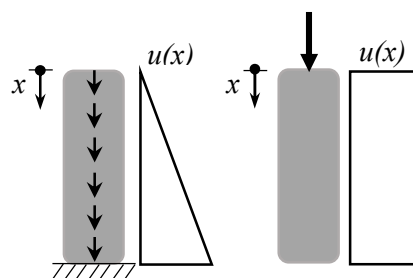
Figure 4.10   The deformation of the drop weight depending on the load application the relation between the stiffness of the beam and the weight.

The transformations factors for the drop weight assuming a triangular or a rectangular deformation shape are presented in Table 4.2.

Table 4.2   Transformation factors for the drop weight depending on displacement shape, from Lovén and Svavarsdóttir (2016).

Transformation factor	Triangular shape	Rectangular shape
κ_m	0.333	1.000
κ_F	0.500	1.000
κ_{mF}	0.667	1.000

4.4.3 Equivalent 2DOF system

When expanding the two SDOF systems into a 2DOF system, the response of the impulse loaded beam can be analysed in a simplified way. The expanded system is shown in Figure 4.11. The falling object is represented by mass m_1 and the interaction between the masses by the resistance, R_1. The beam is represented by mass m_2 and the resistance R_2.
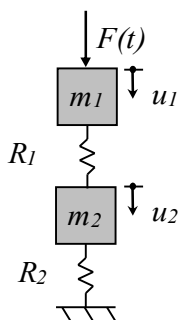
Figure 4.11   The 2DOF system representing the falling object and the beam.

In the same manners as in previous sections, the properties of the drop weight and the beam are transformed into equivalent properties of the 2DOF system, see equations (4.43) to (4.46).

$$m_1 = \kappa_{m,1} m_w \tag{4.43}$$

$$R_1 = \kappa_{k,1} k_{s,w} (u_1 - u_2) \tag{4.44}$$

$$m_2 = \kappa_{m,2} m_b \tag{4.45}$$

$$R_2 = \kappa_{k,2} k_{s,b} u_2 \tag{4.46}$$

Adopting the method of secant stiffness of body 1, as described in Section 4.3.1, and the transformation factors, the equation of motion for the equivalent 2DOF system can be written as:

$$\begin{bmatrix} \kappa_{m,1} m_w & 0 \\ 0 & \kappa_{m,2} m_b \end{bmatrix} \begin{bmatrix} \ddot{u}_1 \\ \ddot{u}_2 \end{bmatrix} + \begin{bmatrix} \kappa_{k,1} k_{s,w} & -\kappa_{k,1} k_{s,w} \\ -\kappa_{k,1} k_{s,w} & \kappa_{k,1} k_{s,w} + \kappa_{k,2} k_{s,b} \end{bmatrix} \begin{bmatrix} u_1 \\ u_2 \end{bmatrix} \dots$$
$$= \begin{bmatrix} \kappa_{F,1} F_w(t) \\ \kappa_{F,2} \cdot 0 \end{bmatrix} \tag{4.47}$$

5 Simplified Analyses

5.1 Introduction

In this project, two simplified methods are used to predict the behaviour of a simply supported reinforced concrete beam subjected to impact loading: the 2DOF system and 2D FE-analysis using 2D beam elements in Abaqus. The results from these analyses are compared with the experimental results as well as results from 3D analyses using solid elements carried out in LS-DYNA, see Chapter 6. In this section, modelling techniques and choices for the two simplified methods are presented. The software Abaqus 6.14 is used to perform analyses of the beam and drop weight modelled in 2D. The theory described in Section 5.3 is based on Simulia (2014 a, b and c).

5.2 2DOF model

5.2.1 Modelling choices for the beam

To model the beam, the response is simplified into a bilinear behaviour according to Figure 5.1. In the elastic part, the beam is assumed to be in state II, i.e. fully cracked, and to have the corresponding stiffness.
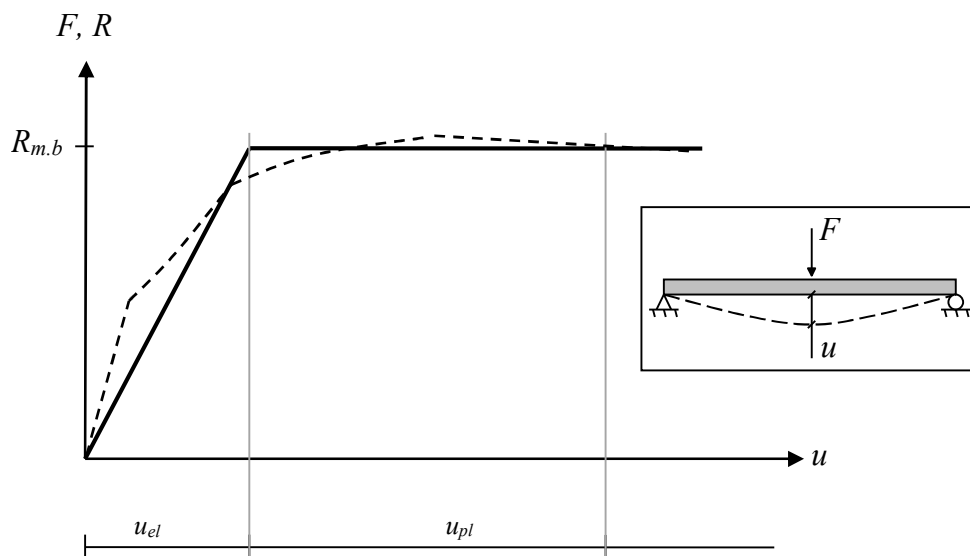
Figure 5.1   Bilinear response assumed for the beam in the simplified analysis using 2DOF.

The resistance limit for the beam, $R_{m,b}$, is calculated using the moment capacity, M_{Rd}, where the capacity utilised for the self-weight, g_b, is subtracted:

$$R_{m,b} = \frac{4\,M_{Rd}}{L} - \frac{g_b L}{2} \tag{5.1}$$

To obtain the stiffness for the linear part, as described in equation (2.4), the expression for the midpoint displacement of a simply supported beam subjected to a point load, F, at the midpoint of the beam can be used:

$$u = \frac{L^3}{48EI_{II}} \cdot F \tag{5.2}$$

This gives an expression for the stiffness, k_b:

$$k_b = \frac{48E_c I_{II}}{L^3} \tag{5.3}$$

In Figure 5.2, the simplified behaviour of the beam is illustrated. In reality, the stiffness of the beam could be different for negative and positive displacements depending on the amount of reinforcement in the top and bottom of the beam. In the negative direction, the self-weight has a favourable effect on the stiffness. However, this is not taken into account in this project.
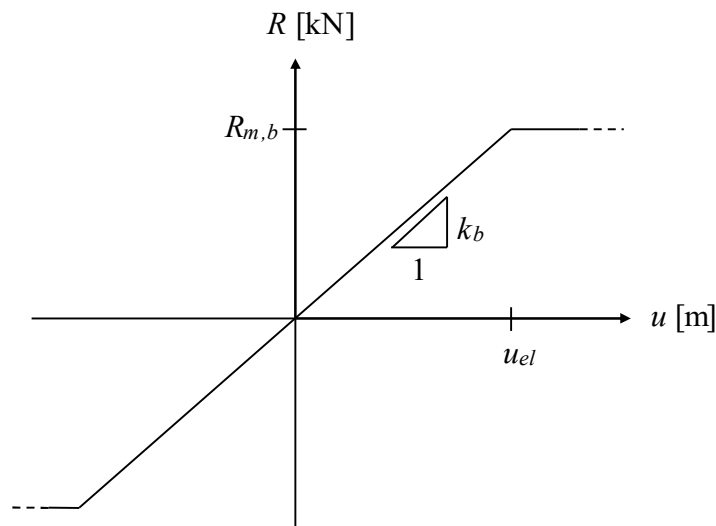
Figure 5.2   Illustration of stiffness and resistance limit for the beam assuming elasto-plastic behaviour.

5.2.2 Modeling choices for the drop weight and the interaction between the drop weight and the beam

The structural response of the fictitious spring representing the interaction between the drop weight and the beam is assumed to be elasto-plastic, see Figure 5.3. When the spring is in tension however, it has no stiffness. This represents that the drop weight and beam are not connected; and hence, no tensile forces can be transferred in between them.
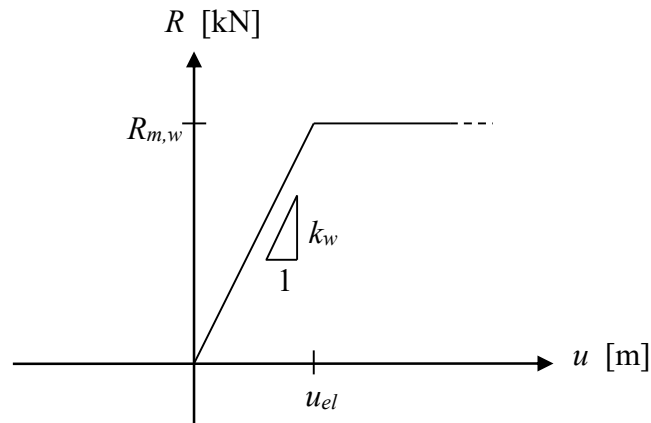
Figure 5.3   Assumed structural response of the spring that represents the contact between the beam and the drop weight.

The stiffness of the drop weight, k_w, is determined from the simplified expression in equation (5.4) including the Young's modulus, E, cross-sectional area, A, and the length, L, of the drop weight.

$$k_w = \frac{EA}{L} \tag{5.4}$$

The resistance limit, $R_{m,w}$, of the spring representing the contact between the weight and the beam is determined by either yielding of the steel in the drop weight or crushing of concrete in the beam. This gives a large span for the resistance which varies between different cases. An evaluation of the choice is made in Section 7.3.1.

The simulation of the impact is made assigning an initial velocity, v_0, to the drop weight and the force, $F_w(t)$, is set to zero. Depending on which height, h, the weight is dropped from, the velocity can be calculated according to:

$$\dot{u}_1 = v_0 = \sqrt{2gh} \tag{5.5}$$

When comparison is made with test results, the measured velocity right before impact is used.

5.2.3 Transformation factors for the system

The deformed shape of the beam will in this project be similar to that of a beam with a plastic response. Therefore, the transformation factors corresponding to plastic response are used.

In the case of an impact load, the boundary conditions of the beam can be said to be time dependent. Directly after impact, the entire beam has not received any information about the impact and only a part of the beam is "active". Initially this results in displacements in the middle part of the beam but no displacement in the outer parts, see Figure 5.4. This is henceforth referred to as the wave propagation effect.
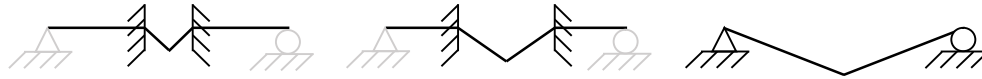
Figure 5.4   Illustration of the deformed shape of the beam at different stages shortly after impact.

The transformation factors, given in Section 4.4.1, are however only valid for a simply supported beam when a plastic hinge has formed in the middle of the beam. The wave propagation effect leads to that the mass of the beam can be considered time dependent. To fully account for this, the transformation factors on the mass could be changed with time. Yi *et al.* (2016) have studied this time dependency for the transformation factor and also provides a suggestion of how it can be approximately accounted for. As a simplification in the present study, though, the boundary conditions, and thereby the transformation factors, are assumed to remain constant.

The stiffness of the drop weight is in this project much stiffer than that of the beam. This means that the drop weight can be considered to move as a rigid body with the same displacement along its entire length. Consequently, the system point of the drop weight can be chosen anywhere along the length. Assuming a stiff drop weight in comparison to the beam also influences the choice of transformation factors for the drop-weight. The assumption that the weight moves as a rigid body means that the displacement shape will be rectangular, and the transformation factors should be chosen accordingly, see Section 4.4.2. In Table 5.1 the chosen transformation factors for the beam and drop-weight are presented.

Table 5.1   Transformation factors for the drop weight and the beam used in the 2DOF.

Transformation factor	Beam Plastic response	Drop weight Rectangular shape
κ_m	0.333	1.000
κ_F	1.000	1.000
κ_{mF}	0.333	1.000

This choice of transformation factors allows for rewriting the equation system given in equation (4.47). Since the transformation factors on the load, κ_F, and on the stiffness, κ_k, for both the drop weight and the beam are equal, the equation system can now be expressed as:

$$\begin{bmatrix} \kappa_{mF,1} m_w & 0 \\ 0 & \kappa_{mF,2} m_b \end{bmatrix} \begin{bmatrix} \ddot{u}_1 \\ \ddot{u}_2 \end{bmatrix} + \begin{bmatrix} k_{w,s} & -k_{w,s} \\ -k_{w,s} & k_{w,s} + k_{b,s} \end{bmatrix} \begin{bmatrix} u_1 \\ u_2 \end{bmatrix} = \begin{bmatrix} 0 \\ 0 \end{bmatrix} \tag{5.6}$$

5.2.4 Central difference method

The central difference method (CDM) is an explicit numerical iteration method that can be used to solve the differential equation of motion for the 2DOF system, see equation (5.6). In this project this is done using Matlab, see Appendix B for the code. The following section on CDM is based on Craig and Kurdila (2006). In CDM, the displacements of the current and previous time steps are used to calculate the displacement of the next step. For the solution to be stable, the timestep, Δt, must be sufficiently small, i.e. the method is conditionally stable.

CHALMERS, *Architecture and Civil Engineering*, Master's Thesis, ACX30-18-36

$$\Delta t < \frac{2}{\omega_{max}} \qquad (5.7)$$

where ω_{max} is the highest eigenfrequency for $|\mathbf{K} - \omega^2 \mathbf{M}| = 0$. Differently put, this means that a stress wave should not propagate more than an element length, l_{el}, in each time step:

$$\Delta t < \frac{l_{el}}{c} \qquad (5.8)$$

Here, c describes the speed of wave propagation in the material with the density ρ, and Young's modulus E, and can be calculated as:

$$c = \sqrt{\frac{E}{\rho}} \qquad (5.9)$$

According to Johansson and Laine (2012), it is preferable to use an even smaller timestep to obtain enough accuracy in the solution. For an impulse loaded structure, they suggest using a timestep smaller than one percent of the load duration, t_1, i.e. equal to:

$$\Delta t < \frac{t_1}{100} \qquad (5.10)$$

CDM is based on the definition of the first and second order derivative. The first order derivative is approximated to:

$$\dot{\mathbf{u}}_n \approx \frac{\mathbf{u}_{n+1} - \mathbf{u}_{n-1}}{2h} \qquad (5.11)$$

Where the subscript n denotes the current timestep, $n-1$ the previous timestep, and $n+1$ the timestep to be calculated. Similarly, the second order derivative is approximated to:

$$\ddot{\mathbf{u}}_n \approx \frac{\dot{\mathbf{u}}_{n+1/2} - \dot{\mathbf{u}}_{n-1/2}}{\Delta t} \approx \frac{\mathbf{u}_{n+1} - 2\mathbf{u}_n + \mathbf{u}_{n-1}}{\Delta t^2} \qquad (5.12)$$

Together with the differential equation of motion for the 2DOF system, see equation (4.29), equations (5.11) and (5.12) gives:

$$\left(\frac{\mathbf{M}_n}{\Delta t^2}\right)\mathbf{u}_{n+1} + \left(\mathbf{K}_n - \frac{2\mathbf{M}_n}{\Delta t^2}\right)\mathbf{u}_n + \left(\frac{\mathbf{M}_n}{\Delta t^2}\right)\mathbf{u}_{n-1} = \mathbf{F}_n \qquad (5.13)$$

This can be rearranged to give an expression for $\boldsymbol{u}_{n+1}$:

$$\boldsymbol{u}_{n+1} = \left(\frac{\boldsymbol{M}_n}{\Delta t^2}\right)^{-1} \left(\boldsymbol{F}_n - \left(\boldsymbol{K}_n - \frac{2\boldsymbol{M}_n}{\Delta t^2}\right)\boldsymbol{u}_n - \left(\frac{\boldsymbol{M}_n}{\Delta t^2}\right)\boldsymbol{u}_{n-1}\right) \tag{5.14}$$

In order to solve the first timestep, initial conditions are needed: $\boldsymbol{u}_0 = \boldsymbol{u}(0)$ and $\dot{\boldsymbol{u}}_0 = \dot{\boldsymbol{u}}(0)$. The initial acceleration $\ddot{\boldsymbol{u}}_0$ is then calculated from the equation of motion as:

$$\ddot{\boldsymbol{u}}_0 = \boldsymbol{M}_0{}^{-1}(\boldsymbol{F}_0 - \boldsymbol{K}_0 \boldsymbol{u}_0) \tag{5.15}$$

To find the displacement of the timestep before that, $n = -1$, a Taylor series expansion is made:

$$\boldsymbol{u}_{-1} \approx \boldsymbol{u}_0 - \Delta t \dot{\boldsymbol{u}}_0 + \frac{\Delta t^2}{2}\ddot{\boldsymbol{u}}_0 \tag{5.16}$$

5.3 Model in Abaqus using 2D beam elements

5.3.1 Modelling of the system

Using 2D beam elements in Abaqus, the drop weight and the beam were modelled according to Figure 5.5. In the same manners as in the 2DOF system, the weight was modelled as a point mass connected to a spring. According to Lovén and Svavarsdóttir (2016), that way of modelling the drop weight is accurate enough, and since it is not the deformations of the drop weight that are of interest, there is no need to model the drop weight in a more detailed way.
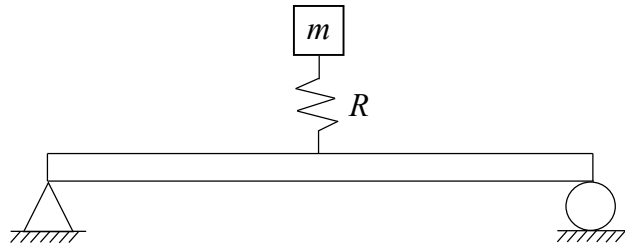
Figure 5.5   Schematic picture of how the system is modelled in Abaqus.

The spring representing the interaction between the beam and the drop weight has no resistance in tension, in the same way as in the 2DOF model. The behaviour of the spring in compression can be modelled as either elastic or elasto-plastic. Lovén and Svavarsdóttir (2016) modelled the interaction as elastic and got reasonable results, but in the 2DOF system the interaction is modelled as elastoplastic. These two ways of modelling the behaviour of the spring have been evaluated in Section 7.3.3. In both cases, the stiffness, k_w, was calculated according to equation (5.4) and in the elasto-plastic case the resistance limit, $R_{m,w}$, was set to the same value as for the 2DOF model. This value of the resistance limit is further evaluated in Section 7.3.1.

In Abaqus, a spring is symmetrically elastic, which means that it is elastic in both directions. To modify the behaviour of the spring, the input file must be changed, see the standard input file in Appendix H. This was done for the elastic spring to remove the resistance in tension.

For the elasto-plastic spring, the behaviour was modified in both tension and compression. The modified spring cannot display any plastic deformation, though, and the loading and unloading for a spring in Abaqus where a resistance limit is added follows the graph in Figure 5.6.
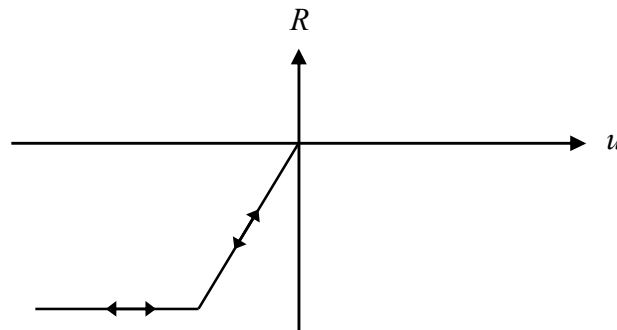
Figure 5.6   Spring behaviour in Abaqus.

To enable for plastic deformations and an elasto-plastic behaviour of the spring, the spring element was modelled together with a bar element, see Figure 5.7. Together they represent the elasto-plastic spring.
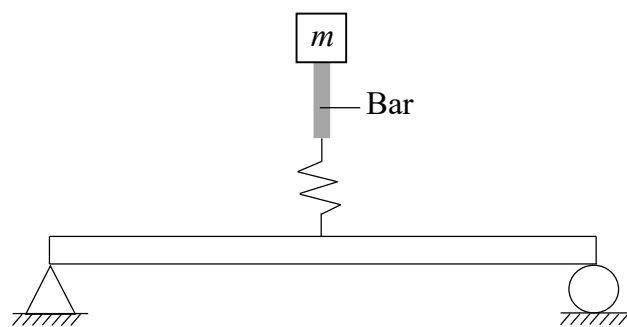
Figure 5.7   Schematic picture of how the system is modelled in Abaqus with the addition of a bar.

The bar was modelled as elasto-plastic with a very high stiffness and the correct resistance limit. The spring element on the other hand has a stiffness somewhat higher than the intended one, but no resistance limit. Together they represent an elasto-plastic spring with the correct stiffness and resistance limit, see Figure 5.8. The relation between the total, effective stiffness and the individual stiffnesses of the spring element and the bar element is defined by:

$$\frac{1}{k_{eff}} = \frac{1}{k_{spring}} + \frac{1}{k_{bar}} \tag{5.17}$$
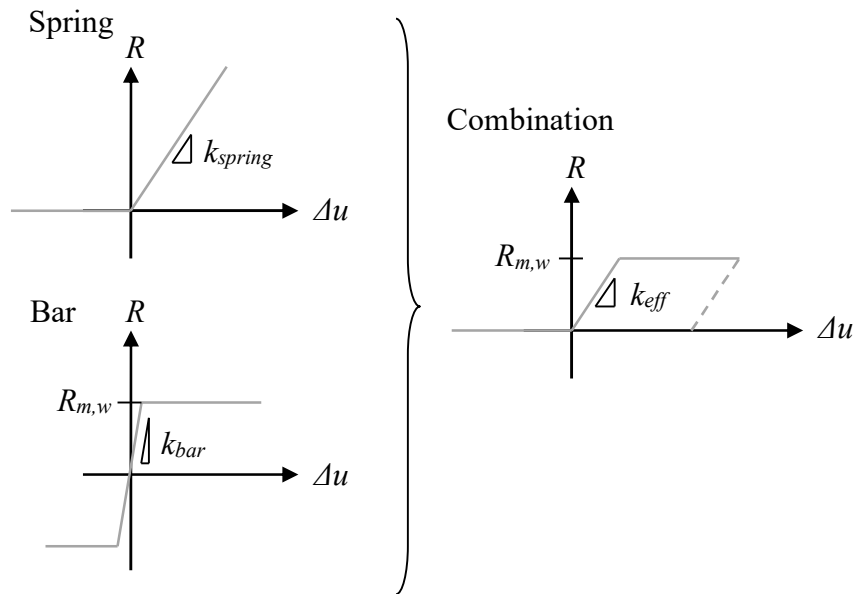
Figure 5.8   Structural behaviour of the combination of a spring and a bar generating an elasto-plastic behaviour, modified from Andersson and Antonsson (2015).

The transformation factors chosen for the drop weight in the 2DOF system, presented in Table 5.1, were included in Abaqus as well. However, since these values are equal to 1 they are not further mentioned. Furthermore, the fall of the mass was represented by an assigned initial velocity in the same way as for the 2DOF system.

In Abaqus, no units are displayed. Instead the user can choose which units to use and it is crucial to keep consistence in these choices. The units used in Abaqus in this project are presented in Table 5.2. These units were chosen to make the handling of the output data more efficient compared to standard SI units.

Table 5.2   The units used in Abaqus.

Mass	Length	Time	Force	Stress	Energy
g	mm	ms	N	MPa	N·mm

5.3.2 Elements

The element type chosen for the beam in Abaqus is a 2D planar beam element that uses linear interpolation and is called B21. This is the default element used when 2D planar and wire elements are chosen in the software. B21 is a Timoshenko beam element which is usually suitable for beams with a high cross section since they allow for transverse shear strains. In Abaqus these beam elements are formulated so that they are suitable for more slender beams as well. According to Simulia (2014 b) the B21 element is one of the element types that are well suited when simulating impact loading.

To find a suitable number of elements, a convergence study was made studying the static capacity of the beam when subjected to a prescribed deformation in the middle of the span. Three different meshes with 50, 100 and 200 elements, respectively, were compared. In Table 5.3, the errors from the theoretical value, calculated in Appendix C, are compared. An error of approximately 1 % was considered good enough and was achieved by a mesh of 100

elements. No further modifications of the input data in the Abaqus model are made to calibrate the model.

Table 5.3   Convergence study of number of elements in the Abaqus model.

	Capacity [kN]	Error [%]
Theoretical	10.38	-
50 elements	10.59	2.0
100 elements	10.49	1.0
200 elements	10.43	0.5

5.3.3 Boundary conditions

In the Abaqus model, the beam is modelled as simply supported. That is, the vertical translation in the beam is tied at the supports while the rotations are set free. In the real case though, the beam is only resting on the supports and not tied to them, which corresponds to boundary conditions were the beam is only fixed downwards. This leads to that the Abaqus-model gives different results than the experiments and the more detailed 3D FE-analysis, but similar to the 2DOF model. However, the Abaqus results does not differ from the test results until the beam rebounds from the supports. Considering that the most interesting results are the maximum values, which are obtained before that, the differences in the later response are deemed to be of minor importance.

5.3.4 Solution method

The analyses are performed with an explicit solution method, described in Simulia (2014c). The method is similar to the central difference method described in Section 5.2.4 and a sufficiently small timestep is needed to make this numerical method work. According to Simulia (2014b), Abaqus gives the possibility to choose between an automatically generated timestep that is small enough or a user specified fixed timestep. In this project the fixed timestep is used to have more control over the analysis.

The explicit solution method is provided in the software Abaqus/Explicit. In Abaqus/Standard, though, the dynamic response is calculated using an implicit solution method. According to Simulia (2014b), the explicit integration method is usually more mathematically efficient for very short-term events, but a comparison between the explicit and implicit solution methods is still of interest to perform.

The implicit solution method is an unconditionally stable integration procedure, where the timestep is less important than for the explicit method. To calculate the displacement, unknown quantities in the timestep to be solved are used which leads to that iteration is required within every timestep, according to (2014c). Compared to the explicit method, explained in Craig and Kurdila (2006), where only known quantities from previous timesteps are used, which leads to that no iteration is required within each timestep, leading to a more computationally efficient solution for short term events.

5.3.5 Modelling of the materials

Since the global response of the beam was of interest, the reinforced concrete could be modelled as an isotropic material with a bilinear response as in Figure 5.9 with the state II (cracked) stiffness.
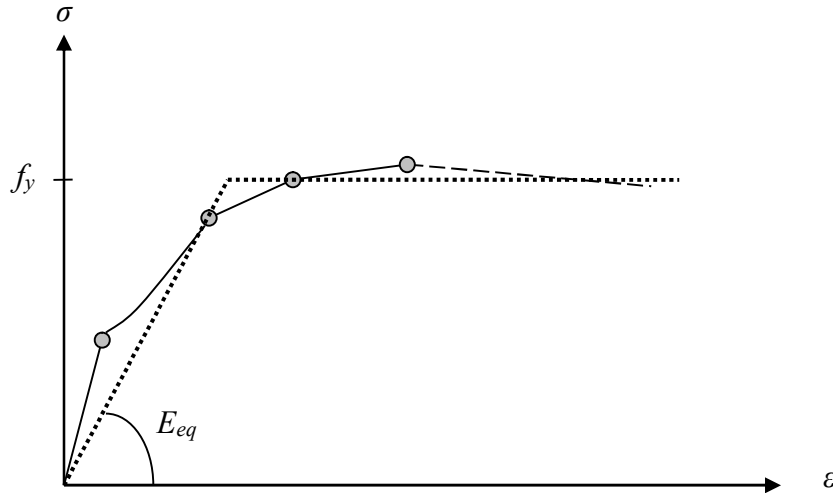
Figure 5.9   Bilinear response with equivalent Youngs modulus.

In standard calculations, Young's modulus for concrete and the moment of inertia for state II would be used. However, in Abaqus the section is assumed to be isotropic and uncracked which means that the software will calculate the moment of inertia for state I. To account for this, an equivalent Young's modulus, E_{eq}, is used in the Abaqus analyses:

$$E_{eq} = E_c \frac{I_{II}}{I_I} \qquad (5.18)$$

This results in the same bending stiffness for the two cases:

$$E_{eq}I_I = E_c I_{II} \qquad (5.19)$$

However, altering the value of Young's modulus also affects the wave speed in the material, see equation (5.9). This has some influence on the response of the model, but Andersson and Karlsson (2012) examined this and found no significant differences until the Young's modulus was changed by a factor of 25. In this project, it is changed by a factor of approximately 6, which implies that the effects on the results are acceptable.

The input value of the yield stress is also calculated for the isotropic material. This is done using the moment capacity, M_{Rd}, and the section modulus for the linear elastic sectional response, W_{el}. To be able to compare the results to the test results, the moment capacity reduced with regard to gravity, $M_{Rd,red}$, must be used. This gives the corresponding value for the yield stress, $f_{y,red}$:

$$f_{y,red} = \frac{M_{Rd,red}}{W_{el}} \qquad (5.20)$$

where the section modulus is calculated using the height, h, and the width, b, of the beam:

$$W_{el} = \frac{bh^2}{6} \tag{5.21}$$

5.3.6 Integration points

In the Abaqus model, three integration points are chosen to describe the height of cross section of the beam. Using three integration points, the sectional response of the model is treated as linear by the software, see Figure 5.10.
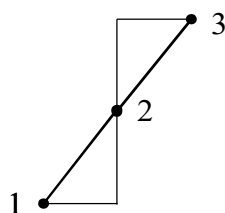
Figure 5.10   Interpretation of three integration points in Abaqus.

Using three integration points gives the user more control of the response of the model compared to e.g. five integration points, which is default. To change to three integration point must be done in the input file, see the standard input file Appendix H. For five integration points, the stress distribution over the section in Abaqus varies in a less obvious way. The stress can be analysed in the integration points only, which means that it is difficult to know how it varies between them. Figure 5.11 shows examples of protentional cross sectional responses using five integration points in Abaqus.
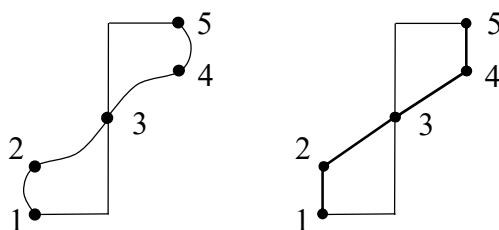
Figure 5.11   Example of possible sectional responses using 5 integration points.

To investigate the program's interpretation of five integration points, a comparison was made of the time-displacement curves from analyses using three and five integration points respectively. Since the stress distribution when five points are used is closer to that of a fully plastic section, the plastic section modulus, W_{pl}, is calculated according to equation (5.22). The input value of the yield strength, $f_{y,red,pl}$, is calculated using the plastic section modulus as in equation (5.23).

$$W_{pl} = \frac{bh^2}{4} \tag{5.22}$$

$$f_{y,red,pl} = \frac{M_{Rd,red}}{W_{pl}} \qquad\qquad (5.23)$$

From the elastic and plastic response, respectively, the values of the equivalent yield strength defined in Abaqus are presented in Table 5.4. See Appendix C for calculations.

Table 5.4   *Equivalent yield strength of the concrete assuming elastic (3 ip) and plastic (5 ip) sectional response.*

	Elastic, 3 ip	Plastic, 5 ip
Equivalent yield strength [MPa]	15.57	10.38

The results of the comparison can be seen in Figure 5.12. It showed that the ultimate capacity of the beam becomes very similar for the two cases.
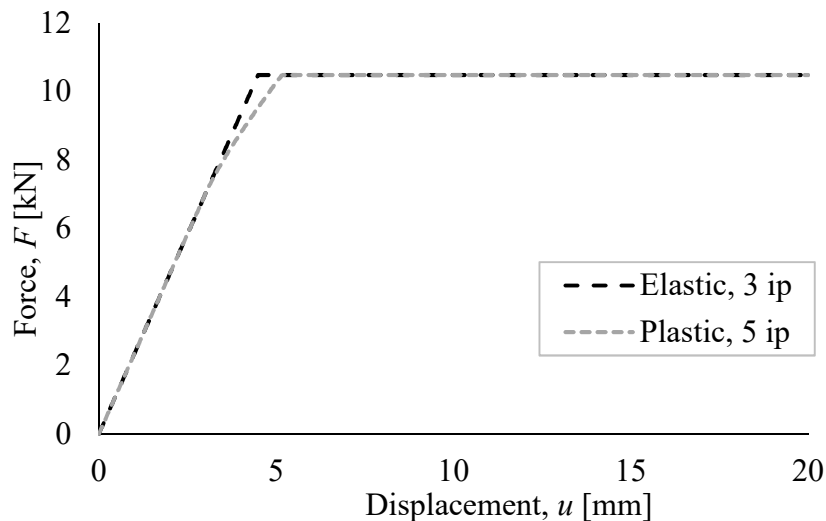
Figure 5.12   *Structural response of the beam assuming elastic section with three Integration points and assuming plastic section with five integration points.*

Using five integration points the bend in the curve is softer, which is closer to the real behaviour of the beam. However, to improve the comparison of the Abaqus model and the 2DOF model, a true bilinear response is desired, which means that the use of three integration points is preferable. The fact that the capacity of the beam becomes almost the same using the plastic section modulus together with five integration points as using the elastic section modulus together with three integration points implies that the stress distribution with five integration points is close to fully plastic. In Figure 5.13, a comparison between the stress distribution for a fully plastic section and a possible assumed stress distribution is showed.

         —— Possible stress distribution
         ...... Fully plastic stress distribution
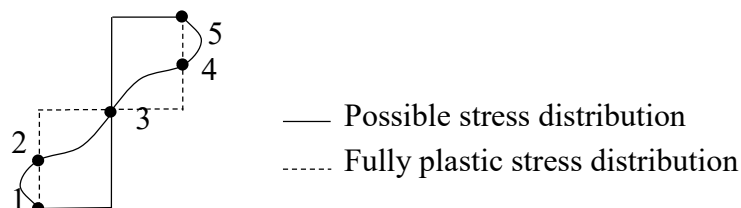
Figure 5.13   *Comparison between possible assumed stress distribution and stress distributions for a fully plastic section.*

6 LS-DYNA Modelling Using 3D Solid Elements

6.1 Introduction

In LS-DYNA, a 3D model using solid elements is created and analysed to simulate the behaviour of a reinforced concrete beam subjected to impact loading. For the modelling, several choices are preformed based on Lovén and Svavarsdóttir (2016) and Lozano and Makdesi (2017). Furthermore, different choices for some parameters are presented and later evaluated in Chapter 7. The information concerning modelling in LS-DYNA described in this chapter is to a large extent based on LSTC (2014 a, b). The input file for the LS-DYNA model can be found in Appendix I.

6.2 Modelling of the system

In the LS-DYNA model, presented in Figure 6.1, the beam and the drop-weight are modelled as solid parts. The beam is resting on two roller supports which are modelled as individual solid parts made of steel.
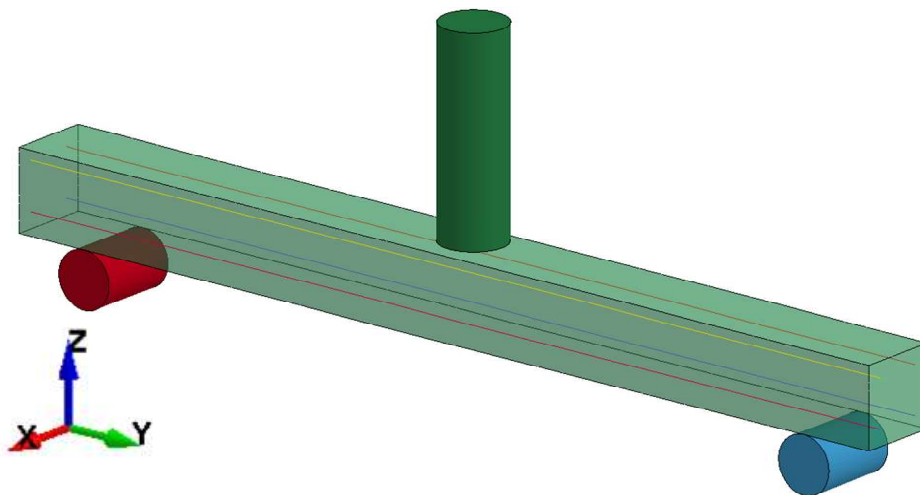
Figure 6.1   LS-DYNA model including the beam, supports and drop weight.

Between the rollers and the beam, a contact was defined. This contact simulates the real behaviour so that it allows the beam to lift; i.e. the beam was not tied to the support. This was done using CONTACT: AUTOMATIC_SURFACE_TO_SURFACE in LS-DYNA. The roller supports, though, were locked in both positive and negative z-direction. They were also locked horizontally in both x- and y-direction. These boundary conditions were obtained by creating sets of nodes and prescribing their displacements in the BOUNDARY: SPC_SET option in LS-DYNA.

The drop weight was initially located 1 mm above the beam and assigned an initial velocity representing the fall. This is made under INITIAL: VELOCITY_GENERATION in LS-DYNA. The contact between the drop-weight and the beam was modelled in the same way as the contact between the beam and the supports. The bottom surface of the drop weight is spherical which was included in the model, see Figure 6.2.

Figure 6.2   Shape of the drop weight in LS-DYNA.

In the same way as in Abaqus, LS-DYNA does not include units on any quantities. Instead, the user must ensure that a consistent system of units is used. In Table 6.1 the units used in this project are presented.

Table 6.1   The units used in LS-DYNA.

Parameter	Mass	Length	Time	Force	Stress	Energy
Unit	g	mm	ms	N	MPa	N·mm

6.3 Elements

In this project, solid tetrahedral elements were used for the beam based on the results from Lozano and Makdesi (2017) who found that the models using tetrahedral elements compared to hexahedral elements corresponded better to test results.

The tetrahedral elements were created by the tetrahedral mesher available in LS-DYNA, see Figure 6.3. The mesh can be created in different ways; with different methods (Method 1-3) of remeshing after a trial mesh is created and with or without skin remesh. If skin remesh is used, it is possible to choose between Method 1 or 2. Lozano and Makdesi (2017) concluded that the tetrahedral mesh is very sensitive to how the mesh looks. Therefore, the mesh was created in the same way as presented in Lozano and Makdesi (2017) where Method 2 was used for the skin remesh and Method 3 for tetrahedral mesh, as well as the element size of 5mm. After the mesh was created, the element type was defined by assigning ELFORM to 10 in the category of solid elements, creating tetrahedral elements with one integration point.
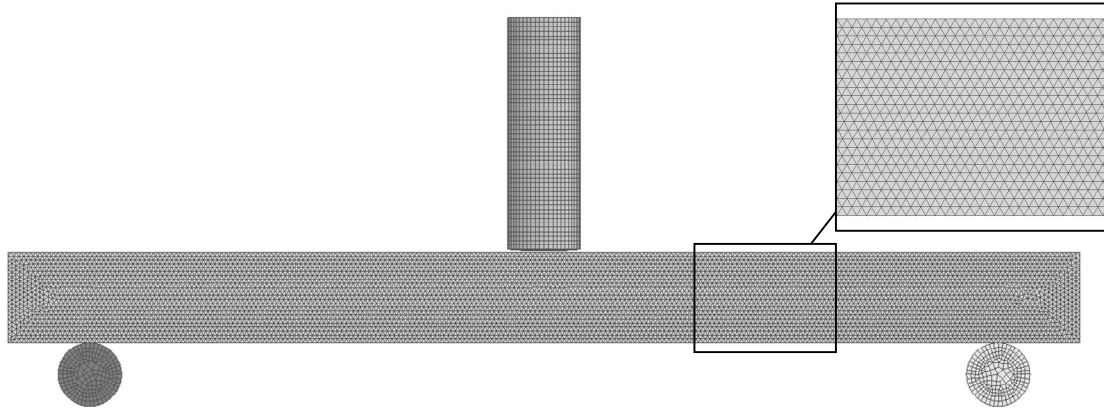
Figure 6.3   Illustration of the meshed model in LS-DYNA.

The drop weight and roller supports were modelled using solid hexahedral elements with constant stress. The mesh was created using the solid mesher and the element type was defined by assigning the parameter ELFORM to 1 in the category solid elements. This kind of element was used for the weight and supports since their response was not of interest in this study.

For the reinforcement, beam or truss elements have been used. Since the reinforcement is mainly acting in tension, it could be argued that truss elements would be well suited. Therefore, a comparison was made in Section 7.5.1 between beam and truss elements for the reinforcement. The number of integration points over the section is specified with the parameter QR/IRID. If beam elements with one integration point over the section is used, an element similar to a truss element is obtained.

Beam elements of the type Hughes-Liu were chosen by assigning ELFORM to 1 while truss elements were defined by choosing ELFORM to 3 in the category of beam elements. When truss elements are used, the section is defined by a cross sectional area and for beam elements, the diameter of the reinforcement is specified. The mesh was created using element generation and the element generation method was set to "curve".

6.4 Solution method

The time integration performed in LS-DYNA is described in LSTC (2018). The method used was CDM, which is described in Section 5.2.4. Since CDM is an explicit method, the timestep is important for the stability. The timestep is not specified by the user but automatically computed in the software. The automatically generated timesteps are calculated differently depending on the element type used. When using tetrahedral solid elements, the critical timestep for each element $h_{crit,i}$ is calculated based on the size of the element and the wave speed. Then the timestep used in the next iteration step, h_{n+1} is calculated as:

$$h_{n+1} = a \cdot \min(h_{crit,i}) \quad i=1,2...n \tag{6.1}$$

where a is a timestep scaling factor defined by default as 0.9 if nothing else is specified and n is the number of elements. The timestep scaling factor is chosen by defining the parameter TSSFAC in CONTROL_TIMESTEP.

6.5 Material models

6.5.1 Concrete

The material model used for the concrete is called CDPM2 and is developed and described by Grassl *et al.* (2013). The material model is suitable for dynamic analyses of concrete structures. In LS-DYNA this material model is named MAT_273 or MAT_CONRETE_DAMAGE_PLASTICITY_MODEL. It contains many input variables, of which some are mentioned in this section. The other parameters were left as the default values. In the manual of CDPM2 by Grassl (2016) and the manual of LS-DYNA, LSTC (2017), a description of each input parameter can be found. In Table 6.2, the parameters that were defined as something different than the default value are presented together with the notation used in LS-DYNA.

Table 6.2   Material parameters defined for CDPM2 in LS-DYNA.

LS-DYNA notation	Parameter
RO	Mass density
E	Young's modulus
PR	Poisson's ratio
ECC	Eccentricity parameter
FT	Uniaxial tensile strength
FC	Uniaxial compressive strength
HP	Hardening parameter
WF	Ultimate crack width
TYPE	Type of tensile damage
EFC	Compressive damage variable

One input variable that was defined is the eccentricity parameter, called ECC in LS-DYNA. According to Grassl *et al.* (2013), the shape of the deviatoric section is handled with this parameter. It is calculated using the mean tensile strength, f_t, and the mean compressive strength, f_c, of the concrete used. According to Grassl *et al.* (2013), f_{bc} represents the equiaxial compressive strength and the expression is obtained through experiments.

$$\text{ECC} = \frac{1+\epsilon}{2-\epsilon}, \quad \epsilon = \frac{f_t(f_{bc}^2 - f_c^2)}{f_{bc}(f_c^2 - f_t^2)}, \quad f_{bc} = 1.16f_c \tag{6.2}$$

Another parameter that was defined is the hardening parameter which is dependent on if the strain rate effects are included. The default value is HP = 0.5 and is only valid if the strain rate effects are included. However, if these effects are not included the recommended value is HP = 0.01. The effect of strain rate effect on the concrete can be treated in CDPM2 by putting the variable STRFLG to 1.0, however this was not done in this project.

The compressive damage variable ε_{fc}, EFC in LS-DYNA, which controls the behaviour of concrete after the maximum compressive stress is reached, were increased from the default of 0.0001 value to a larger value of 0.001. This is recommended by Grassl *et al.* (2018) when using tetrahedral elements to avoid local compressive failure where the drop weight hits the

beam. For some cases when the risk of local compressive failure is extra high, the damage variable can be increased further.

The damage when the tensile strength is reached is described by the stress-inelastic displacement law as described in Section 2.2.2. This relation can in LS-DYNA be described as linear, bilinear or exponential. The damage formulation is linear by default. However, Grassl (2016) states that a bilinear damage formulation gives the best results which is also shown in the previous project by Lozano and Makdesi (2017). A comparison of how the result is affected by the choice of the damage formulation is of interest since Lovén and Svavarsdóttir (2016) used the linear formulation in their project.

The linear damage formulation is defined by TYPE = 0 and can be seen in Figure 6.4. Using the value for fracture energy, G_F the ultimate crack width, w_f for a linear damage formulation is calculated according to equation (6.3).
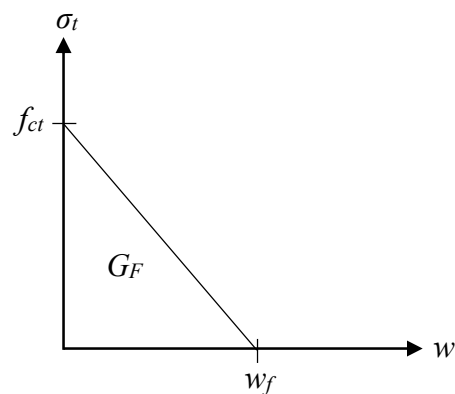
Figure 6.4   Linear tensile damage formulation applied in LS-DYNA.

$$w_f = \frac{2G_F}{f_{ct}}$$

(6.3)

The bilinear damage formulation is illustrated in Figure 6.5 and is defined in LS-DYNA by assigning the parameter TYPE = 1.
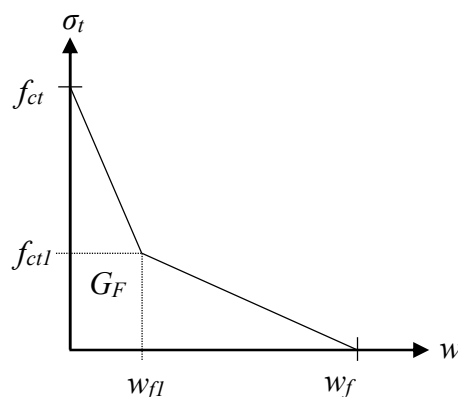
Figure 6.5   Bilinear tensile damage formulation applied in LS-DYNA.

The ultimate crack width, w_f for a bilinear damage formulation is calculated using the value for fracture energy, G_F, according to equation (6.4). From the input value of w_f the values of w_{f1} and f_{ct1} are calculated by default according to equations (6.5) and (6.6).

$$w_f = \frac{4.444 G_F}{f_{ct}} \tag{6.4}$$

$$w_{f1} = 0.15 \cdot w_{f,tetra} \tag{6.5}$$

$$f_{ct1} = 0.3 \cdot f_{ct} \tag{6.6}$$

According to Grassl (2016), the input value of the ultimate crack width in models with tetrahedral elements should be modified:

$$w_{f,tetra} = 0.56 \cdot w_f \tag{6.7}$$

6.5.2 Reinforcement

The steel in the reinforcement can be modelled in different ways, Lovén and Svavarsdóttir (2016) and Lozano and Makdesi (2017) modelled it as bilinear. However, to model the reinforcement in a more realistic way, a multilinear relationship for the stress-strain curve can be introduced. An investigation of the different ways of modelling the stress-strain relation for the concrete is made in Section 7.5.4.

The bilinear behaviour is defined with the material model MAT_003, which is called MAT_PLASTIC_KINEMATIC in LS-DYNA. According to LSTC (2014 b), this material model is effective and well suited for isotropic materials with hardening plasticity. In Figure 6.6, the structural response of the reinforcement in LS-DYNA is illustrated.
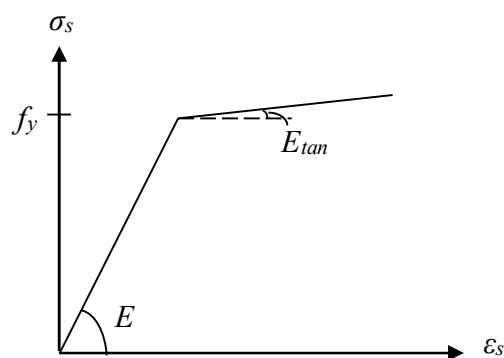
Figure 6.6   Structural response of the plastic kinematic material model.

There are several material parameters in the material model that can be defined. The parameters for the bilinear model that are defined as something other than the default value are presented together with the LS-DYNA notation of the parameter in Table 6.3.

Table 6.3   Input material parameters for the bilinear model in LS-DYNA.

LS-DYNA notation	Parameter
RO	Mass density
E	Young's modulus
PR	Poisson's ratio
SIGY	Yield stress
ETAN	Tangent modulus

The multilinear behaviour is in LS-DYNA introduced using the material model 024-PIECEWISE_LINEAR_PLASTICITY. This material behaviour is illustrated in Figure 6.7.
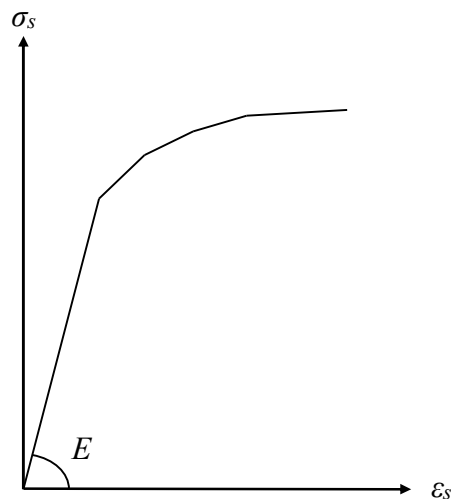
Figure 6.7   Structural response for the multilinear material model.

For the multilinear model, SIGY and ETAN mentioned in Table 6.3 are not used. Instead, stresses and corresponding strains are defined by assigning values to the parameters ES and EPS. Only the plastic strains are considered, which means that the first value of strain is zero and the corresponding stress is equal to the yield stress. In Figure 6.8, the values of plastic strain and stress defined in LS-DYNA are illustrated.
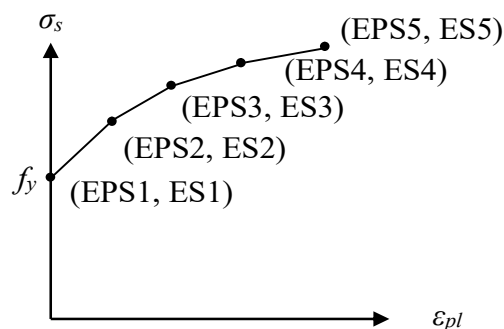
Figure 6.8   Schematic illustration of the stress-plastic strain relationship defined in LS-DYNA.

To calculate the plastic strain defined for this material model in LS-DYNA, the elastic part of the strain is subtracted from the total strain, as schematically illustrated in Figure 6.9.
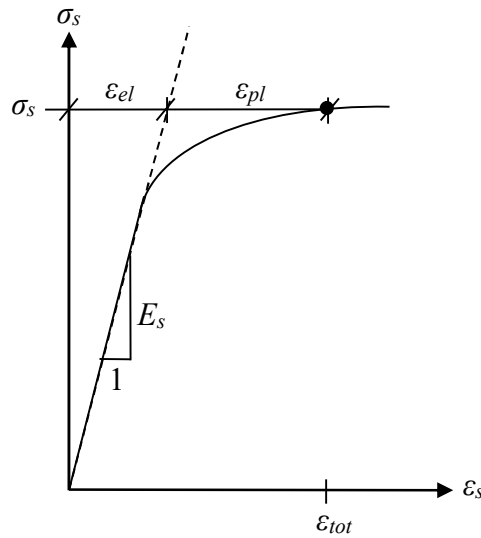
Figure 6.9   Schematic illustration of the stress strain relationship for the reinforcement.

The plastic strain for the corresponding stress is calculated for the points according to equation (6.8).

$$\varepsilon_{pl} = \varepsilon_{tot} - \varepsilon_{el} = \varepsilon_{tot} - \frac{\sigma_s}{E_s} \tag{6.8}$$

There is an option to include strain rate effects with this material model, this was however not done in this project.

6.5.3 Supports and drop weight

For the drop weight and the supports the isotropic hypoelastic material model MAT_001, called MAT_ELASTIC in LS-DYNA, was used. According to LSTC (2014b) this material model is suitable if the strains are suspected to be small which is the case for these parts. The input variables are presented in Table 6.4 together with the corresponding notations in LS-DYNA.

Table 6.4   Input parameters for the material of the supports and drop weight in LS-DYNA.

LS-DYNA notation	Parameter
RO	Mass density
E	Young's modulus
PR	Poisson's ratio

6.6 Interaction between reinforcement and concrete

In reinforced concrete, forces are transferred from the reinforcement to the concrete by shear stress acting in the contact between the concrete and reinforcement. These stresses are referred to as the bond stress. The bond between the reinforcement bars and the concrete is developed during a certain distance from a free edge or a crack, this is explained by e.g. Engström (2014). The reinforcement slides in relation to the concrete until the full bond is developed. If the stress then has reached the tensile strength of the concrete, a new crack is formed. The relative displacement that occurs between the concrete and the reinforcement is referred to as the slip. The bond-slip relation can be determined by experiments or calculated.

The interaction between concrete and reinforcement can be modelled in different ways. One common way of treating the interaction is to model the reinforcement as embedded. This means that the bond between the reinforcement and concrete is complete. In LS-DYNA a complete bond is set by defining CONSTRAINED where the SLAVE is defined as the reinforcement bars and the MASTER as the solid beam. This means that the nodes of the reinforcement bars and the concrete elements coincide and that the bars are constrained to move perfectly together with the concrete. This, though, does not simulate a fully realistic behaviour.

To approach a more realistic behaviour of the structure in an FE-model, the bond-slip relation between the reinforcement bars and the concrete can be included. The bond-slip relationship is described by defining an axial force, F, depending on the bond, τ_b, which in turn is dependent on the slip, s. The force is defined as:

$$F = \tau_b(s) \cdot \pi\phi \cdot l_{el} \tag{6.9}$$

where l_{el} is the average element length. The bond stress is described in the CEB-FIP Model Code (2012). In Figure 6.10 the relation assuming good bond conditions is illustrated.
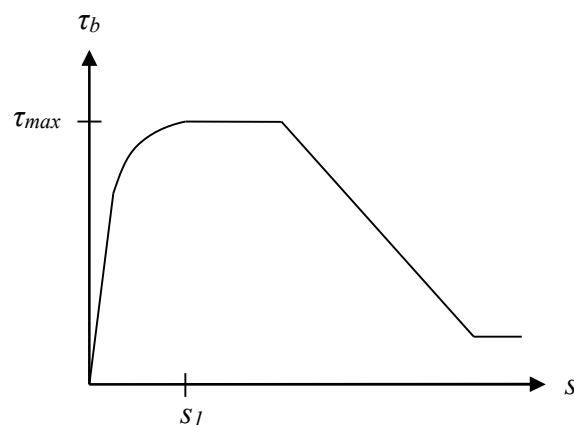
Figure 6.10   Schematic illustration of Bond-slip relation according to CEB-FIP (2012).

In this project a simplification of this relation was used based on Grassl *et al.* (2017) and Lockhart (2017). This function is also given as an example in the new version of the LS-DYNA Keyword User's Manual from LSTC (2017). The assumed bond-slip relation can be seen in Figure 6.11.
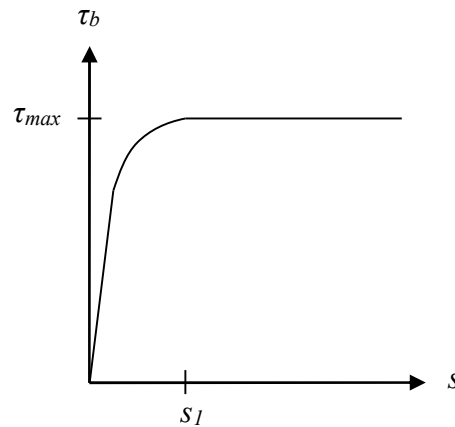
Figure 6.11   Assumed bond-slip relation in LS-DYNA.

The first part of the bond-function is adopted directly from the model code, while the second part is assumed constant, see equation (6.10). The value of the slip at which the simplified bond stress function becomes constant is defined according to CEB-FIP (2012), for good bond conditions, as in equation (6.11), and the maximum value of the bonds stress according to equation (6.12).

$$
\tau_b(s) = \begin{cases} \tau_{max} \left(\dfrac{s}{s_1} \right)^{0.4} & if \ s < s_1 \\ \tau_{max} & if \ s \geq s_1 \end{cases}
\tag{6.10}
$$

$$
s_1 = 1.0 \ mm
\tag{6.11}
$$

$$
\tau_{max} = 2.5\sqrt{f_{cm}}
\tag{6.12}
$$

Grassl *et al.* (2017) explains how this bond-slip can be modelled in LS-DYNA either by constraining the reinforcement in the concrete using bond-slip laws or using nonlinear spring elements. If the bond-slip is introduced by making the reinforcement constrained into the concrete using bond-slip functions, Lockhart (2017) states that the modelling is less complicated compared to including springs. In this case, the nodes of the reinforcement and the concrete, respectively, are constrained to move according to the bond-slip function. This is made using a built-in function in LS-DYNA. As for the case of perfect bond, CONSTRAINED is defined. But to include bond-slip, the parameter AXFOR is used to enable the user to specify the bond-slip relation of the reinforcement. In this project, bond-slip was included using this option since it was considered the simplest way to model, and the easiest method to repeat in future projects. The bond-slip relation is defined by DEFINE_FUNCTION, for the code used, see Appendix I. When AXFOR is used, the parameter CDIR must be changed from the default value to 1 to remove the constraint along the axial direction of the reinforcement and allow for a movement.

7 Validation and Improvements of Models

7.1 Introduction

Previously, tests have been conducted where actual concrete beams have been subjected to a drop-weight corresponding to the scenario modelled in this project. The tests were originally carried out and analysed by Ekström (2017). Lovén and Svavarsdóttir (2016) used some of those tests results to create models and analyse and compare results. Lozano and Makdesi (2017) carried out a new series of drop weight tests. In this chapter a brief description of the tests studied in Lovén and Svavarsdóttir (2016) are described. Time-displacement curves for the midpoint of the beam and crack patterns from these tests were used in this project. For more detailed information and deeper analyses of these tests, the reader is referred to the original studies.

Some different choices were compared and analysed to evaluate the modelling techniques in the simplified models as well as in the LS-DYNA model. The 2DOF model and the Abaqus model were then validated by comparing them to each other, to hand calculations and to some extent test results. The LS-DYNA model was validated by comparison to test results.

7.2 Reference experimental procedure and material properties

Dynamic tests were carried out on simply supported concrete beams by means of a guided fall of a weight hitting the beam. The basic geometry and support conditions of the beams that were tested can be seen in Figure 7.1.
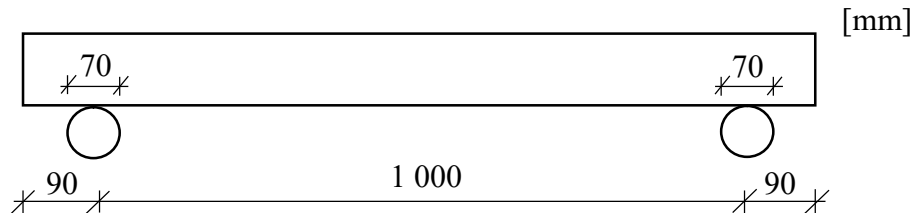
Figure 7.1   Dimensions of the beams used in experiments.

The beams were reinforced with four rebars, divided in one top and one bottom layer and the square cross sections of the beams and the reinforcement layout is shown in Figure 7.2. The dimensions of the cross section are presented in Table 7.1.
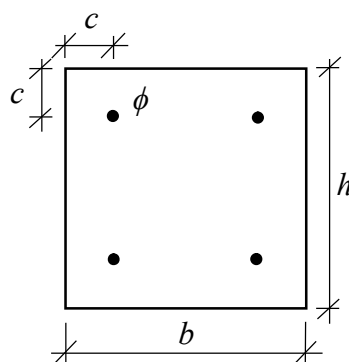
Figure 7.2   Cross section of the beam.

Table 7.1   Dimensions of the cross section.

Property	Dimension
Height, h [mm]	100
Width, b [mm]	100
Cover, c [mm]	20
Diameter, ϕ [mm]	6

The drop-weight, illustrated in Figure 7.3, is cylindrical and made of steel. There is a cavity inside the weight intended for measuring devices and the bottom of the drop-weight has a rounded surface. Since the weight is modelled as solid in LS-DYNA, the input value of the density has been modified to represent the correct mass. The dimensions and properties of the drop-weight are presented in Table 7.2. For more detailed information on the drop-weight, refer to e.g. Lovén and Svavarsdóttir (2016).
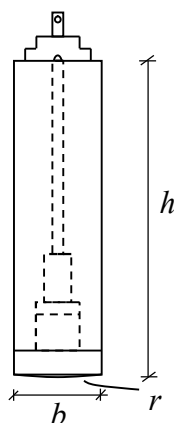
Figure 7.3   Geometry of the drop-weight, modified from Lovén and Svavarsdóttir (2016).

Table 7.2   Properties of the drop-weight, according to Lovén and Svavarsdóttir (2016).

Property	Value
Height, h [mm]	260
Width, b [mm]	80
Radius of rounded tip, r [mm]	400
Mass, m_w [g]	10 093
Young's modulus [GPa]	200

Material tests were carried out on the concrete and reinforcement. The average mechanical properties of the concrete at the day of the dynamic tests, according to Lovén and Svavarsdóttir (2016), as well as the ultimate tensile strength of the reinforcement are presented in Table 7.3. These are also the values used for validation of the models in this report. The values of Young's modulus and theoretical fracture energy for the concrete were calculated using the mean compressive strength at the day of the tests, see Appendix C for calculations.

Table 7.3　　*Mechanical properties of the concrete and reinforcement, from Lovén and Svavarsdóttir (2016).*

Parameter	Value
Mean compressive strength of concrete cylinders, f_{cm} [MPa]	45.5
Mean tensile strength of concrete cubes, f_{ctm} [MPa]	3.28
Modulus of elasticity of concrete, E_{cm} [GPa]	34.7
Fracture energy from tests of concrete, G_F [N/m]	113
Mean ultimate tensile strength of reinforcement, f_u [MPa]	665

Tensile tests were performed on the reinforcement and the results of these tests can be seen in Figure 7.4. From this, the mean ultimate strength was obtained. Mean values for the stresses and strains were calculated to obtain a curve representing the average behaviour of the reinforcement. For the input data used in the models, see Appendix A.
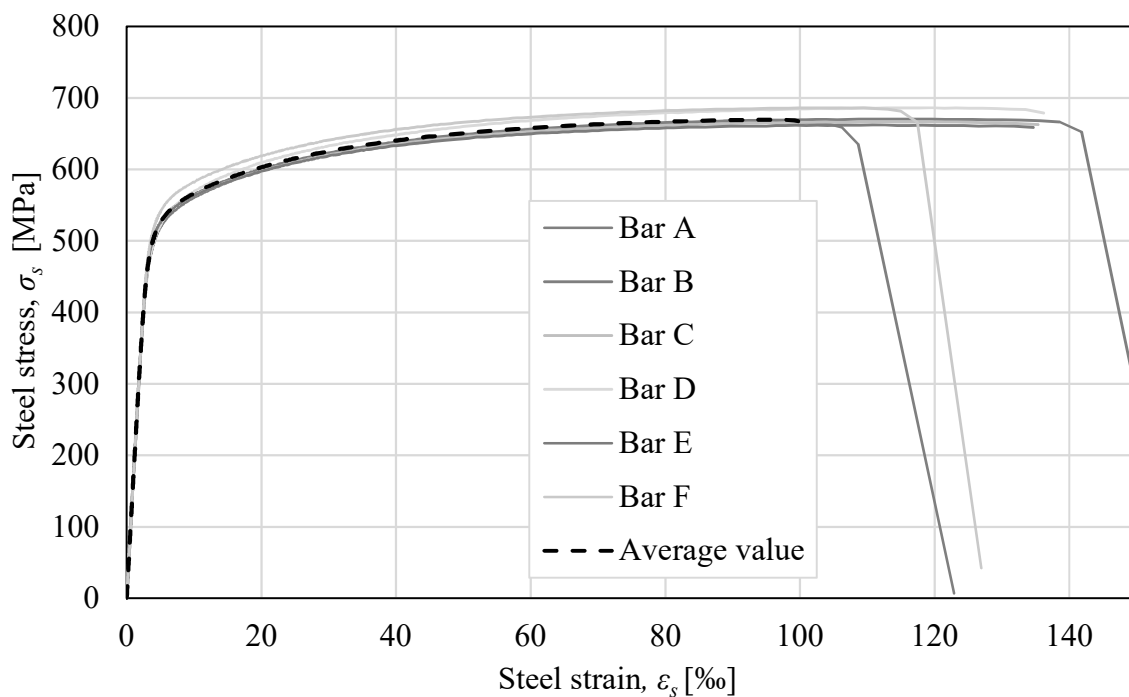
Figure 7.4　　*Result from the tensile tests of the reinforcement bars.*

Several different dynamic tests were carried out, dropping the weight from different heights. The reference test for this project was from 5.5 meters, resulting in a measured velocity of 10.35 m/s of the drop weight just before impact. There were five beams tested in the test series with a drop height of 5.5 meters. The test results from the dynamic tests showed some variation, see Figure 7.5.

Lovén and Svavarsdóttir (2016) used the beam RPC2 as a reference since it was considered representative for the results in total. In this project, RPC2 was mostly used for comparison, but it was desirable to achieve results from the models that are on the safe side. Therefore, the entire test series was sometimes used in the comparison.
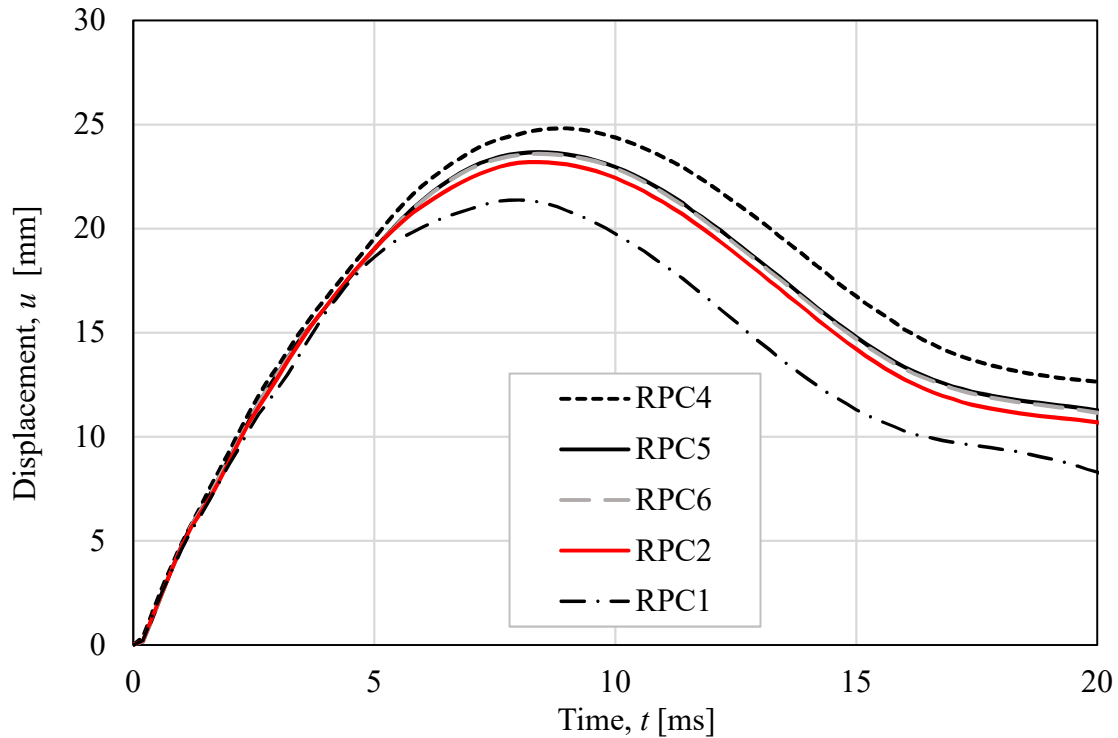
Figure 7.5   Displacement with time for the tested beams.

The cracks for two beams from the experiments are presented in Table 7.4, at the time of the maximum displacement. The beam RPC2 was previously chosen as the reference beam for the time-displacement curve. RPC5 was considered more representative concerning the crack pattern since the crack closest to the middle region in RCP2 is more inclined and has merged with the middle cracks. Therefore, these two beams were used for comparison of crack patterns in this project. The scale for the crack patterns from the tests were chosen by Lovén and Svavarsdóttir (2016) so that the red colour represents an open crack.

Table 7.4   Crack patterns at maximum displacement for two tested beams that were used as reference.

Description	Crack pattern
RPC2	
RCP5	
Principle strain [%]	0 1.4

7.3 Comparison of modelling techniques in simplified models

7.3.1 Resistance limit for the interaction in the 2DOF model

The resistance limit of the spring representing the interaction between the beam and the drop weight is chosen based on the properties of the specific beam and load case, as mentioned in Section 5.2.2. Lovén and Svavarsdóttir (2016) evaluated the choice of resistance limit with respect to velocity and concluded that a limit of 50 kN proved to give reasonable results in comparison to their test results. Lozano and Makdesi (2017) also used 50 kN. To evaluate the effects of the choice of resistance limit, the displacements with time using a limit of 20, 50, 100, 200, 500 and 1 000 kN were evaluated in this project and are presented in Figure 7.6.
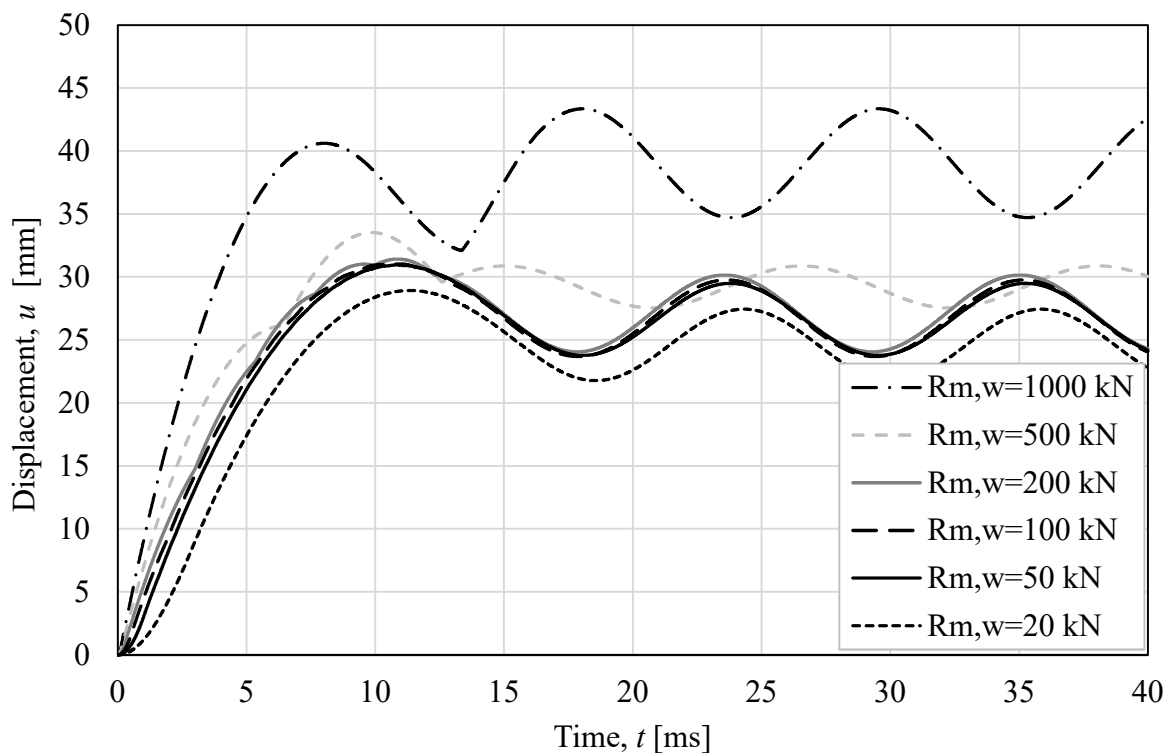
Figure 7.6   Difference in response depending on how the resistance limit of the spring representing the interaction was chosen.

It can be seen that the displacement does not differ much if a value between 50 or 100 is chosen. The shape of the response starts to differ though when a limit of 200 kN is used and when using a limit of 500 kN the resulting response is quite different. Based on this sensitivity analysis and previous experience, the resistance limit was set to 50 kN in this project as well. For the elasto-plastic spring in Abaqus, the same limit was used.

7.3.2 Implicit or explicit solution method in Abaqus

A comparison between the two solution methods in Abaqus, explained in Section 5.3.4, was made to evaluate the influence of the solution method on the displacement with time. The result can be seen in Figure 7.7. The results from the two solution methods correspond well, but since the explicit method is more efficient for this type of analysis, the explicit method was used henceforth.
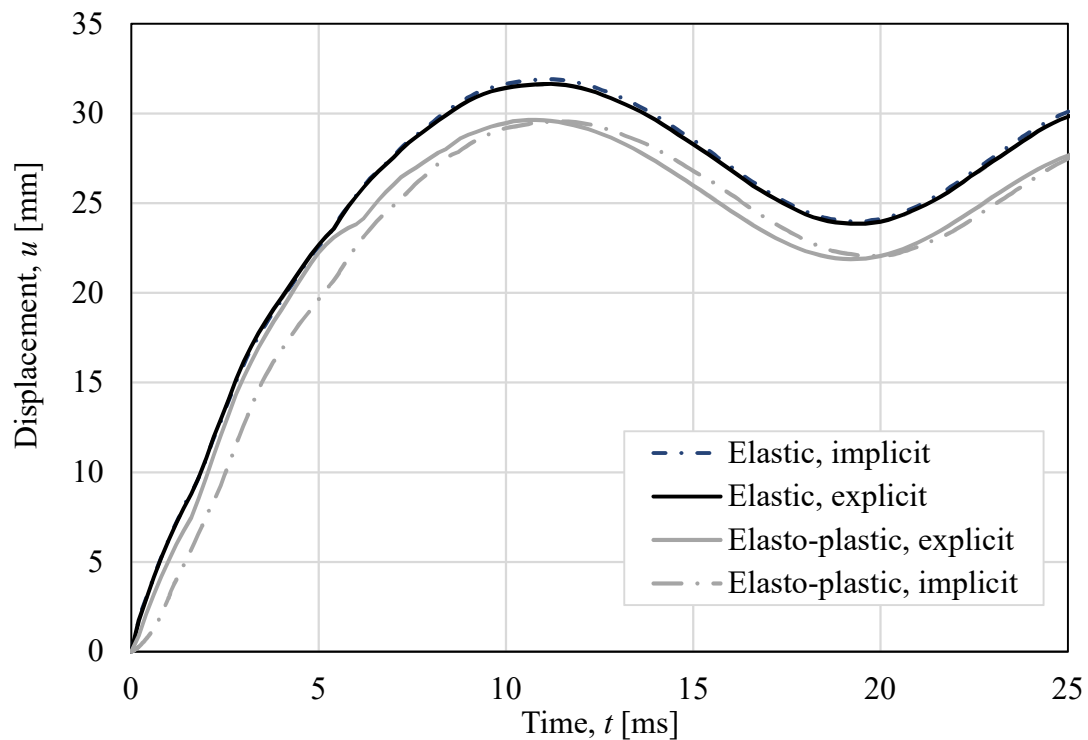
Figure 7.7   *Comparison of implicit and explicit solution method using an elastic and elasto-plastic spring in Abaqus.*

7.3.3 Structural behaviour of the spring in the Abaqus model

The elastic and elasto-plastic structural behaviour of the spring in Abaqus, mentioned in Section 5.3.1, were evaluated and are presented in Figure 7.8.
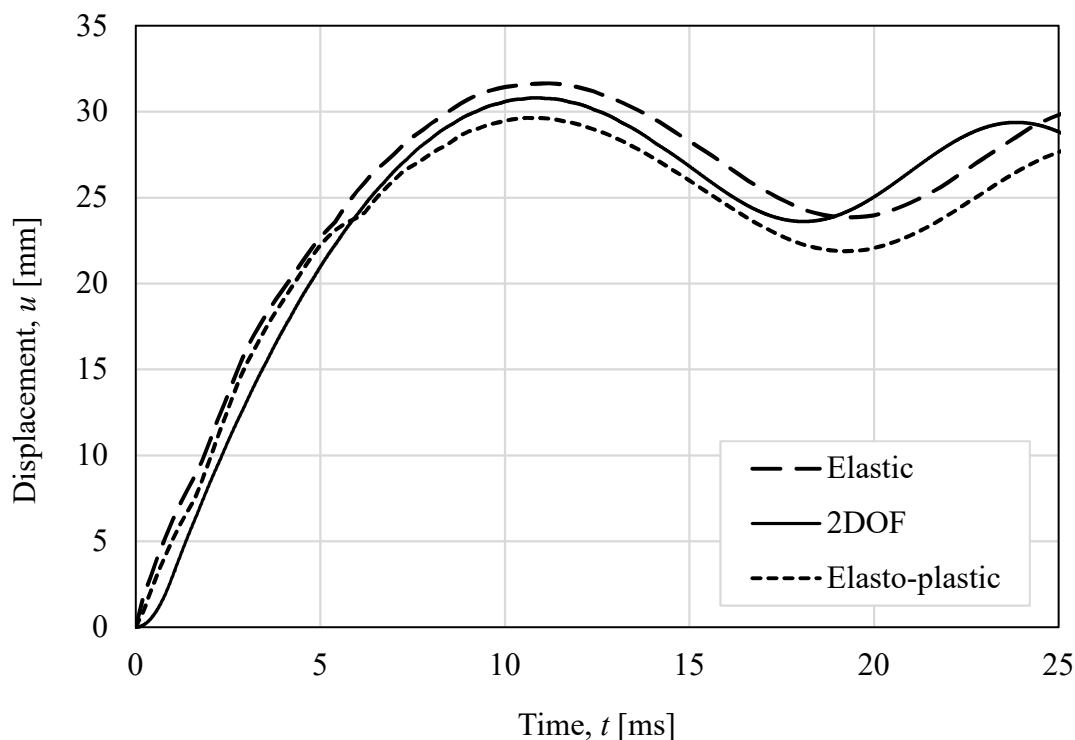
Figure 7.8   Comparison of midpoint displacement with time from the 2DOF model and from Abaqus using elastic and elasto-plastic springs.

As can be seen, the difference in results using an elasto-plastic or an elastic spring was not significant. In the 2DOF model, on the other hand, the resistance limit of the spring had a large influence. This can be seen in Figure 7.6 where an elasto-plastic spring with a very high resistance limit gave larger displacements. An elasto-plastic spring with a high resistance limit approaches the behaviour of an elastic spring. The difference in influence from the structural behaviour of the spring in the different models may be explained by the different ways of modelling the beam. In the 2D model in Abaqus, the wave propagation effect, explained in Section 5.2.3, was captured. In the 2DOF model in 1D it was not captured, and an elasto-plastic spring was needed to simulate the more realistic behaviour. Therefore, elasto-plastic behaviour of the spring was not needed in Abaqus and an elastic structural behaviour was sufficient.

7.4 Validation of simplified models

The time-displacement curves for the 2DOF model and the Abaqus model, compared in Figure 7.9, are similar. Regarding the maximum displacement, there is a difference of 0.7 millimetres, which was considered accurate enough considering the different levels of detail in the models.
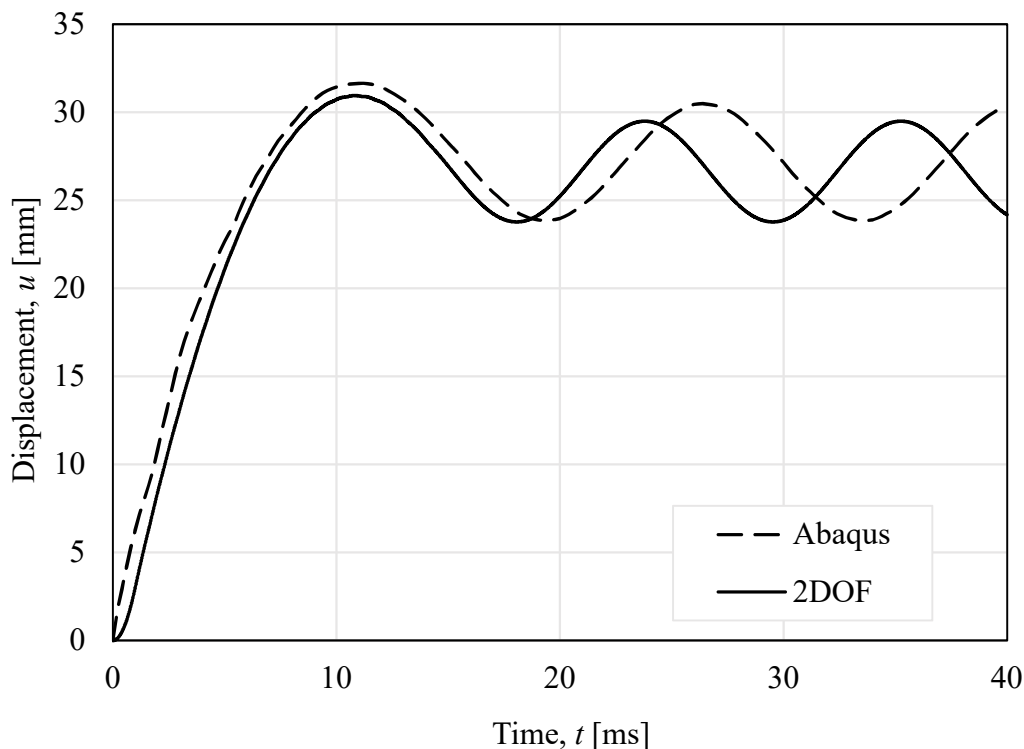
Figure 7.9   Displacement of the midpoint of the beam comparing 2DOF and Abaqus.

The results from the simplified models are compared to hand calculations with respect to transferred energy in the system and maximum displacement. The energy in the system was calculated from the value of the maximum displacement from the two models using equations (3.8) and (4.8). In the hand calculations, a plastic impact was assumed, and the energy was calculated as the external work described by equation (3.16). From the external work, the maximum displacement was obtained. The equations used are also presented in Appendix F. From the maximum values, the quota η_u for the displacements and the ratio η_{W_y} for the energy were calculated as described in equations (7.1) and (7.2). The results are presented in Table 7.5.

$$\eta_u = \frac{u_i}{u_{2DOF}} \qquad\qquad i = Abaqus, Hand\ calculations \qquad\qquad (7.1)$$

$$\eta_{W_y} = \frac{W_{y_i}}{W_{y_{2DOF}}} \qquad\qquad i = Abaqus, Hand\ calculations \qquad\qquad (7.2)$$

Table 7.5   Comparison of transferred energy into the system calculated using different methods.

Method	Maximum displacement [mm]	η_u [-]	Energy [J]	η_{W_y} [-]
2DOF	30.9	1.00	298.3	1.00
Abaqus	31.6	1.02	305.6	1.02
Hand calculations	31.1	1.00	299.8	1.00

From the results, it can be seen that the assumption of a plastic impact and the elasto-plastic response with a resistance limit of 50 kN in the 2DOF model was a good approximation to capture a more realistic response. In the Abaqus model, the behaviour of the system was captured well with the more simple, elastic response. As previously mentioned, one possible explanation to why an elasto-plastic modification was needed in the 2DOF model and not in Abaqus can be that the wave propagation effect discussed in Section 5.2.3 is automatically captured in Abaqus.

The results from the 2DOF model and the Abaqus model were compared to the test results regarding the time-displacement curves, see Figure 7.10. The simplified models were only compared to the test results with respect to global behaviour since the models are not detailed enough to describe e.g. crack patterns.
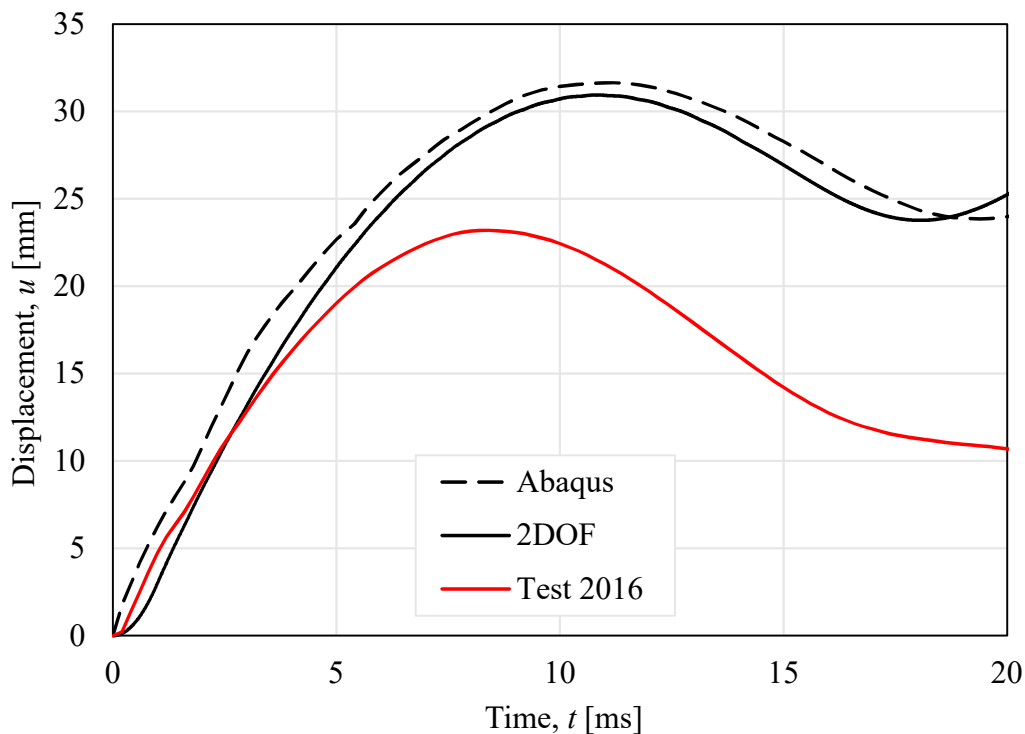
Figure 7.10   Time-displacement curves from the 2DOF model, Abaqus model and test results.

The models are less stiff than the real beam and one contributing factor is that the simplified models do not take strain rate effects into account for either the reinforcement or the concrete. Another contributing explanation may be that static tests, performed by Lozano and

Makdesi (2017) and by Jönsson and Stenseke (2018), showed that the capacity of the beams was higher than predicted (reason unknown) with hand calculations.

No adjustments of the models were made to make them fit better to the test results. It was investigated, though, how much the capacity would need to be modified in the 2DOF to obtain results close to the test results. If the yield strength of the reinforcement were to be increased, an increase of 45 % would be needed to reduce the displacement to that obtained in the test, see Figure 7.11.
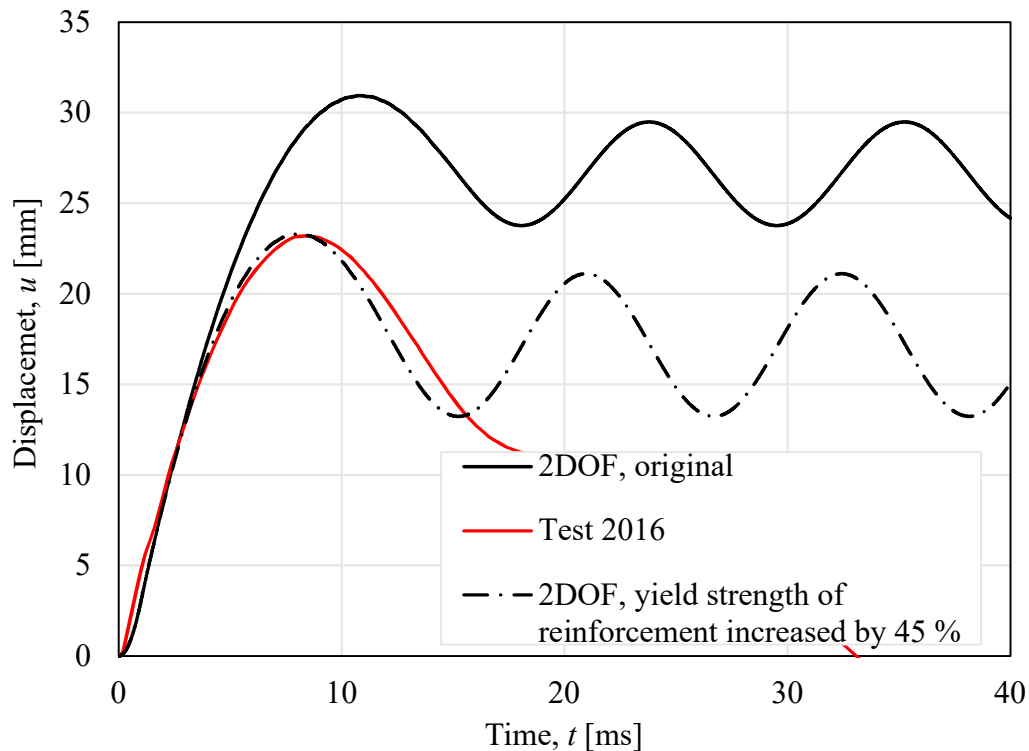
Figure 7.11   An attempt to modify the 2DOF model to obtain results closer to the test results.

Another attempt was made to get closer to the test results by modelling the interaction between the parts in a more sophisticated way using contact mechanics. See Appendix D for an evaluation of this more thorough method of modelling the contact. This evaluation, though, showed that there is a neglectable difference between the simplified way and the more detailed way since the stiffness of the interaction is still so much larger than the stiffness of the beam. Since the difference in results was neglectable, and the fact that the stiffness has been modelled in the simplified way previous years, the stiffness based on contact mechanics has not been used in this project.

7.5 Comparison of different modelling choices in LS-DYNA

7.5.1 Element type for the reinforcement

The different element types for the reinforcement, described in Section 6.3, were evaluated. The time-displacement curves for the analyses showed that very similar results were obtained using beam elements with 1 x 1 integration point and truss elements. The displacements when using beam elements with 2 x 2 integration points were smaller, see Figure 7.12. There were some convergence issues for the model with truss elements and 1x1 beam elements where the analyses terminated after approximately 15 ms. However, the time of main interest is when the maximum displacement is reached, which happens after approximately 8 ms. Hence, this means that the problem with convergence later is not of major concern.
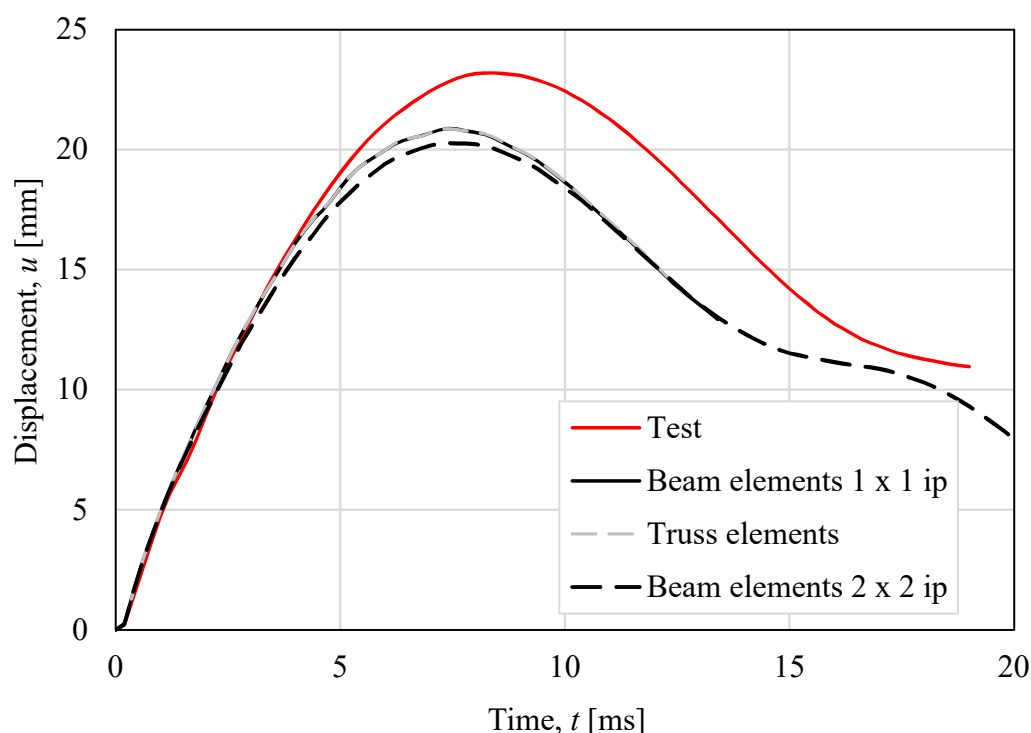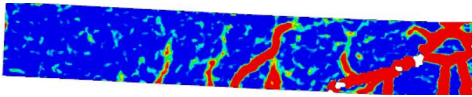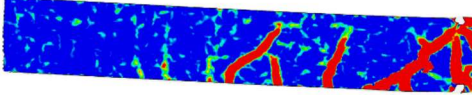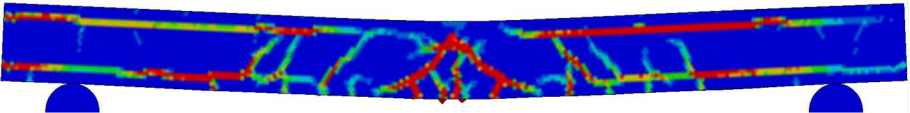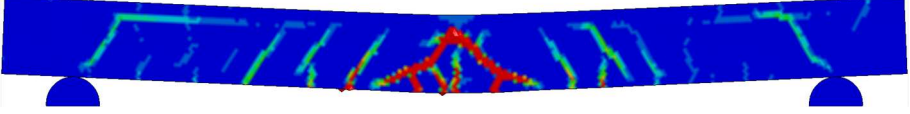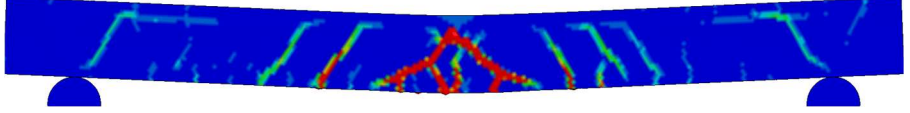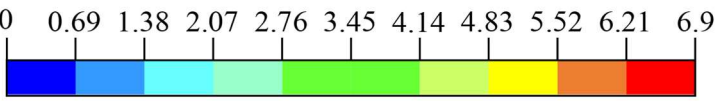
Figure 7.12   Comparison between beam elements with 1 x 1 integration points, 2 x 2 integration point and truss elements.

The crack patterns from the LS-DYNA model were compared to test results. In the plots from the LS-DYNA model, the strain representing a fully open crack, i.e. no tensile force can be transferred over it, is represented with red colour. That strain value was calculated, in Appendix C, using an equivalent element length according to Lozano and Makdesi (2017). The strain from the tests and LS-DYNA, though, are not directly comparable since the strain presented refers to different lengths.

The results showed that more realistic crack patterns were achieved when using truss elements and 1 x 1 beam elements, see Table 7.6. Using beam elements with 2 x 2 integration points, unrealistic horizontal strains along the reinforcement occurred. The fact that truss elements and beam elements with 1 x 1 integration points resulted in more realistic crack patterns than beam elements with 2 x 2 integration points was considered more important

than the convergence issues in a later stage even if 2 x 2 integration points would have been the most realistic choice for modelling the reinforcement.

Table 7.6 *Crack patterns for test results and models with different element types for the reinforcement at the time for maximum displacement.*

Description	Crack pattern
Test (RPC2)	
Test (RCP5)	
Principle strain [%]	0 1.4
Beam elements (2 x 2 ip)	
Beam elements (1 x 1 ip)	
Truss elements	
Principle strain [%]	0 0.69 1.38 2.07 2.76 3.45 4.14 4.83 5.52 6.21 6.9

7.5.2 Interaction between concrete and reinforcement

A comparison was made between a model with embedded reinforcement and a model with a bond-slip function included. The displacements when bond-slip was included were noticeable larger and closer to the test results, see Figure 7.13.
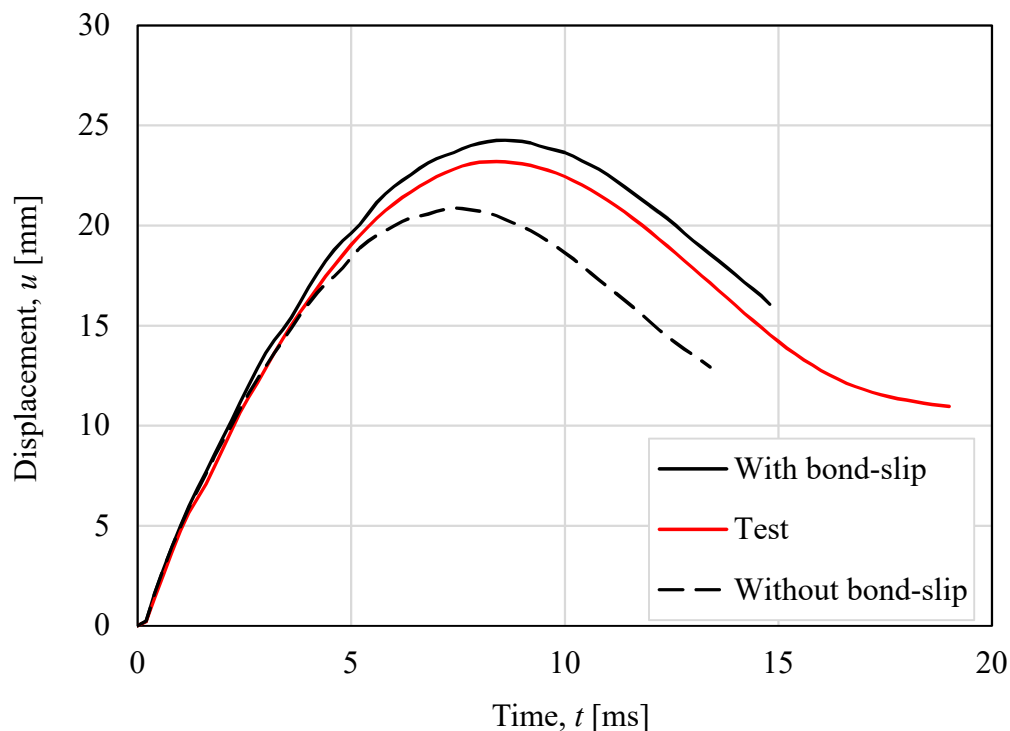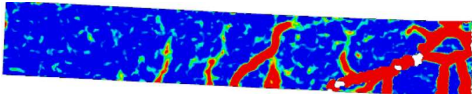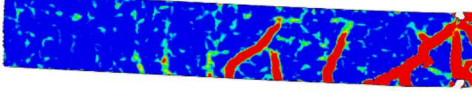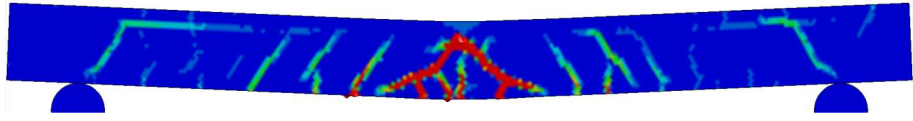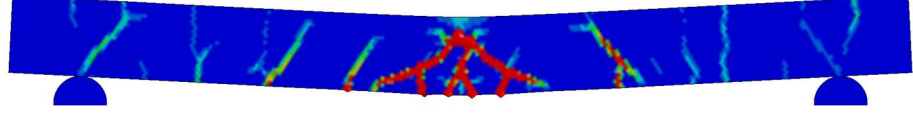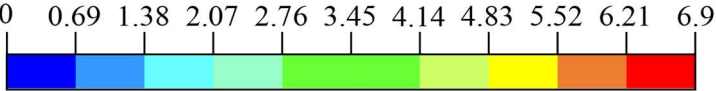
Figure 7.13   Time-displacement curve with and without bond-slip, using beam elements with 1 x 1 integration point for the reinforcement.

The crack patterns for the models without and with bond-slip are presented together with the crack patterns from the test in Table 7.7. It can be seen that there are some horizontal strains along the reinforcement for the model without bond-slip but that they are less prominent in the model including bond-slip. As expected, the crack pattern has changed somewhat when the bond-slip is introduced, and the cracks are distributed with a larger crack distance.

Table 7.7   *Crack patterns from the test and LS-DYNA models without and with bond-slip at the time for maximum displacement. The reinforcement is modelled with beam elements with 1 x 1 integration point.*

Description	Crack pattern
Test (RPC2)	
Test (RCP5)	
Principle strain [%]	0 1.4
Without bond-slip	
With bond-slip	
Principle strain [%]	0 0.69 1.38 2.07 2.76 3.45 4.14 4.83 5.52 6.21 6.9

Based on that the horizontal strains were less prominent for the beam elements using 1 x 1 integration points there was an idea that the horizontal strains for 2 x 2 beam elements, discussed in Section 7.5.1, would be reduced when the full constraint between the reinforcement and the concrete was released. Therefore, different element types for the reinforcement were compared when bond-slip was included.

In Figure 7.14, the displacements for beam elements with 1 x 1 and 2 x 2 integration point and truss elements are compared when bond-slip is included. The displacements for 1 x 1 integration points and truss elements were larger than and closer to the test results. Furthermore, the crack pattern is shown in Table 7.8, and it were concluded that the horizontal strains for beam elements with 2 x 2 integration points remained. It can also be seen that the crack patterns for beam elements with 1 x 1 integration point and for truss elements are very similar.
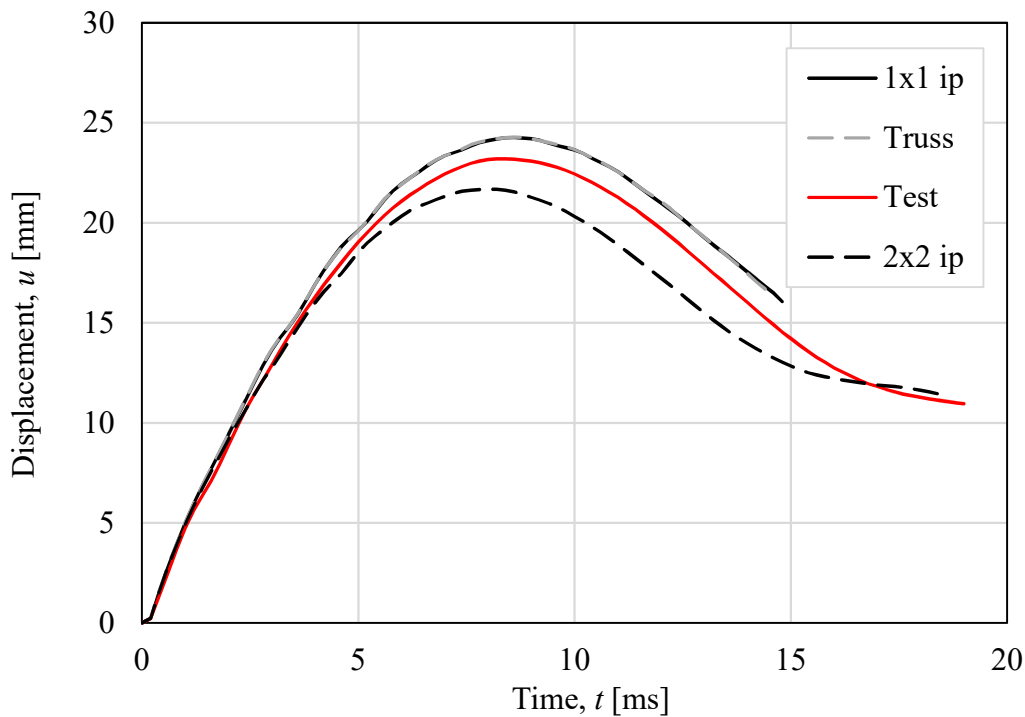
Figure 7.14   Displacements for different element types for the reinforcement when bond-slip interaction is included in the modelling.

Table 7.8   Crack patterns from models with different element types for the reinforcement when bond-slip is included.

Description	Crack pattern
Beam elements (2 x 2 ip)	
Beam elements (1 x 1 ip)	
Truss elements	
Principle strain [%]	0 0.69 1.38 2.07 2.76 3.45 4.14 4.83 5.52 6.21 6.9

When beam elements with 1 x 1 integration points or truss elements were used, the influence of bond-slip on the displacement was larger than for beam elements with 2 x 2 integration points. For truss elements and beam elements with 1 x 1 integration points, the increase in displacement when bond-slip was included was 16 %. For beam elements with 2 x 2 integration points the difference was 7 %. Based on that it was considered desirable to achieve larger displacements in the model compared to the tests and that the horizontal strains

remained for the beam elements with 2 x 2 integration points, bond-slip was included in further analyses and beam elements with 2 x 2 integration points were excluded.

The way of modelling the interaction, using the built-in function CONSTRAINT, the nodes of the reinforcement is probably linked to the closest nodes in the concrete. This leads to that the interaction is spread out over the element size. In this case, when the diameter of the reinforcement and the element size is almost the same, this can be favourable. However, if the element size would be larger than the diameter of the reinforcement, this is something that may be needed to be considered.

7.5.3 Damage formulation for the concrete

A comparison was made between linear and bilinear damage formulation for the concrete in tension. In Figure 7.15 it can be seen that the difference in displacement for the two models was small.
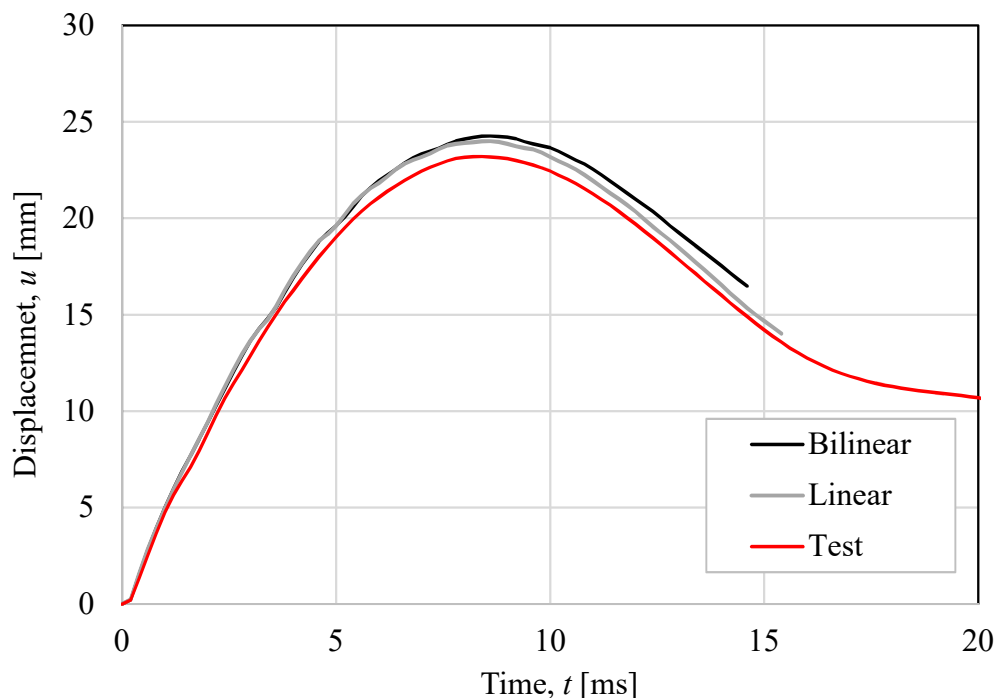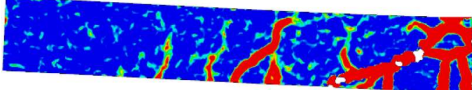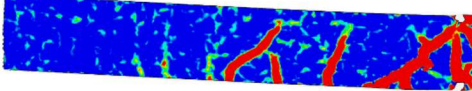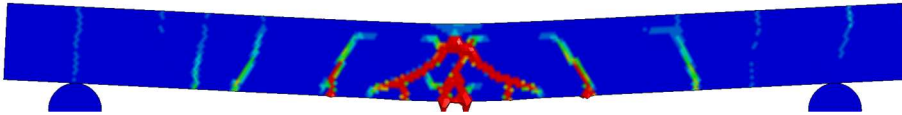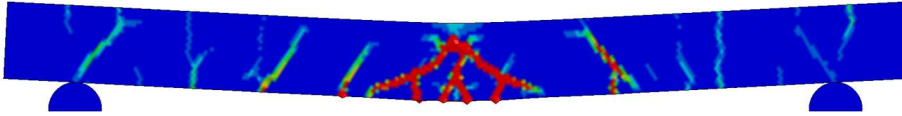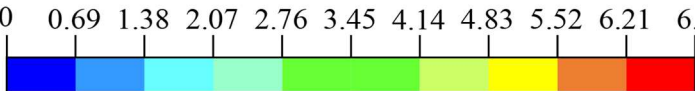
Figure 7.15   *Displacements for the models with linear and bilinear damage formulations for concrete in tension. The reinforcement is modelled with beam elements with 1 x 1 integration point.*

In Table 7.9, the crack patterns for the model with linear and bilinear damage formulations for concrete in tension are presented. There is a small difference, but it is not significant. Therefore, the bilinear response was considered to be the best model since it is a better approximation of the real behaviour.

Table 7.9   *Crack patterns for the models with linear and bilinear damage formulations for concrete in tension. The reinforcement is modelled with beam elements with 1 x 1 integration point.*

Description	Crack pattern
Test (RPC2)	
Test (RCP5)	
Principle strain [%]	0 1.4
Linear damage formulation	
Bilinear damage formulation	
Principle strain [%]	0 0.69 1.38 2.07 2.76 3.45 4.14 4.83 5.52 6.21 6.9

7.5.4 Modelling of stress-strain relation for the reinforcement

The two ways to model the structural behaviour of the reinforcement that were studied is the bilinear and a multilinear behaviour, see Figure 7.16. The bilinear curve is a very rough estimation of the real behaviour while the multilinear curve captures the behaviour of the reinforcement more realistically.
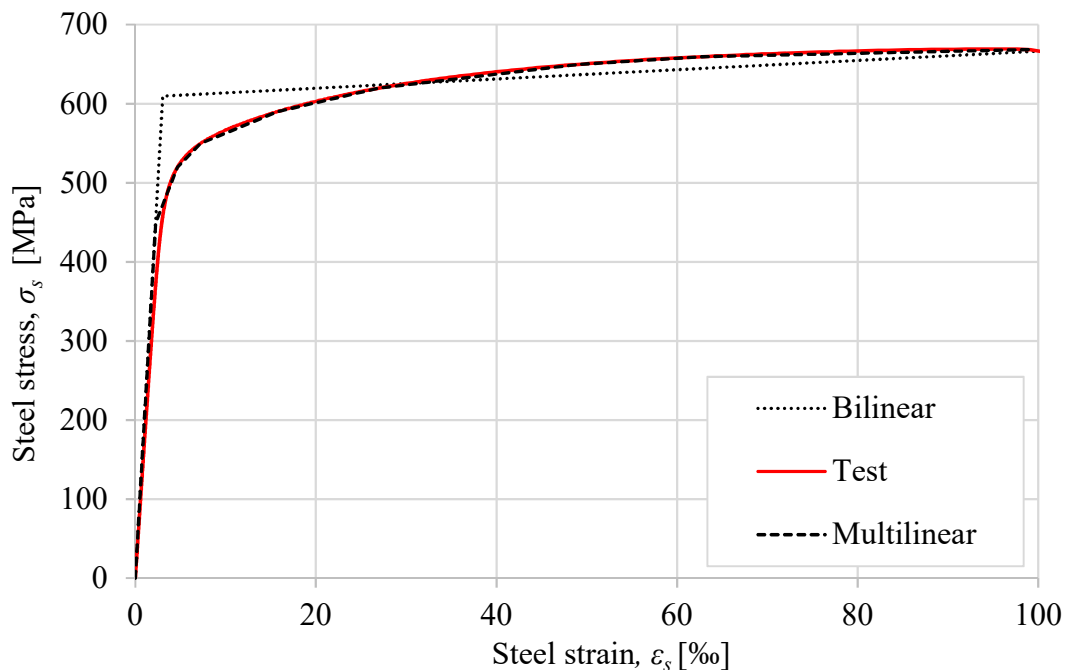
Figure 7.16   *The mean value from tests of the reinforcement in comparison with the bilinear and multi-linear behaviour modelled in LS-DYNA.*

Since the experimental stress-strain relation does not show a distinct yield behaviour, and there is no clear point where the nonlinear part of the curve begins, the multilinear curve is designed to fit the curve from the tests and not only starting from the yield plateau.

It was concluded when running analyses that the truss elements and the multilinear behaviour of the reinforcement were not compatible in LS-DYNA. Since the results from truss elements and beam elements with 1 x 1 integration point have proved to be similar, beam elements with 1 x 1 integration points are used in all further analyses made in this thesis.

The displacements for the models with multilinear and bilinear stress-strain relation are compared in Figure 7.17. The model with bilinear behaviour can absorb more energy since the area under the stress-strain graph in is also larger. This is confirmed by the somewhat smaller displacements for the model with bilinear behaviour.
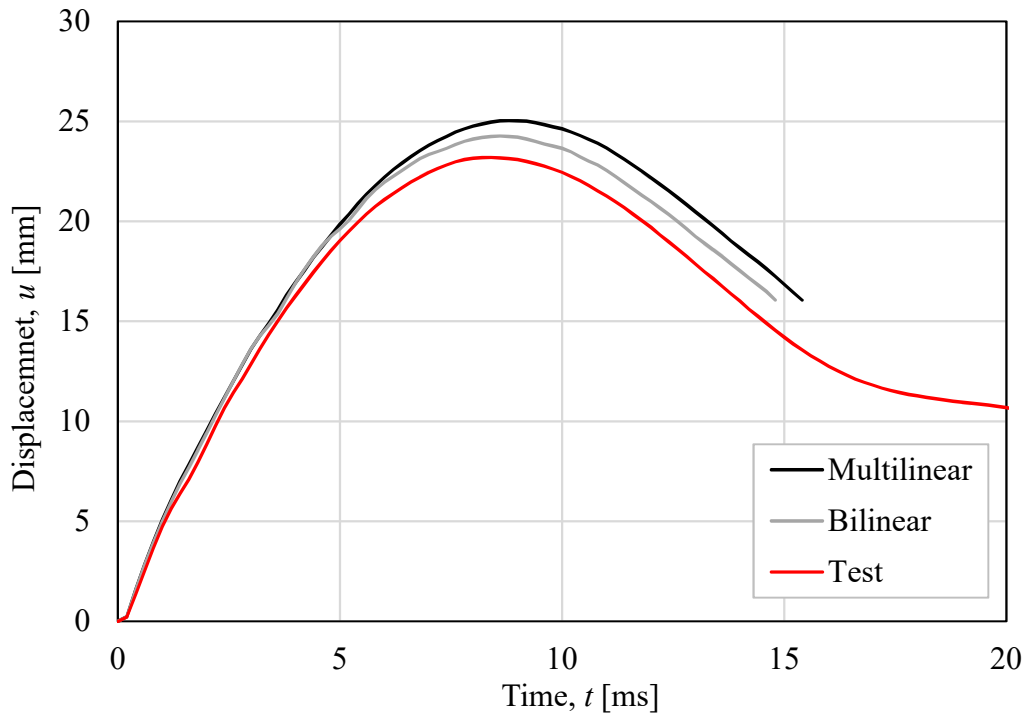
Figure 7.17   Displacements for models with multilinear and bilinear behaviour of the reinforcement.

The multilinear behaviour is closer to reality than the bilinear and gave results that are more on the safe side. The crack patterns from the different models showed to be very similar. Therefore, the model with multilinear behaviour were used in all further analyses.

7.6 Validation of the final LS-DYNA model

From the comparisons made for different modelling choices, a final version of the model, referred to as the standard model, was obtained. The modelling choices for this model are presented in Table 7.10.

Table 7.10   Conclusions from comparison of modelling choices.

Modelling parameter	Chosen method
Element type for the reinforcement	Beam elements, 1x1 integration point
Interaction between concrete and reinforcement	Bond-slip included
Damage formulation for concrete in tension	Bilinear
Structural behaviour of the reinforcement	Multilinear

The displacements for the final model is compared to the beams in the test series, see Figure 7.18. The results from the final model are just above the weakest test beam, which is deemed to be a satisfactory result since the model was close to reality while still on the safe side. No strain rate effects were considered, but the beam still showed a stiffness that corresponds well to the reality. This may be explained by volumetric locking effects in the model when tetrahedral elements are used. Volumetric locking effects can be caused by the shape of the tetrahedral elements and the irregular pattern they create in the beam. This inhibits the movements that would occur in more regular shaped elements.
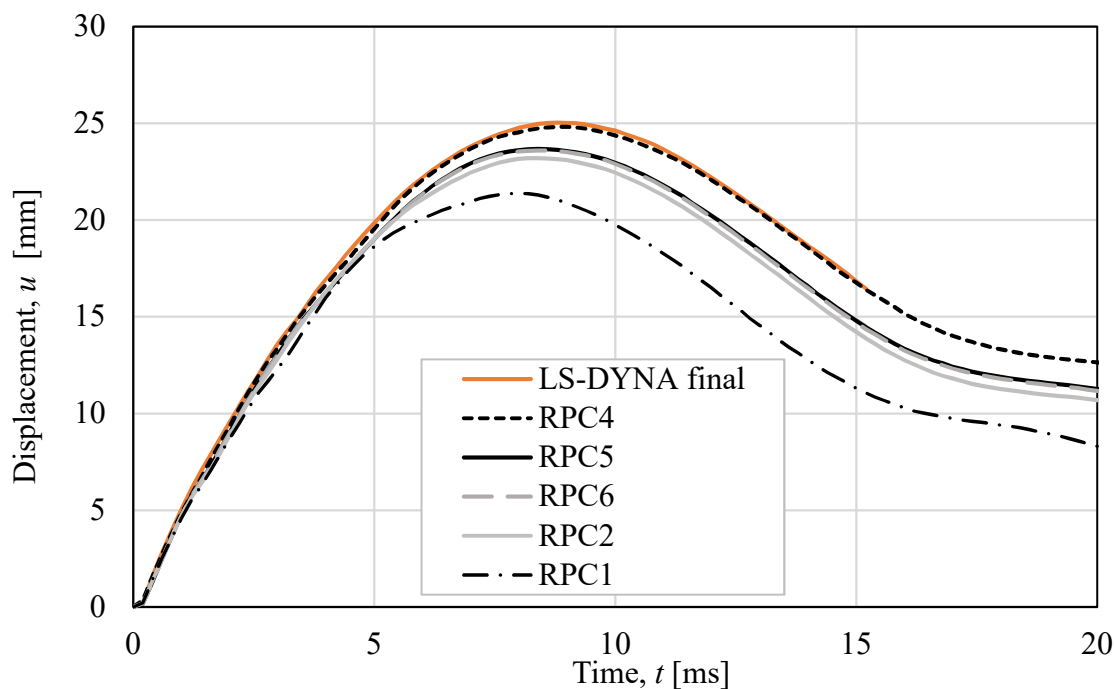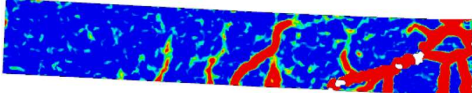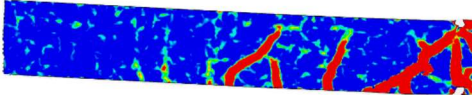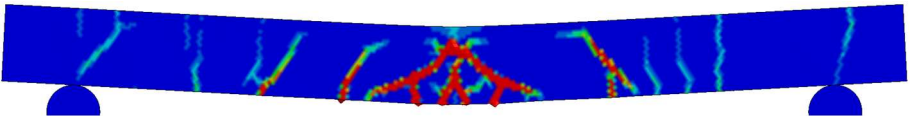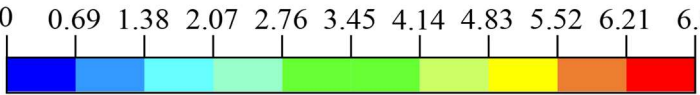
Figure 7.18   Comparison of the standard LS-DYNA model and the tested beams.

The crack pattern for the final model is compared to the test results, see Table 7.11, and the overall expression of the crack patterns corresponds well. The strain pattern in LS-DYNA is not symmetric which is realistic since the real material of the beam is not totally homogenous. In LS-DYNA an asymmetric element mesh may be an explanation for these unsymmetrical crack pattern. The middle part of the LS-DYNA beam is more similar to RCP5, but as mentioned in Section 7.2, the crack closest to the middle region of RCP2 is more inclined and has probably merged with the middle cracks.

Table 7.11   Crack patterns for the final LS-DYNA model compared to the tests.

Description	Crack pattern
Test (RPC2)	
Test (RCP5)	
Principle strain [%]	
LS-DYNA final	
Principle strain [%]	

7.7 Summary of results from the final models

The results from the final, now considered standard, models from 2DOF, Abaqus and LS-DYNA, can be seen in Figure 7.19. The settings used in these models were used as a basis for the parametric studies in Chapter 8.
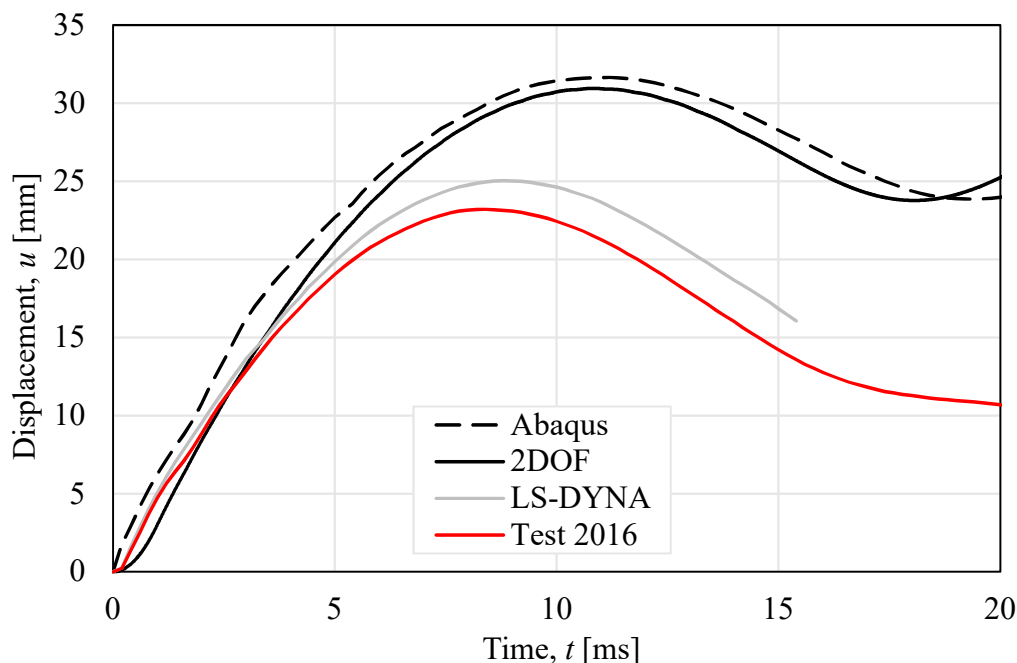
Figure 7.19   Time-displacement curves for the test and final models 2DOF, Abaqus and LS-DYNA.

The shapes of the time-displacement curves are different when comparing the 2DOF and Abaqus results to the test results and LS-DYNA. In the test results and LS-DYNA, the displacement oscillates around a descending branch, while in the results from the simplified models it oscillates around a constant value equal to the plastic deformation. This can be explained with how the support conditions were modelled in the simplified models compared to the actual conditions in the test. In the simplified models, the beam was prevented from lifting from the supports, while in reality it lifted from the supports when the beam rebounded after reaching the maximum displacement. In LS-DYNA the support conditions were modelled realistically enough to capture this behaviour. Since the maximum displacement and not the plastic displacement is the main interest in this study, it is of minor importance to extract the relative displacement for the LS-DYNA model.

8 Adaption to New Test Series and Parametric Study

8.1 Introduction

Having validated the different models, they were adapted to simulate new tests carried out by Jönsson and Stenseke (2018). In these tests, new beams were casted with new reinforcement, which means that some material parameters for concrete and reinforcement were modified. The adaption to the new tests was done to enable for future studies to continue the work.

A variation of load, geometry and reinforcement parameters was then studied to investigate how sensitive the different models are to certain parameters. In LS-DYNA the mass of the drop weight, the drop height and the amount of reinforcement were varied. In the simplified model these parameters as well as the height, width and length of the beam were varied.

8.2 Adaption of models to new test results and future studies

In the new tests, the radius of the rounded bottom surface of the drop weight was decreased from 400 to 200 mm. Since new reinforcement was used and new concrete was mixed and casted, the properties of the concrete and reinforcement was different compared to previous years. The new material properties of the reinforcement were adopted in this project to enable for future studies using the same reinforcement. Several bars were tested, and the average material behaviour of the reinforcement is shown in Figure 8.1.
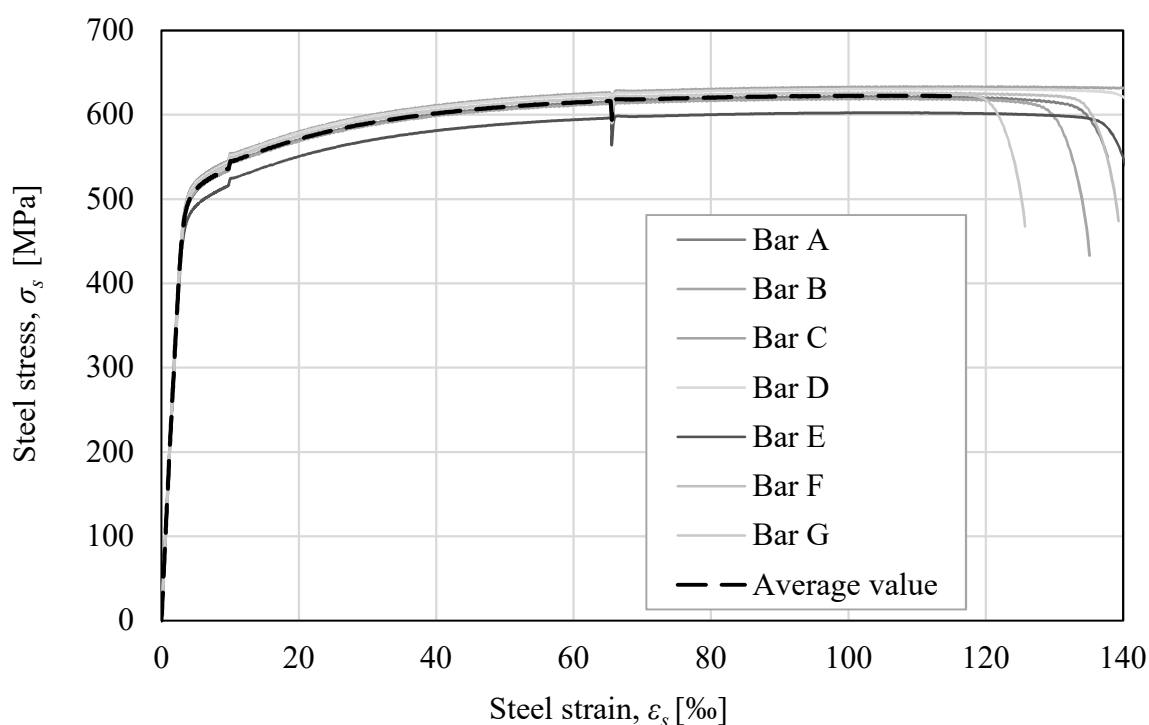
Figure 8.1   Structural behaviour of the tested reinforcement bars and average value.

The measured properties of the concrete were however not used since the properties of the concrete varies slightly from each batch. Instead, the target values for the concrete when casting the new concrete were used. The properties are presented in Table 8.1.

Table 8.1   *Target values for the material properties of concrete used in Jönsson and Stenseke (2018).*

Parameter	Value
Compressive mean strength, f_{cm} [MPa]	36
Tensile mean strength, f_{ctm} [MPa]	2.8
Young's modulus, E_{cm} [GPa]	32.0

In the 2DOF model, the ultimate strength of the reinforcement was used as the limit in the elasto-plastic curve. The ultimate strength was chosen instead of the yield strength since static tests performed by Jönsson and Stenseke (2018) showed that the static capacity of the beams was higher than expected. Furthermore, this limit was used when calculating the input data for the Abaqus model. In the LS-DYNA model, the structural behaviour of the reinforcement was modelled as multilinear and adopted to the real behaviour. The elasto-platic behaviour as well as the multilinear curve used in LS-DYNA are shown in Figure 8.2 together with the average relation of the stress-strain curve for the reinforcement. Based on this new data, all the needed parameters for the models were calculated, see Appendix C. All the input data for the different models are presented in Appendix A.
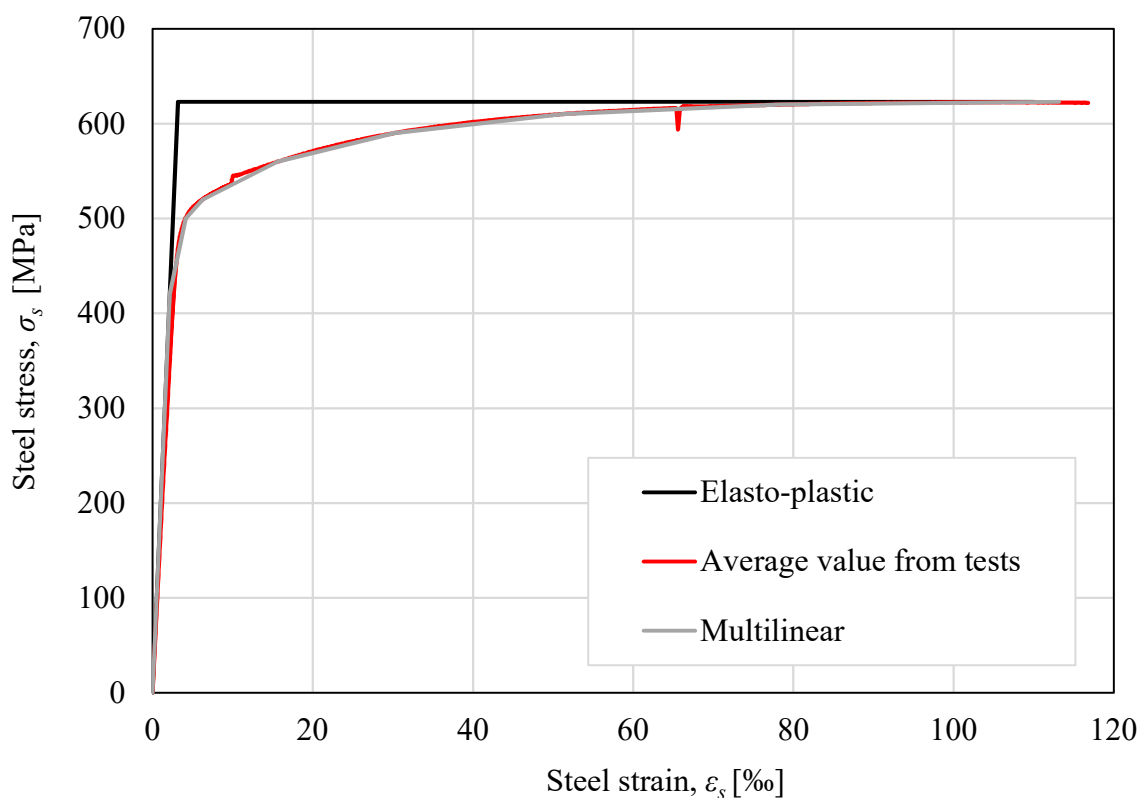
Figure 8.2   *Structural behaviour of the reinforcement from tests and in the different models.*

8.3 Parametric studies in 2DOF and Abaqus

8.3.1 Studied cases

In the parametric study, different load cases were created combining different masses and drop heights of the drop weight. It was of interest to see how the response of the models was affected by different combinations of the mass and drop height resulting in the same kinetic energy before impact. In Table 8.2, the different load cases that were studied are presented. The darker grey boxes represent twice the kinetic energy of the drop weight just before impact compared to the lighter grey boxes. All load cases were studied for nine different beams with properties presented in Table 8.3.

Table 8.2   Load cases studied in the 2DOF and Abaqus models combining mass and drop height of the drop weight.

		Drop height of the drop weight h [m]					
		1.25	2.5	5	10	20	40
Mass of drop weight m [kg]	2.5					E	J
	5				D	I	
	10			C	H		
	20		B	G			
	40	A	F				

Table 8.3   Properties of the beams studied in the parametric studies.

Beam	Width, b [m]		Height, h [m]		Length, L [m]		Reinforcement			
	0.1	0.2	0.1	0.2	1.0	2.0	$2\phi5$	$2\phi6$	$2\phi8$	$4\phi6$
1	●		●		●		●			
2	●		●		●			●		
3	●		●		●				●	
4		●	●		●			●		
5	●			●	●			●		
6	●		●			●	●			
7	●		●			●		●		
8	●		●			●			●	
9	●		●			●				●

To change the mass of the drop weight in Abaqus and the 2DOF model for the different load cases in the parametric study, only the point mass was altered. This corresponds to that the density of the drop weight would be modified, while in practise it is more reasonable to modify the height of the drop weight. When the height is changed, the stiffness is as well. However, since the study in Appendix D showed that a change of the stiffness of the interaction between the weight and the beam in this range does not influence the response of the beam significantly, the stiffness is kept the same when the mass is altered.

8.3.2 Complete results for one selected beam

The time-displacement curves from all the load cases for Beam 2 can be seen in Figure 8.3. Comparing 2DOF and Abaqus, the overall look of the curves is similar. In Appendix F, Section F.2, the results can be found for all beams and the appearance have the same correspondence.
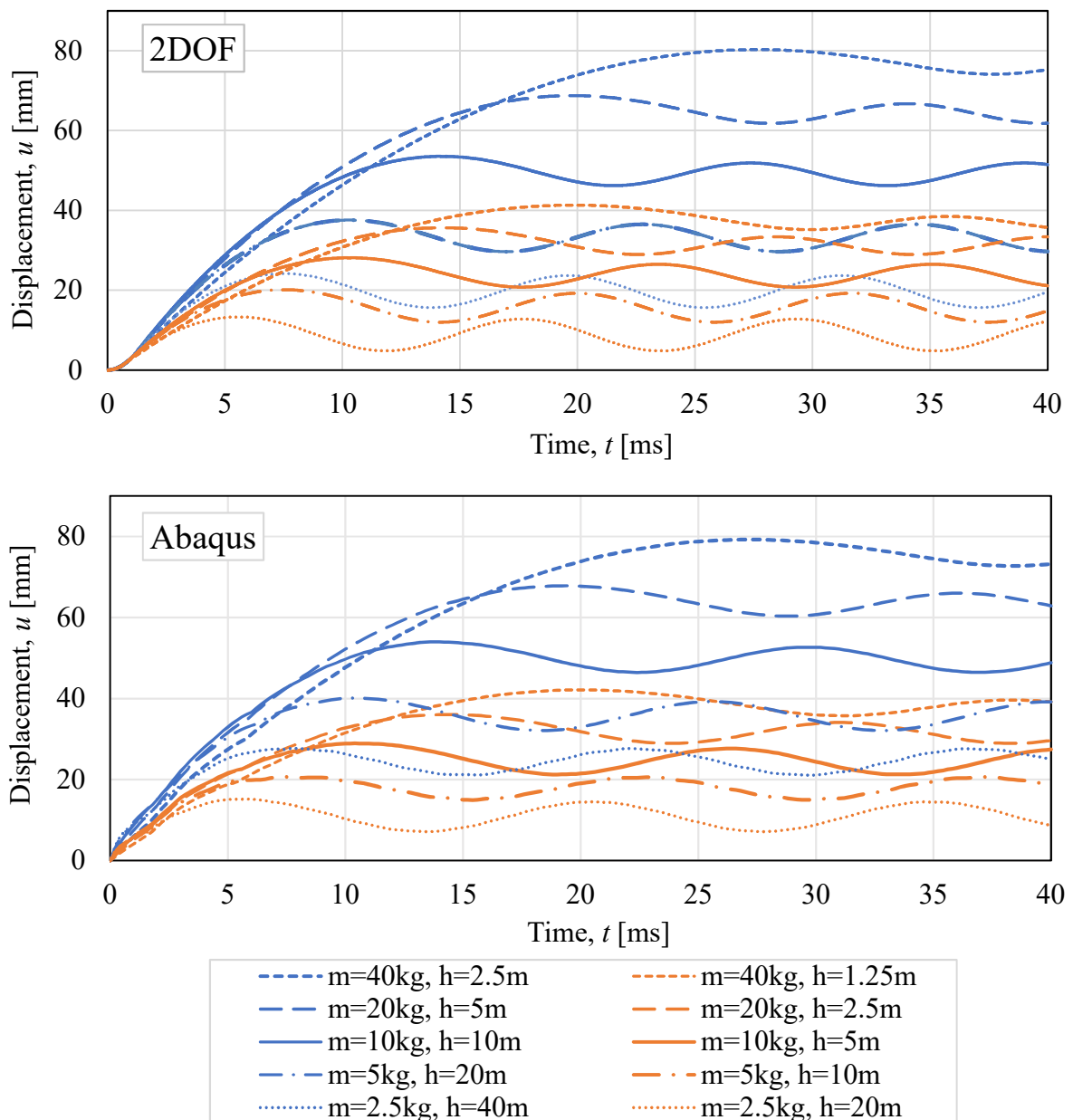
Figure 8.3   Time-displacement relation for all load cases for Beam 2. The upper graph is from the 2DOF model and the lower one from the Abaqus model.

It can be seen that a larger mass of the drop weight, m_w, gives larger displacements in both 2DOF and Abaqus. This may be related to the expression for the external work performed on the system in a plastic impact, which is calculated as:

$$W_y = \frac{m_w}{m_w + m_b} E_{k,0} \qquad (8.1)$$

To evaluate the results more thoroughly, the results from Abaqus and hand calculations were compared to the results from the 2DOF model with regard to maximum displacement and transferred energy calculated as described in Appendix F. From the maximum values, the ratio for the displacements, η_u , and the ratio for the energy, η_{W_y} , were calculated as described in equations (7.1) and (7.2). The comparison of results for Beam 2 is presented together with the values of the maximum displacement in Table 8.4. The values and comparisons for the other beams are presented in Appendix F.

Table 8.4   Displacements and comparison of displacements and transferred energy from all load cases in Abaqus and hand calculations (Calc.) compared to 2DOF for Beam 2.

Load case	m [kg]	h [m]	Displacement, u [m]			η_u [−]		η_{W_y} [−]	
			2DOF	Abaqus	Calc.	Abaqus	Calc.	Abaqus	Calc.
A	40	1.25	41.3	42.1	41.4	1.02	1.00	1.02	1.00
B	20	2.5	35.7	36.0	35.8	1.01	1.00	1.01	1.00
C	10	5	28.1	28.9	28.3	1.03	1.01	1.03	1.01
D	5	10	20.1	20.7	20.3	1.03	1.01	1.03	1.01
E	2.5	20	13.3	15.2	13.4	1.14	1.01	1.17	1.01
F	40	2.5	80.3	79.2	80.5	0.99	1.00	0.99	1.00
G	20	5	68.8	67.8	69.3	0.99	1.01	0.99	1.01
H	10	10	53.5	54.0	54.4	1.01	1.02	1.01	1.02
I	5	20	37.6	40.1	38.4	1.07	1.02	1.07	1.02
J	2.5	40	24.2	27.7	24.6	1.15	1.02	1.16	1.02

In this load case the correspondence of the results is quite good, especially the 2DOF in comparison with the hand calculation. This shows that the resistance limit of 50 kN used here, see Section 7.3.1, is a valid assumption to capture a plastic response. In comparison with the Abaqus result, the correspondence is good for most load cases, but a trend can be seen that the correspondence is less accurate when the mass of the drop weight becomes smaller in relation to the mass of the beam. Hence, the assumption of a plastic impact in the hand calculations and the choices made for the 2DOF system are valid approximations when the mass ratio of the weight and the beam is higher.

8.3.3 Overall comparison of 2DOF and hand calculations

In Figure 8.4 and Figure 8.5, the comparisons with regard to energy in the hand calculations compared to 2DOF for all beams and all load cases are presented. As for Beam 2, the correspondence is good in all cases except for Beam 5. This is discussed more further down.
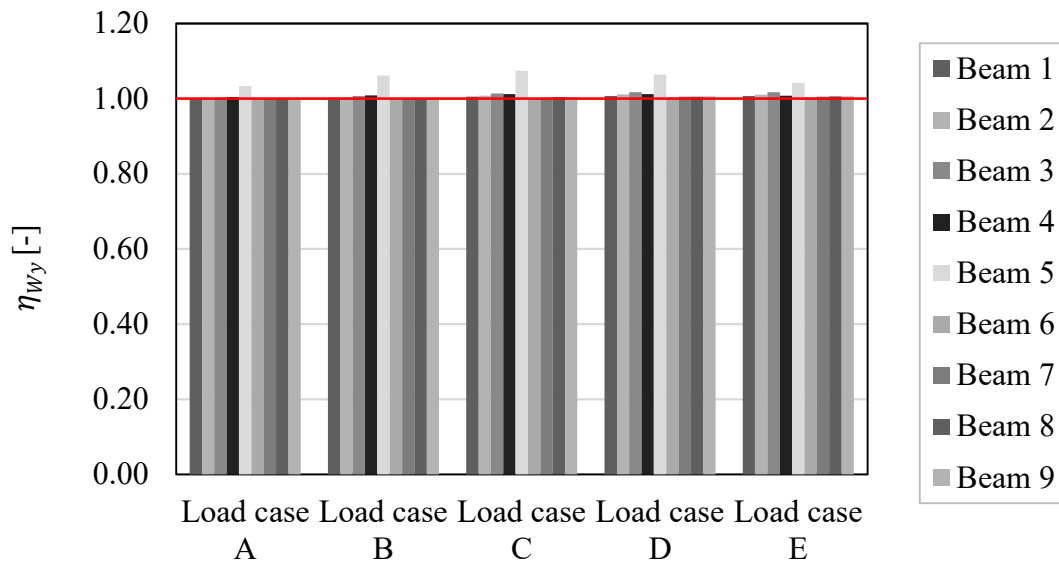
Figure 8.4   Comparison of transferred energy from the hand calculations compared to 2DOF for load cases A-E.
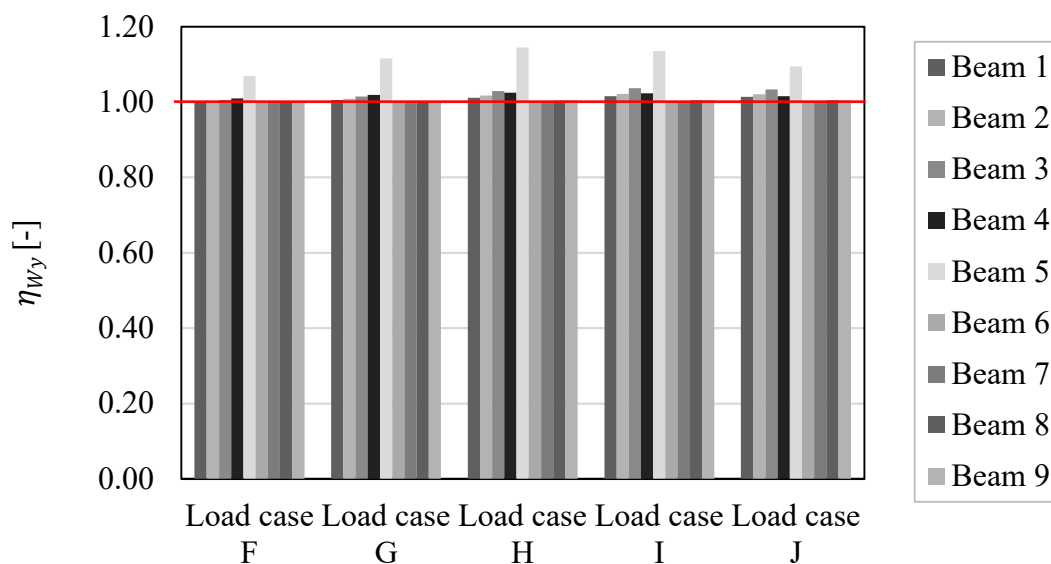
Figure 8.5   Comparison of transferred energy from the hand calculations compared to 2DOF for load cases F-J.

Since the 2DOF model was created and calibrated to fit Beam 2, as described in Section 7.3.1, one reason for the deviation of Beam 5 showed to be that the resistance limit for the interaction between the drop weight and the beam, $R_{m,w}$, was not accurate. In Figure 8.6, a new calibration of the resistance limit for Beam 5 is presented. The load case that had the worst correspondence, i.e. load case J, was chosen for the calibration.
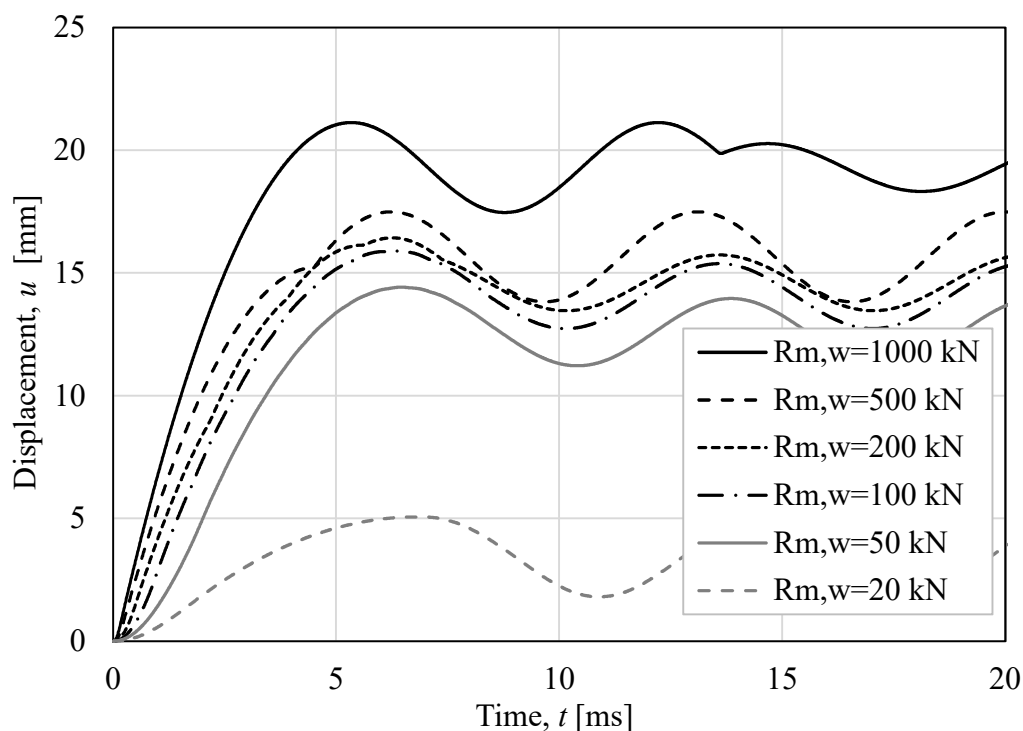
Figure 8.6   *Difference in response depending on how the resistance limit of the spring representing the interaction for Beam 5.*

The result of the calibration for Beam 5 shows that the range, for which the resistance limit, $R_{m,w}$, is accurate, is higher than for Beam 2. Here a value of about $100 - 200$ kN seems to be more accurate. This means that $R_{m,w} = 50$ kN is not the best choice for the resistance limit for Beam 5. When instead a resistance limit of 100 kN or 200 kN was chosen, the correspondence with the hand calculation was also improved significantly, see Table 8.5.

Table 8.5   *Displacement and quota between the result from hand calculations and 2DOF for different resistance limit for the interaction between the weight and beam.*

$R_{m,w}$ [kN]	u [mm]	η_u [-]	η_{W_y} [-]
50	14.4	1.14	1.14
100	15.9	1.03	1.03
200	16.4	1.00	1.00

It was of interest to investigate why Beam 5 required another resistance limit for the interaction between the drop weight and the beam. Things that separate the different beams and affect the response are their mass, m_b, stiffness, k_b, and capacity, $R_{m,b}$. An attempt to investigate which one of these properties that has the largest effect of the resistance limit for the interaction between the weight and the beam, $R_{m,w}$, was made. Since the mass is the same

for Beam 4-9, this difference was excluded. The stiffness, k_b, and the resistance limit, $R_{m,b}$, for Beam 5 are both much higher than for the other beams. Due to this, two beams with almost the same resistance limit, and different stiffnesses were chosen for the comparison (Beam 4 and Beam 9). The properties of these beams are presented in Table 8.6. It could be seen in Figure 8.4 and Figure 8.5, that the load also has an influence since the correspondence is better for some load cases, therefore load case J was chosen for all the beams in this investigation. The calibration of Beam 4 and 9 is presented in Figure 8.7 and Figure 8.8.

Table 8.6   Stiffness and resistance limit for the beams in the calibration study.

Beam	k_b [N/m]	$R_{m,b}$ [kN]
4	$2.59 \cdot 10^6$	10.68
5	$13.33 \cdot 10^6$	24.42
9	$0.50 \cdot 10^6$	9.62
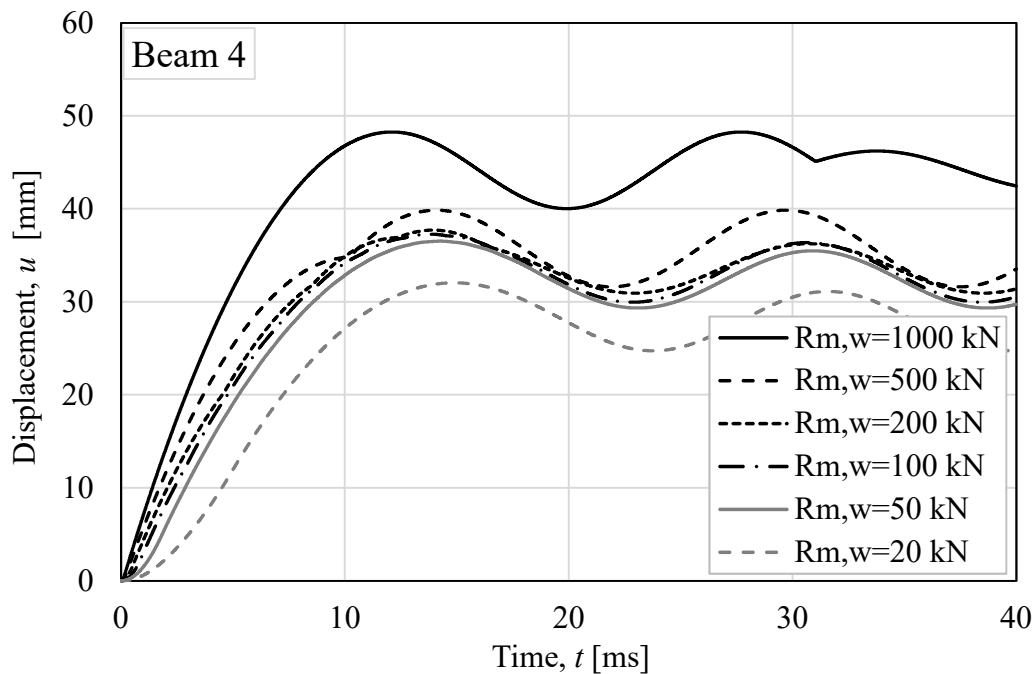
Figure 8.7   Difference in response depending on how the resistance limit of the spring representing the interaction for Beam 4.
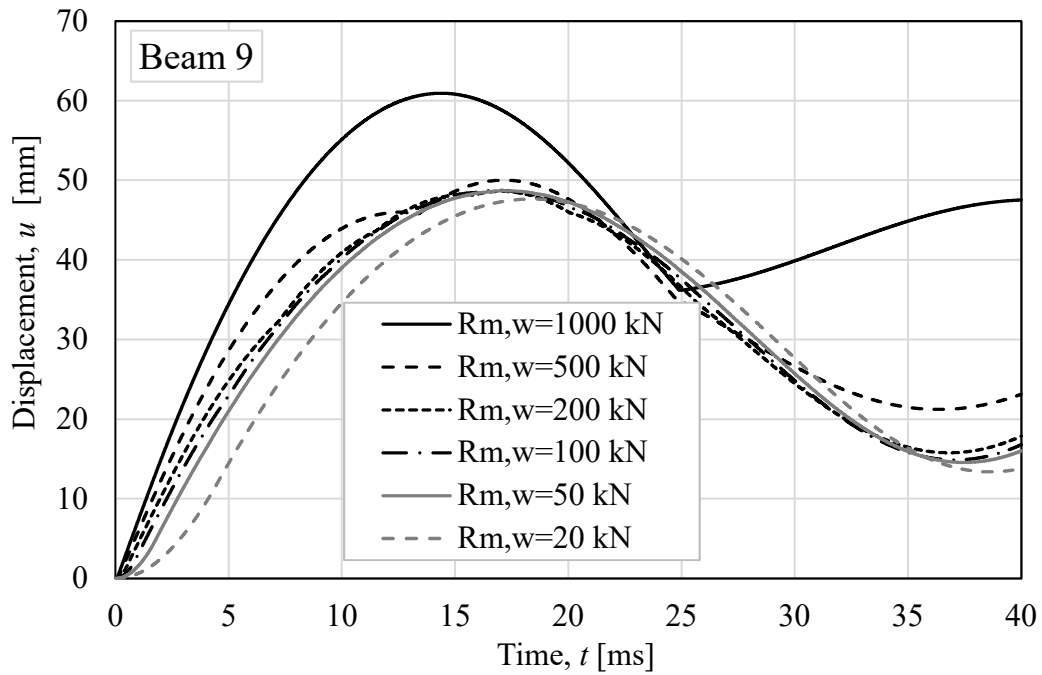
Figure 8.8   *Difference in response depending on how the resistance limit of the spring representing the interaction for Beam 9.*

From this limited comparison it is difficult to draw a clear conclusion. However, for Beam 4 a value of 50 – 200 kN for the resistance limit, $R_{m,w}$, is acceptable while for Beam 9, a value of 20 kN and 500 kN is almost acceptable as well. Since they have almost the same capacity, $R_{m,b}$, this indicates that the stiffness has an influence. The lower the stiffness, the larger the span of acceptable values to be used for $R_{m,w}$ in a 2DOF model. However, further and more extensive evaluations need to be conducted but is not further done in this report.

Furthermore, this calibration study indicates that when the capacity of the beam is changed, the resistance limit for the interaction between the weight and the beam should be calibrated for each separate beam.

8.3.4 Overall comparison of 2DOF and Abaqus

In Figure 8.9 and Figure 8.10, the comparisons with regard to energy in Abaqus and 2DOF for all beams and all load cases are presented. A deviation for the different beams can be seen within each load case. In the Abaqus model a more realistic behaviour including the wave propagation effect is captured, but in the 2DOF model it is not. The deviation between the 2DOF model and Abaqus model is larger for the longer beams, which is an indication of this may be one reason for these deviations.
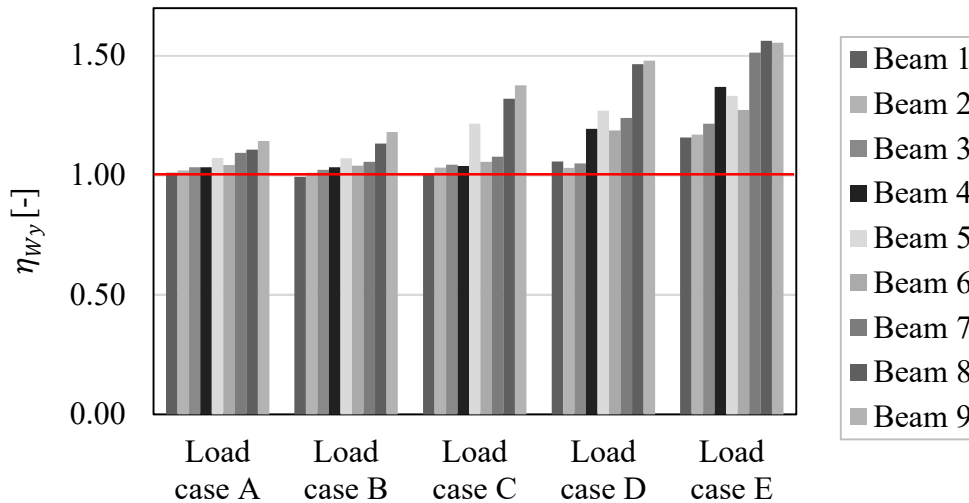
Figure 8.9   *Comparison of transferred energy calculated from Abaqus compared to 2DOF for load cases A-E.*
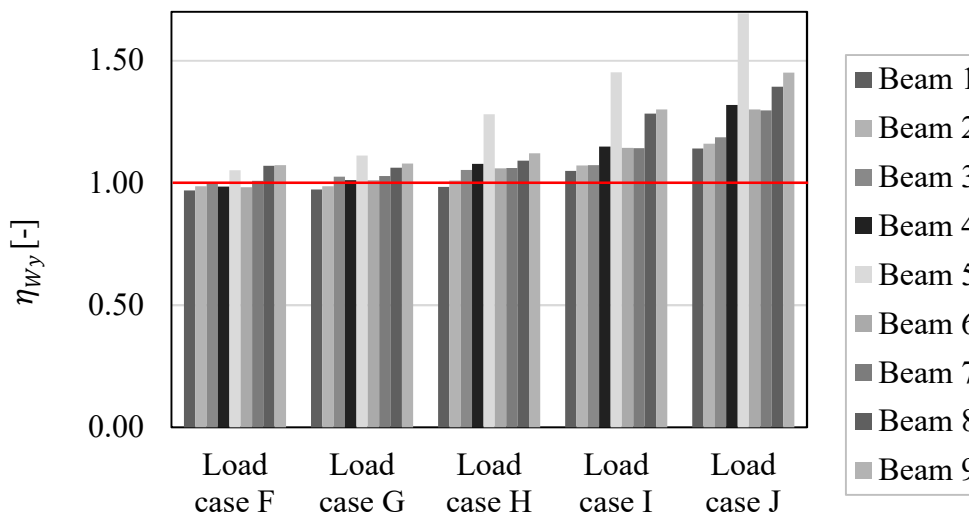
Figure 8.10   *Comparison of transferred energy calculated from Abaqus compared to 2DOF for load cases F-J.*

The result deviates more when the drop height of the drop weight was increased, and the mass of the drop weight decreased. Looking at load case E and J that have the same mass of the drop weight, they correspond better than E and I that have the same velocity. This indicates that the mass of the drop weight influences more than the velocity. When the mass of the weight, m_w, is decreased, the quota between the mass of the drop weight and the total mass decreases. This can be connected to that the external work on the system, calculated as

described in equation (8.1), decreases. This indicates that when the mass ratio decreases, the assumption of a plastic impact is no longer valid to capture the realistic response of the beam regarding the time dependency.

Beam 5 deviates from the pattern, but this can be explained by the choice of resistance limit in the 2DOF model, as discussed in Section 8.3.3. If the resistance limit was chosen to 200 kN instead of 50 kN, the displacements for load case H would be in the same range as the other beams, see Figure 8.11.
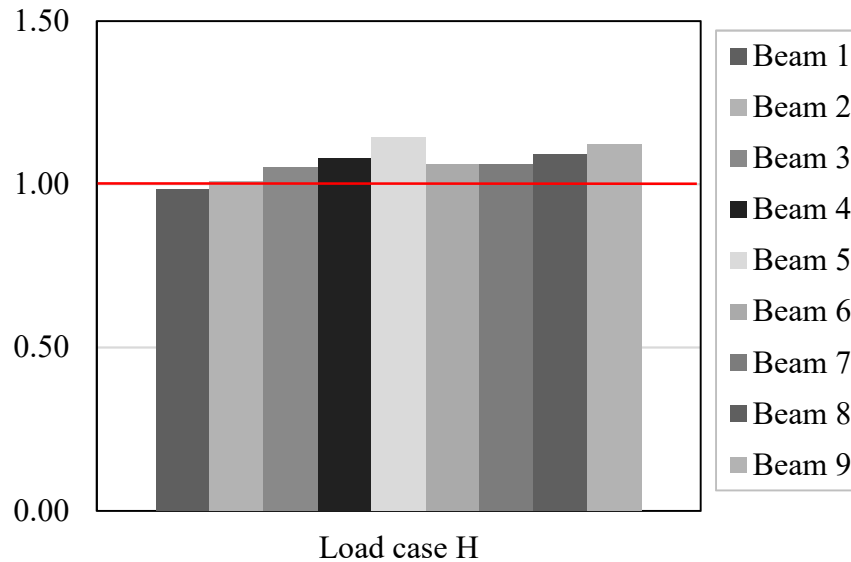
Figure 8.11   Load case H for all beams when $R_{m,w}$ for Beam 5 is updated.

A suggestion of how to avoid these deviations between the models can be to use time dependent transformation factors where the mass and resistance of the beam is changed with time. Thereby, an elastic spring for the interaction between the drop weight and the beam could be used in the 2DOF model as in Abaqus. Thereby the wave propagation effects would be included and the problem with choosing the correct resistance limit would be solved.

8.4 Parametric studies in LS-DYNA

Due to the extensive computing time in LS-DYNA, the parametric study was limited to mainly load case F-J for Beam 1-3. For comparison, though, load case A-E for Beam 2 were analysed as well, see Table 8.7 and Table 8.8. When the mass of the drop weight was changed in LS-DYNA the density was modified to give the correct value of the mass instead of changing the height of the drop weight.

Table 8.7   Load cases studied in LS-DYNA.

		Drop height of the drop weight h [m]					
		1.25	2.5	5	10	20	40
Mass of drop weight m [kg]	2.5					E	J
	5				D	I	
	10			C	H		
	20		B	G			
	40	A	F				

Table 8.8   Beams studied in LS-DYNA.

Beam	Width, b [m]		Height, h [m]		Length, L [m]		Reinforcement			
	0.1	0.2	0.1	0.2	1.0	2.0	2ϕ5	2ϕ6	2ϕ8	4ϕ6
1	●		●		●		●			
2	●		●		●			●		
3	●		●		●				●	

The time-displacement curves from the analyses of Beam 2 for the load case A-J can be seen in Figure 8.12. In the same way as for the simplified analyses, the largest mass gives the largest displacements. This can be observed for Beam 1 and 3 as well, see Appendix G.
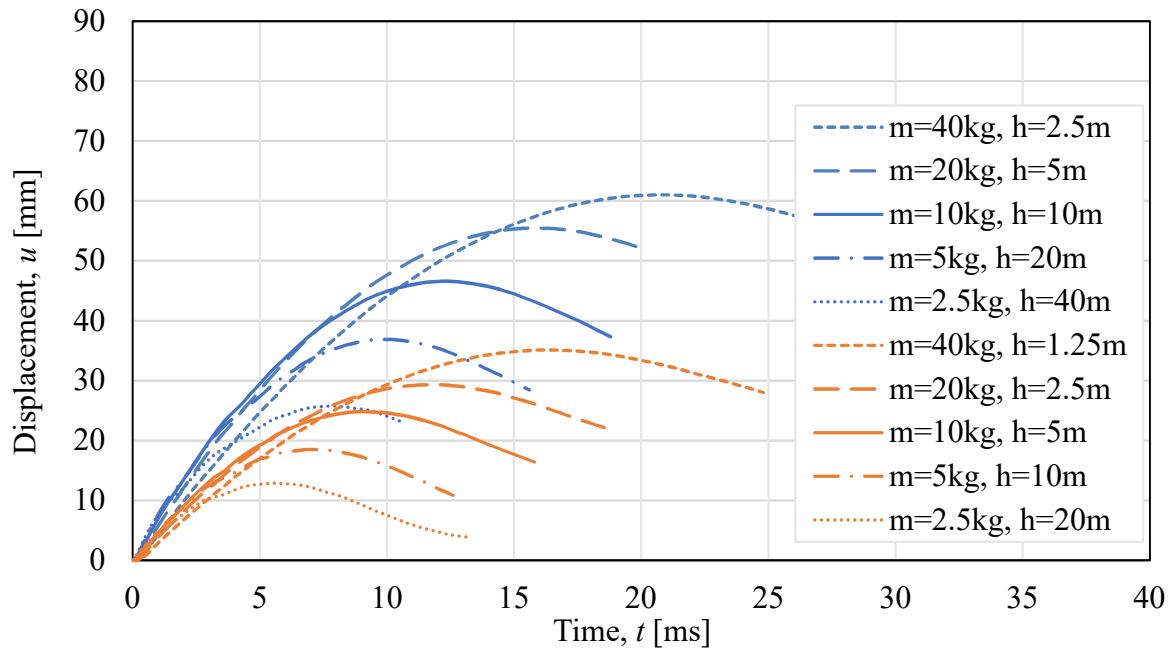
Figure 8.12   Time-displacement curves for Beam 2 for load case A-J.

The crack pattern from the time of maximum displacement for load case A-E for Beam 2 can be seen in Table 8.9, and load case F-J in Table 8.10.

In load case A-E the magnitude of the kinetic energy before impact is halved compared to load case F-J, which leads to less extensive cracking. The differences of the cracks depending on a high mass or a high velocity for the gentler cases are not as distinct as for the severe cases.

Comparing load case F-J, higher impact velocity caused more extensive shear cracks. There are more cracks in the middle section for the cases with higher velocity and they have a lower inclination. In the rest of the beam, there are fewer cracks due to the smaller displacement compared to the cases with a higher mass of the drop weight. These tendencies can be observed for Beam 1 and 3 as well, see Appendix G.

Table 8.9   *Crack pattern at the time om maximum displacement for load case A-E for Beam 2.*

Load case	Crack pattern
A	
B	
C	
D	
E	
Principle strain [%]	0 0.99 1.98 2.97 3.96 4.95 5.94 6.93 7.92 8.91 9.9

CHALMERS, *Architecture and Civil Engineering*, Master's Thesis, ACX30-18-36
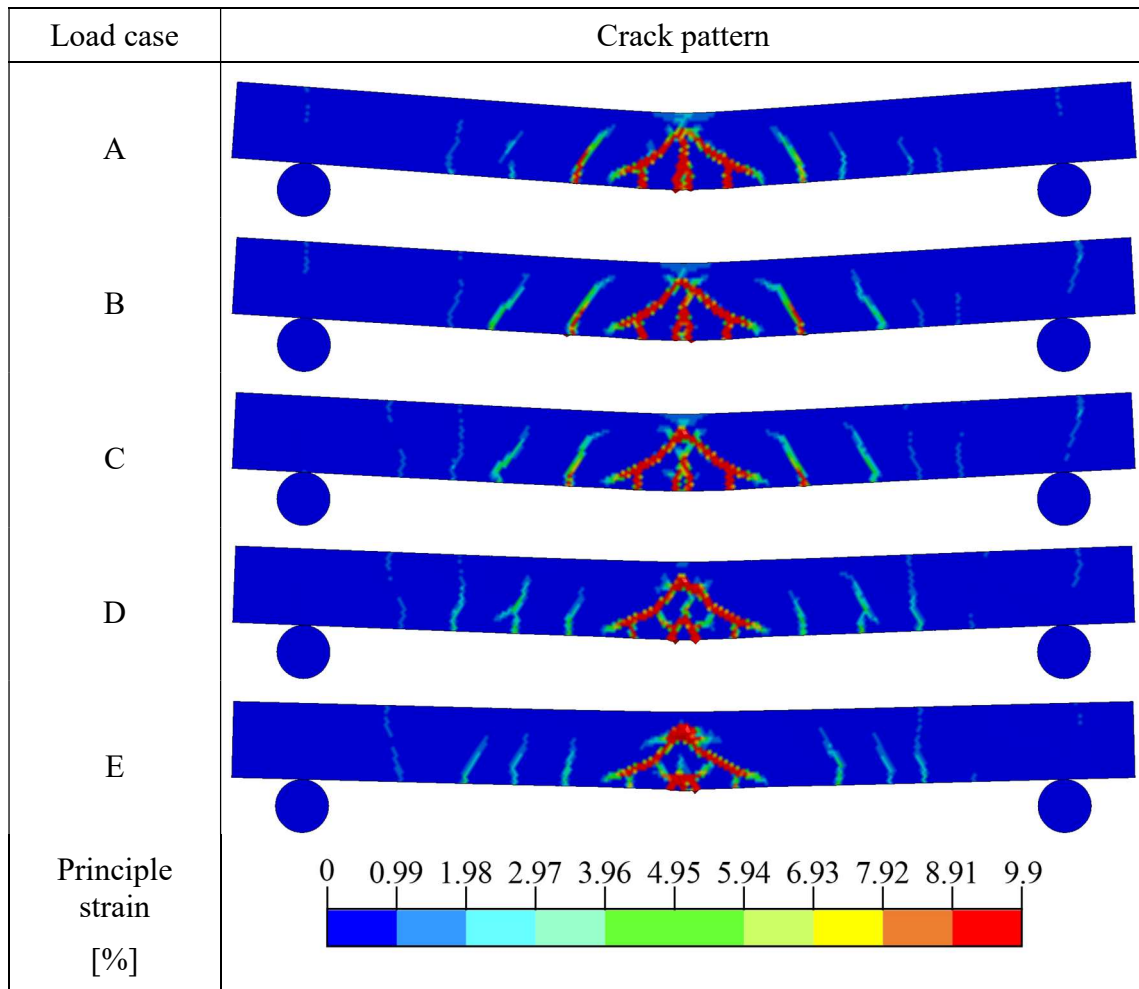
Table 8.10   Crack pattern at the time om maximum displacement for load case F-J for Beam 2.

Load case	Crack pattern
F	
G	
H	
I	
J	
Principle strain [%]	0 0.99 1.98 2.97 3.96 4.95 5.94 6.93 7.92 8.91 9.9
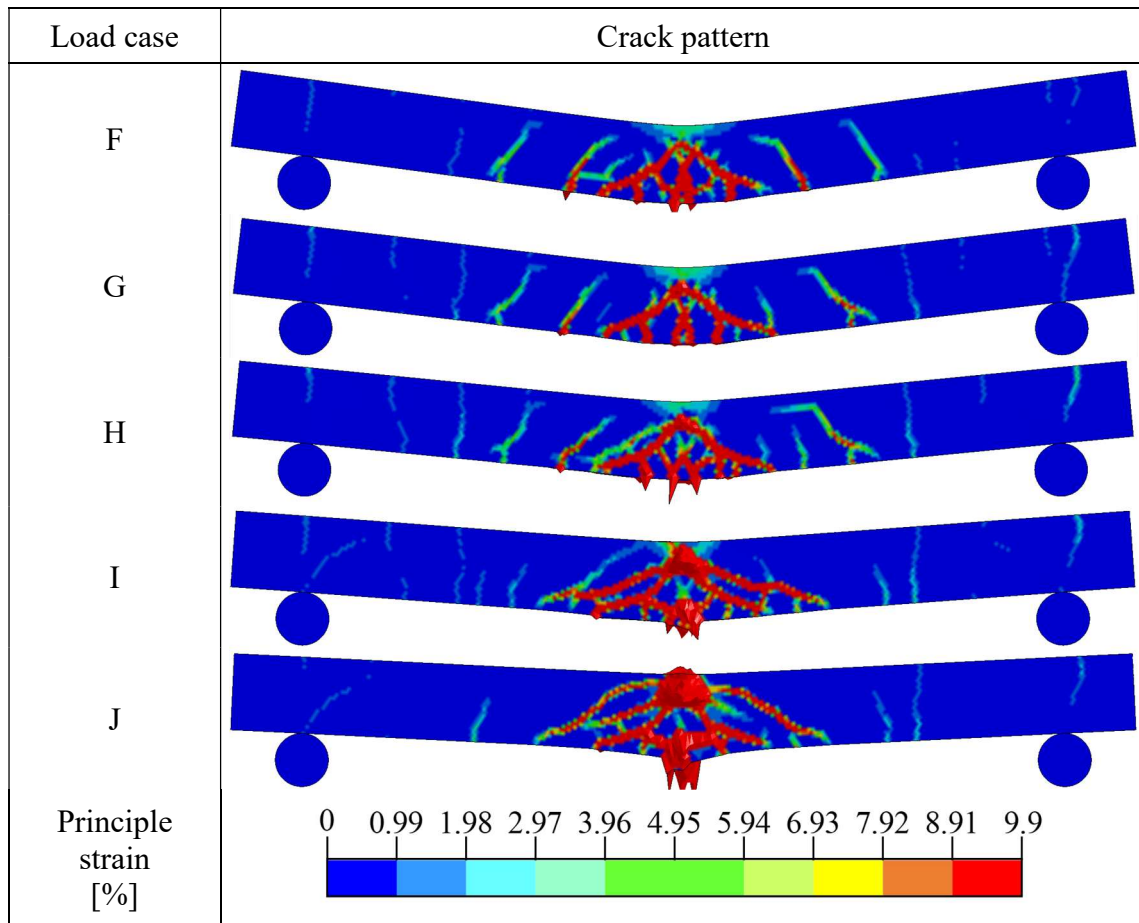
In the load cases with high impact velocity, extruded parts of the beam can be observed, see Figure 8.13. The extruded parts appear in the middle of the beam, in and under the impact zone. These may represent concrete that is spalled of due to the pressure wave caused by the high velocity impact. An argument for this is that the extruded parts continue to grow during the entire analysis, even after the beam has reached its maximum displacement.
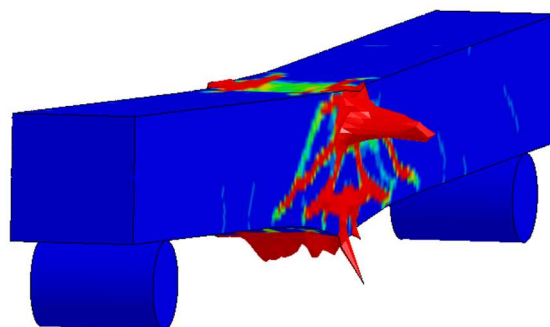
Figure 8.13   Visualization of the extruded parts appearing in Beam 2, load case J.

A possible improvement of the model could be to include so called erosion of elements, so that elements with a strain large enough to make them disconnected from the other elements are removed. In this way the extrusion of parts might be avoided.

When the different load cases were analysed in LS-DYNA, there were trouble with convergence in some cases, probably due to concrete compressive failure, and the analyses did not reach the timestep of maximum displacement. In some cases, the extruded parts could be a contributing factor, but there was no indication that this would be the main reason since it was not observed at all in several cases with convergence issues. Instead, the compressive failure variable, ε_{fc}, was increased for the cases with convergence issues. This was considered to be acceptable since the post peak behaviour of local compressive failure was not of interest and should not influence the global result significantly.

In Appendix E an evaluation of how the displacements and the crack patterns are influenced by an increase of two, five and ten times the standard value of the compressive failure variable is made. The conclusion is that the influence was not significant. In the parametric study, the standard value was used if no converges issues arose before the maximum displacement was reached. If it did, the compressive damage variable was first increased to two times the standard value, secondly five times and thirdly ten times. The different values that were finally used in the analyses presented in this report can be seen in Table 8.11.

Table 8.11   Summary of the values that have been used of the compressive damage variable for the different beams and load cases, 0.001 being the standard value in this project.

Beam	Load case	ε_{fc} [-]
1	F	0.005
	G	0.002
	H	0.010
	I	-
	J	-
2	A	0.001
	B	0.001
	C	0.001
	D	0.001
	E	0.001
	F	0.002
	G	0.001
	H	0.002
	I	0.002
	J	0.002
3	F	0.001
	G	0.001
	H	0.002
	I	0.005
	J	0.005

There was no obvious correlation between the load case and the value of the compressive damage variable that was needed, but for higher velocities, a higher value was often required. However, in the less severe load cases for Beam 2, the standard value of the compressive damage variable could be used. This implies that not only the impact velocity, but also the total loading affects how the variable should be chosen.

For load case I and J for the weakest beam (Beam 1), the analyses stopped after approximately 1-2 milliseconds for all four values of the compressive damage variable. In Abaqus and the 2DOF model, they reach maximum displacement after approximately 14 milliseconds for load case I and approximately 11 milliseconds for load case J. These cases are the ones with the highest velocity right before impact and theses load cases have required a higher value for the compressive damage variable for Beam 2-3 as well. In the analyses for these two load cases the compressive damage variable was not increased above the studied values and the reasons for the issues were not further investigated. The analyses for these two load cases were instead ran with the value of $\varepsilon_{fc} = 0.01$ until convergence issues arose.

8.5 Comparison between models

To compare the results from LS-DYNA to the results from the simplified model, ratios for the maximum displacements were calculated. In this case, energy calculations were excluded since the final force-displacement relation in LS-DYNA is unknown.

$$\eta_{u,LS-DYNA} = \frac{u_{LS-DYNA}}{u_i} \qquad i = 2DOF, Abaqus \qquad (8.2)$$

In Figure 8.14 load case A-E for Beam 2 are compared to Abaqus and in Figure 8.15 load case F-J for Beam 1-3 are compared.
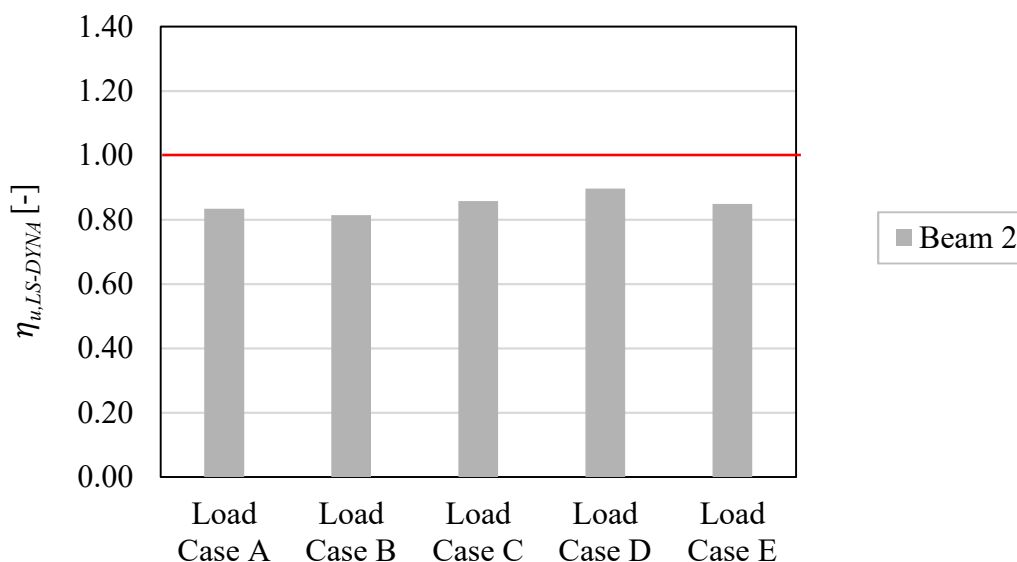
Figure 8.14   The maximum displacement in LS-DYNA compared to in Abaqus for Beam 2, load case A-E.
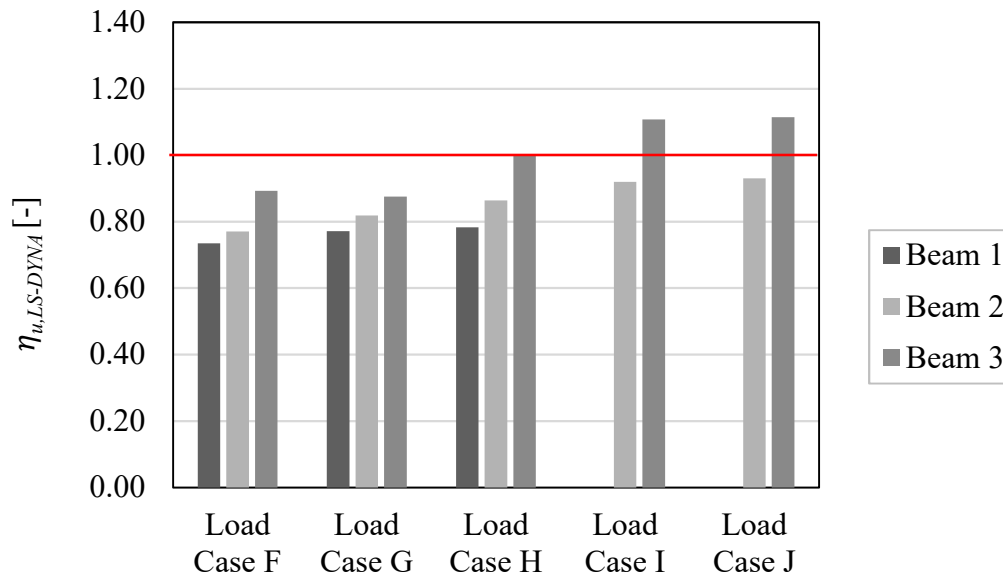
Figure 8.15   The maximum displacement in LS-DYNA compared to in Abaqus for all beams, load case F-J.

In general, the LS-DYNA model gave smaller displacements than the simplified models. For the more severe load cases with high velocity, the displacements from LS-DYNA approach the displacements from Abaqus, and for some cases, even exceed them. For these load cases extensive shear cracks can be observed in middle of the beam, see Table 8.10. These extensive cracks lead to a lowering of the capacity and a softer behaviour of the beam and may be an explanation for this deviation. There are also indications of that crushing of concrete in the impact zone could be more extensive in these cases, which also lowers the capacity and creates a softer behaviour.

For the less severe cases, A-E, the deviation is not as prominent and to take a closer look at this, the gentler load cases were compared to the severe load cases for Beam 2 in Figure 8.16. The comparison indicates that the relation between LS-DYNA and Abaqus is more constant when the load level is lower. It could also be seen in Table 8.9 that there is a smaller variation in crack pattern for these load cases.
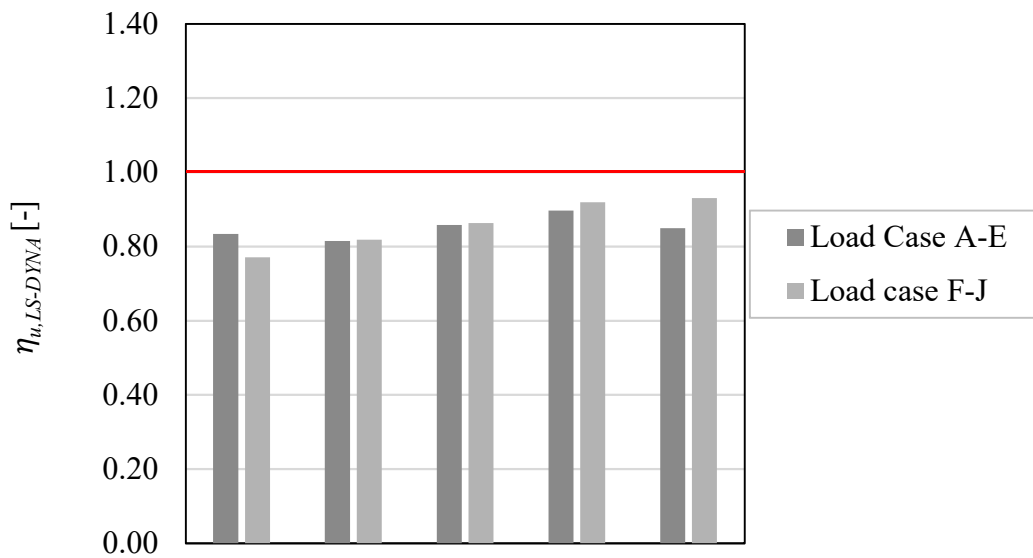
Figure 8.16   Comparison of LS-DYNA to Abaqus for Beam 2, Load cases A-E and F-J.

This indicates that the LS-DYNA model can represent the behaviour of lowered capacity due to cracking or crushing of concrete more realistically. However, since no experiments have been conducted on the different beams and load cases, it cannot be determined how reliable the results from the LS-DYNA model are.

9 Final Remarks

9.1 Conclusions

This project aimed to increase the understanding of dynamically loaded structures by using different levels of numerical modelling. The 2DOF system proved to give different levels of accuracy for different beams and load cases compared to the beam element model in Abaqus where a more realistic behaviour is captured. One thing that the Abaqus model cannot capture is the cracking which proved to have an influence of the results in comparison to the LS-DYNA model.

In the 2DOF model, a plastic impact was assumed. It was discovered that the suitable range for the value for the resistance limit of the spring, representing the interaction between the drop weight and the beam, varied mainly depending on properties of the beam, such as the stiffness and the capacity. To use this kind of 2DOF model, it was found to be necessary to calibrate the model for each separate case.

Results from the 2DOF model and the Abaqus model for cases with the same kinetic energy before impact were compared. It could be seen that for the cases when the mass of the drop weight was small in relation to the beam, the results differed more. This indicates that the assumption of a plastic impact in the 2DOF model was not valid to capture a more realistic behaviour in these cases.

The time dependency of the response of the beam is captured in the Abaqus model, but not in the 2DOF model. It is believed that using time dependent transformation factors would make it possible to model the spring, representing the interaction between the drop weight and the beam, in the 2DOF model as elastic. Thereby, the problems with the value for the resistance limit could be solved. Time dependent transformation factors in the 2DOF model would also make it possible to capture a behaviour similar to that in Abaqus and achieve a model that is applicable for all load cases.

The further development of the LS-DYNA model by including a bond-slip relation and a non-linear structural behaviour of the reinforcement gave satisfying results. In the parametric study, it was concluded that there is a need to further develop the model to be able to analyse all kind of load cases since convergence issues arose for some analyses. In some of these cases the issues where to some extent solved by increasing the variable describing the descending branch of the post-peak behaviour of concrete in compression. In the parametric study using the LS-DYNA model of the severe load cases, a high velocity showed to give more extensive shear cracks in the middle section of the beam and crushing of concrete in the impact zone. For these cases, the difference between the LS-DYNA model and the Abaqus model also showed a deviant trend. It is therefore believed that this deviation can be an indication that the LS-DYNA model captures the lowering of capacity due to cracking and crushing of concrete and thereby a more realistic behaviour.

9.2 Future studies

In this project bond-slip, by the built-in function CONSTRAINED in LS-DYNA, as well as a nonlinear structural behaviour of the reinforcement were included. However, further development of the model could be made as a future study. The different ways of modelling bond-slip could be evaluated. The description of the structural behaviour of the reinforcement can be further developed by including an ultimate strain where the bar would be torn off.

Furthermore, the model used in this thesis showed convergence issues and the problem behind this is a question to be answered.

In future studies it would be of interest to include erosion of elements in the LS-DYNA model since it could be seen in this study that parts of the beam were extruded. Including erosion leads to that elements with a strain large enough to make them disconnected from the other elements are removed. The extrusion can probably be spalling of concrete and when these elements would be removed a more realistic behaviour might be obtained.

In this thesis, a simplified way of model the stiffness for the spring representing the interaction between the weight and the beam was used. A brief study of the use of contact mechanics was conducted but not applicated in this project. However, a further evaluation of how this more advanced and realistic way of modelling the stiffness would be of interest.

The parametric study showed that the 2DOF model used in this project is sensitive to some parameters. It was discovered that the suitable range of the resistance limit for the interaction between the drop weight and the beam change depending on the properties on the weight. It would be of interest to evaluate which parameters that affect the model and how to be able to make it applicable for a general case.

However, it would be desirable to have a 2DOF model of universal application. An idea of how to achieve this can be by including time dependent transformation factors and to use an elastic spring for the interaction between the drop weight and the beam. Thereby a response of the beam similar to that obtained in the Abaqus model (i.e. considering wave propagation effects) could be simulated.

From the parametric study that was made, some of the studied load cases and beams would be interesting to conduct experiments on, even though many of the load cases would be hard to realise. Performing more experiments could give a further indication of when the models are valid. Since it was seen that when the results from the 2DOF model deviated when the mass of the drop weight was small in relation to the mass of the beam, it would be of interest to conduct experiments on heavier beams. It would also be interesting to conduct experiments on beams with different relations between the height and the length than the beams that have been included in previous experiments.

10 References

Andersson, J. and Antonsson, J. (2015). *Design with Regard to Collision Impact,* Gothenburg: Chalmers University of Technology.

Andersson, S. and Karlsson, H. (2012). *Structural response of reinforced concrete beams subjected to explosions,* Gothenburg: Chalmers University of Technology.

Biggs, J. M. (1964). *Introduction to structural dynamics.* New York: McGraw-Hill.

CEB-FIP12 (2012). CEB-FIP Model Code 2010, Design code. *fib Bulletin 65,* Volume 1.

CEB-FIP91 (1991). *CEB-FIP Model Code 1990, Design Code.* London: s.n.

Chen, Y. and May, I. M. (2009). Reinforced concrete members under drop-weight impacts. *Strutures and Buildings,* 162(SB1), pp. 45-56.

Craig, R. R. and Kurdila, A. J. (2006). *Fundamentals of structural dynamics.* Second Edition ed. New Jersey: Wiley.

Dassault Systems, Simulia (2014a). *Abaqus/CAE User's Guide.* [Online] Available at: http://abaqus.software.polimi.it/v6.14/books/usi/default.htm [Accessed 02 03 2018].

Dassault Systems, Simulia (2014b). *Abaqus Analysis User's Guide.* [Online] Available at: http://abaqus.software.polimi.it/v6.14/books/usb/default.htm [Accessed 020318].

Dassault Systems, Simulia (2014c). *Abaqus Theory Guide.* [Online] Available at: http://abaqus.software.polimi.it/v6.14/books/stm/default.htm [Accessed 020318].

Ekström, J. (2017). *Blast and Impact Loaded Concrete Structures,* Gothenburg: Chalmers University of Technology.

Engström, B. (2014). *Restraint cracking of reinforced concrete structures,* Gothenburg: Chalmers university of technology .

Engström, B. (2015). *Design and analysis of continuous beams and columns,* Gothenburg: Chalmers University of Technology.

Fujikake, K., Senga, T., Ueda, N., Ohno, T. and Katagiri, M. (2006). Study on Impact Response of Reactive Powder Concrete Beam and Its Analytical Model. *Journal of Advanced Concrete Technology,* 4(1), pp. 99-108.

Grassl, P., 2016. *petergrassl.com.* [Online] Available at: http://petergrassl.com/tempFiles/MAT_CDPM_Grassl.pdf [Accessed 120318].

Grassl, P., Johansson , M. and Leppänen, J. (2018). On the Numerical Modelling of Bond for the Failure Analysis of Reinforced Concrete. *Engineering Fracture Mechanics,* Volume 189, pp. 13-26.

Grassl, P., Xenos, D., Nyström, U., Rempling, R. and Gylltoft, K. (2013). CDPM2: A damage-plasticity approach to modelling the failure of concrete. *International Journal of Solids and Structures,* 50(24), pp. 3805-3816.

Johansson, M. (2000). *Structural behaviour in concrete frame corners of civil defence shelters - Non-linear finite element analyses and experiments,* Gothenburg: Chalmers University of Technology.

Johansson, M. (2014). *B03-101, Beräkning av impulsbelastad konstruktion - Strukturrespons vid impulsbelastning.* [Online]
Available at: https://www.msb.se/sv/Insats--beredskap/Hantera-olyckor--kriser/Skyddsrum/Berakningar-losningar-och-komponenter/
[Accessed 020218].

Johansson, M. (2014). *Beräkningsmetodik stötlast (Working document)*, Gothenburg: Norconsult AB

Johansson, M. and Laine, L. (2012). *Bebyggelsens motståndsförmåga mot extrem dynamisk belastning, Del 3 - Kapacitet hos byggnader,* Gothenburg: Myndigheten för samhällsskydd och beredskap.

Johansson, M., Leppänen, J., Jansson, H. and Ekengren, B. (2014). *Seminarium om impulsbelastade konstruktioner 2014,* Gothenburg: Myndigheten för samhällsskydd och beredskap.

Jönsson, J. and Stenseke, A. (2018). *Concrete Beams Subjected to Repeated Drop-Weight Impact and Static Load,* Gothenburg: Chalmers University of Technology.

Lockhart, E. (2017). *Modelling the Failure of Reinforced Concrete Subjected to Dynamic Loading Using CDPM2 in LS-DYNA,* Glasgow: University of Glasgow.

Lovén, J. and Svavarsdóttir, E. S. (2016). *Concrete beams subjected to drop weight impact,* Gothenburg: Chalmers University of Technology.

Lozano Mendoza, F. and Makdesi Aphram, J. (2017). *Concrete Beams Subjected to Drop-Weight Impact and Static Load,* Gothenburg: Chalmers University of Technology.

LSTC (2014a). *LS-DYNA Keyword User's Manual - Volume I R7.1.* California: Livermore Software Technology Corporation.

LSTC (2014b). *LS-DYNA Keyword User's Manual - Volume II R7.1.* California: Livermore Software Technology Corporation.

LSTC (2017). *LS-DYNA Keyword User's Manual - Volume I R10.0.* California: Livermore Software Technology Corporation.

LSTC (2018). *LS-DYNA Theory Manual.* California: Livermore Software Technology Corporation .

Plos, M. (2000). *Finite element analyses of reinforced concrete structures,* Gothenburg: Chalmers University of Technology.

Yi, W.-J., Zaoh, D.-B. and Kunnath, S. K. (2016). Simplified Approach for Assessing Shear Resistance of Reinforced Concrete Beams under Impact Loads. *ACI STRUCTURAL JOURNAL,* 113(4), pp. 747-756.

Appendix A   Material input data

A.1   Input data to the 2DOF model for validation

The material input data used in the 2DOF model for validation, made in Sections 7.3 and 7.4, is presented in Table A-1 and Table A-2.

Table A-1   Material parameters for the beam in the 2DOF model.

Parameter	Value
Mass density, ρ [kg/m^3]	2400
Stiffness, k_b [N/m]	$2.405 \cdot 10^6$
Resistance limit, R_m [kN]	10.377

Table A-2   Parameters for the weight and the interaction between the weight and the beam in the 2DOF model.

Parameter	Value
Mass of the weight, m [kg]	10.093
Stiffness, k_w [N/m]	$3.99 \cdot 10^9$
Resistance limit, R_m [kN]	50
Initial velocity, v_0 [m/s]	10.35

To calculate the resistance limit for the beam, the simplification of the structural behaviour of the reinforcement seen in Figure A-1 was used. The resistance limit is based on a value for the yield stress of the reinforcement which is approximated to 610 MPa.
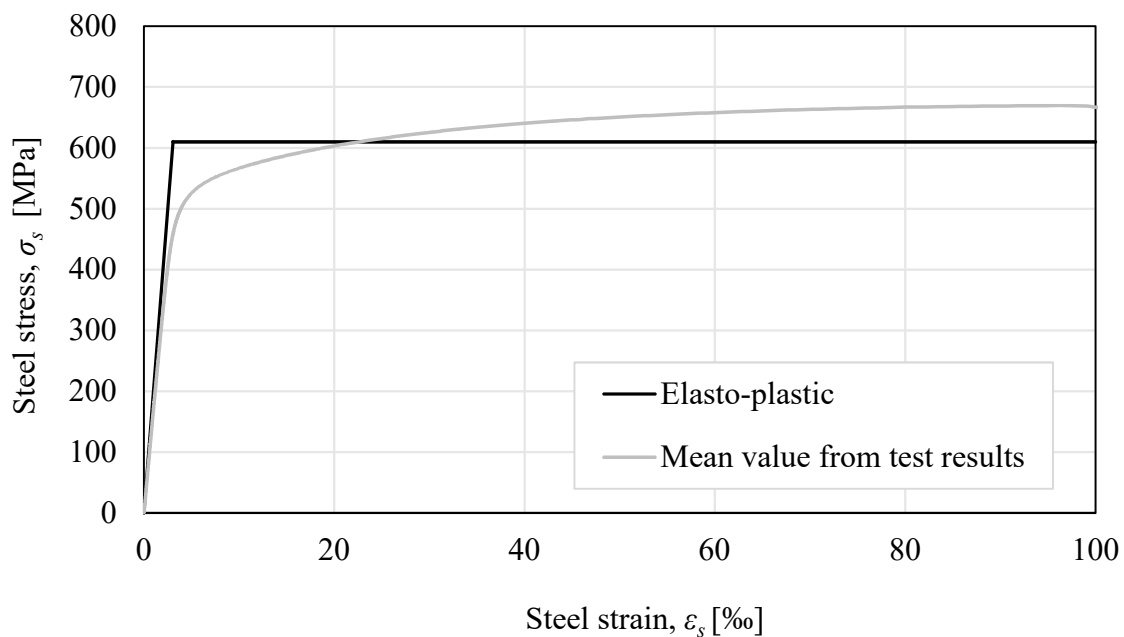
Figure A-1   The mean value from the tensile test of the reinforcement in comparison with the elasto-plastic behaviour used in the simplified models.

A.2 Input data in Abaqus for validation

In Table A-3 and Table A-4, the material input data used in Abaqus for validation of the model, made in Sections 7.3 and 7.4, is presented. The units used in Abaqus are presented in Section 5.3.1, Table 5.2.

Table A-3   Material input parameters for the drop weight.

Element	Parameter	Value
Bar	Density, ρ [kg/m^3]	5 000
	Height, h [mm]	50
	Young's modulus, E [GPa]	133 100
	Corresponding stiffness, k_{bar} [N/m]	4.342e12
	Yield stress, f_y [MPa]	50
	Fictitious area, A [m^2]	0.001
Point mass	Mass, m [kg]	10.093
	Initial velocity, v_0 [m/s]	10.35
Spring	Stiffness, k_{spring} [N/m]	4.0e9

Table A-4   Material input parameters for the beam in Abaqus.

Parameter	Value
Mass density, ρ [kg/m^3]	2 400
Equivalent Young's modulus, E_{eq} [GPa]	6.0
Poisson's ratio, v [-]	0.2
Equivalent yield stress, $f_{y.mod}$ [MPa]	15.57

A.3   Input data in LS-DYNA for validation

The material input data used in LS-DYNA for validation of the model, made in Sections 7.5 and 7.6, is presented in Table A-5 to Table A-9. The units used in LS-DYNA are presented in Section 6.2, Table 6.1.

Table A-5   Material parameters in LS-DYNA for CDPM2

LS-DYNA notation	Parameter	Value
RO	Mass density, ρ [kg/m^3]	2 400
E	Young's modulus, E_c [GPa]	34.7
PR	Poisson's ratio, v [-]	0.2
ECC	Eccentricity parameter, e [-]	0.516
FT	Uniaxial tensile strength, f_t [MPa]	3.28
FC	Uniaxial compressive strength, f_c [MPa]	45.5
HP	Hardening parameter [-]	0.01
WF	Ultimate crack width, w_f [mm]	0.086
TYPE	Type of tensile damage	Bi-linear [1.0]
EFC	Compressive damage variable [-]	0.001

Table A-6   Material parameters in LS-DYNA for the reinforcement.

LS-DYNA notation	Parameter	Value
RO	Mass density, ρ [kg/m^3]	7 850
E	Young's modulus, E_c [GPa]	200
PR	Poisson's ratio, v [-]	0.3
TS1	Diameter of bar, ϕ [mm]	6
TS2	Diameter of bar, ϕ [mm]	6

Table A-7   Parameters in LS-DYNA for the bilinear structural behaviour of the reinforcement.

LS-DYNA notation	Parameter	Value
SIGY	Yield stress, f_y [MPa]	609.8
ETAN	Tangent modulus, E_{tan} [MPa]	584
E	Young's modulus, E_c [GPa]	200

Table A-8   *Parameters in LS-DYNA for the nonlinear structural behaviour of the reinforcement. This reinforcement was used in tests in 2016.*

LS-DYNA notation	Parameter	Value
E	Young's modulus, E_c [GPa]	200
ES1	Stress, σ_1 [MPa]	450
ES2	Stress, σ_2 [MPa]	520
ES3	Stress, σ_3 [MPa]	550
ES4	Stress, σ_4 [MPa]	590
ES5	Stress, σ_5 [MPa]	620
ES6	Stress, σ_6 [MPa]	650
ES7	Stress, σ_7 [MPa]	660
ES8	Stress, σ_8 [MPa]	668
EPS1	Plastic strain, $\varepsilon_{pl,1}$ [‰]	0.0
EPS2	Plastic strain, $\varepsilon_{pl,2}$ [‰]	2.1
EPS3	Plastic strain, $\varepsilon_{pl,3}$ [‰]	4.5
EPS4	Plastic strain, $\varepsilon_{pl,4}$ [‰]	12.7
EPS5	Plastic strain, $\varepsilon_{pl,5}$ [‰]	23.9
EPS6	Plastic strain, $\varepsilon_{pl,6}$ [‰]	45.9
EPS7	Plastic strain, $\varepsilon_{pl,7}$ [‰]	59.5
EPS8	Plastic strain, $\varepsilon_{pl,8}$ [‰]	95.8
TS1	Diameter of bar, ϕ [mm]	6
TS2	Diameter of bar, ϕ [mm]	6

Table A-9   *Material parameters in LS-DYNA for the drop weight and supports.*

LS-DYNA notation	Parameter	
RO	Mass density, ρ [kg/m^3]	7 753
E	Young's modulus [GPa]	205
PR	Poisson's ratio [-]	0.3

A.4   Input data to the 2DOF model 2018

The material input data used in the 2DOF model for the material data from 2018 is presented in Table A-10 and Table A-11. The input data that was varied is calculated in Appendix C based on the different parameters.

Table A-10   Material parameters for the beam in the 2DOF model.

Parameter	Value
Mass density, ρ [kg/m^3]	2 400
Stiffness, k_b [N/m]	Varied
Resistance limit, $R_{m,b}$ [kN]	Varied

Table A-11   Parameters for the weight and the interaction between the weight and the beam in the 2DOF model.

Parameter	Value
Mass of the weight, m [kg]	Varied
Stiffness, k_w [N/m]	$3.99 \cdot 10^9$
Resistance limit, $R_{m,w}$ [kN]	50
Initial velocity, v_0 [m/s]	Varied

To calculate the resistance limit for the beam, the simplification of the structural behaviour of the reinforcement seen in Figure A-2 was used. The resistance limit is based on the mean value of the ultimate strength of the reinforcement bars which is calculated from the measured values to 623 MPa.
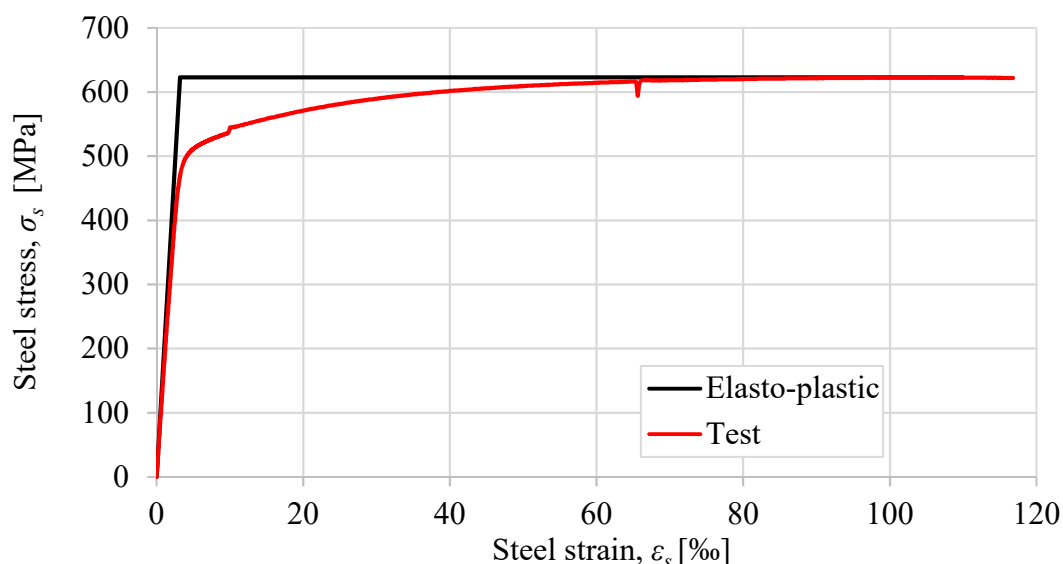
Figure A-2   Structural behaviour of the reinforcement in the 2DOF model compared to in the test 2018.

A.5 Input data in Abaqus 2018

In Table A-12 and Table A-13, the material input data used in Abaqus 2018 is presented. The units used in Abaqus are presented in Section 5.3.1, Table 5.2. The input data that was varied is calculated in Appendix C based on the different parameters.

Table A-12   Material input parameters for the drop weight in Abaqus 2018.

Element	Parameter	Value
Point mass	Mass, m [kg]	Varied
	Initial velocity, v_0 [m/s]	Varied
Spring	Stiffness, k_{spring} [N/m]	3.99e9

Table A-13   Material input parameters for the beam in Abaqus 2018.

Parameter	Value
Mass density, ρ [kg/m^3]	2400
Equivalent Young's modulus, E_{eq} [GPa]	Varied
Poisson's ratio, v [-]	0.2
Equivalent yield stress, $f_{y.mod}$ [MPa]	Varied

A.6 Input data in LS-DYNA 2018

The material input data used in LS-DYNA 2018 is presented in Table A-14, Table A-15, and Table A-16. The units used in LS-DYNA are presented in Section 6.2, Table 6.1.

Table A-14   Material parameters in LS-DYNA for CDPM2 2018.

LS-DYNA notation	Parameter	Value
RO	Mass density, ρ [kg/m^3]	2400
E	Young's modulus, E_c [GPa]	32
PR	Poisson's ratio, v [-]	0.2
ECC	Eccentricity parameter, e [-]	0.518
FT	Uniaxial tensile strength, f_t [MPa]	2.8
FC	Uniaxial compressive strength, f_c [MPa]	36.0
HP	Hardening parameter	0.01
WF	Ultimate crack width, w_f [mm]	0.124
TYPE	Type of tensile damage	Bi-linear [1.0]
EFC	Compressive damage variable	0.001

Table A-15   Material parameters in LS-DYNA for the reinforcement used in tests in 2018.

LS-DYNA notation	Parameter	Value
RO	Mass density, ρ [kg/m^3]	7800
E	Young's modulus, E_c [GPa]	196
PR	Poisson's ratio, v [-]	0.3
ES1	Stress, σ_1 [MPa]	420
ES2	Stress, σ_2 [MPa]	500
ES3	Stress, σ_3 [MPa]	520
ES4	Stress, σ_4 [MPa]	560
ES5	Stress, σ_5 [MPa]	590
ES6	Stress, σ_6 [MPa]	610
ES7	Stress, σ_7 [MPa]	620
ES8	Stress, σ_8 [MPa]	623
EPS1	Plastic strain, $\varepsilon_{pl,1}$ [‰]	0
EPS2	Plastic strain, $\varepsilon_{pl,2}$ [‰]	1.6
EPS3	Plastic strain, $\varepsilon_{pl,3}$ [‰]	3.6
EPS4	Plastic strain, $\varepsilon_{pl,4}$ [‰]	12.8
EPS5	Plastic strain, $\varepsilon_{pl,5}$ [‰]	27.2
EPS6	Plastic strain, $\varepsilon_{pl,6}$ [‰]	48.0
EPS7	Plastic strain, $\varepsilon_{pl,7}$ [‰]	75.0
EPS8	Plastic strain, $\varepsilon_{pl,8}$ [‰]	110.0
TS1	Diameter of bar, ϕ [mm]	Varied
TS2	Diameter of bar, ϕ [mm]	Varied

Table A-16   Material parameters in LS-DYNA for the drop weight and supports.

LS-DYNA notation	Parameter	
RO	Mass density, ρ [kg/m^3]	Varied
E	Young's modulus, E_s [GPa]	205
PR	Poisson's ratio, v [-]	0.3

Appendix B   Matlab script for the 2DOF model

```matlab
%% 2DOF
%%
clc
clear all
close all
%%
% Chosen timestep
h=0.01;                                  % [ms]

%% Data for the beam

L_b=1000;                   % Length [mm]
b_b=100;                    % Width [mm]
H_b=100;                    % Height [mm]
A_b=b_b*H_b;                % Area of section [mm^2]
rho_b=2.4e-3;               % Density [g/mm^3]

g=9.82e-3;                  % [mm/ms^2] Gravity
m_b=rho_b*A_b*L_b;          % Mass [g]
kel_b=2.3240e3;             % Stiffness for the bilinear response [N/mm]
Rm_b=10.45e3;               % Resistance limit [N]
uel_b=Rm_b/kel_b;           % Maximal elastic displacement [mm]

% Transformation factors (Plastic)
kappampl_b=1/3;             % For the mass of the beam
kappaFpl_b=1;               % For the stiffness and force of the beam
kappamFpl_b=1/3;            % For the ratio mass/force for the beam

uRd_b=100000;               % Displacment limit [mm]. Set to a large value.

%% Data for the drop weight
v0_1=9.9;                   % Initial velocity for the weight [mm/ms]

H_w=258;                    % Height [mm]
r_w=40;                     % Radius [mm]
A_w=pi*r_w^2;               % Area of section [mm^2]
E_w=205e3;                  % Youngs modulus [MPa]
m_w=10000;                  % Mass [g]

kel_w=3.99e6;               % stiffness for elasto-platic response [N/mm]
Rm_w=50e3;                  % Resistance limit [N]

uel_w=Rm_w/kel_w;           % Maximal elastic displacement [mm]

% Transformation factors (Rectangular shape)
kappampl_w=1;               % For the ratio mass of the beam
kappaFpl_w=1;               % For the ratio force and stiffness of the
weight
kappamFpl_w=1;              % For the ratio mass/force for the weight

uRd_w=100000;               % Displacment limit [mm]. Set to a large value.

%% Critical Timestep
```

```matlab
Kel=[kel_w -kel_w; -kel_w kel_w+kel_b];    % Stiffness matrix for the
elastic part
M=[kappamFpl_w*m_w 0; 0 kappamFpl_b*m_b]; % Mass matrix

[L,X]=eigen(Kel,M);             % Solve for the eigenfrequencies
hcrit_1=2/sqrt(max(L));         % Critical timestep 1
hcrit=min(hcrit_1);

% The program is terminated if the timestep is to large
if h>hcrit
 fprintf('Choose a timestep that is smaller than %1.1e [ms]',hcrit)
 return
end

%% Initial conditions

t=0:h:40;                       % Load duration [ms]
% Force vector, constant and zero.
f=zeros(2,1);

% Initial plastic deformation for the beam
upl_w=0;
upl_b=0;

% Allocate space for the displacement, velocity and acceleration
u=zeros(2,length(t));           % [mm]
v=zeros(2,length(t)-1);         % [mm/ms]
a=zeros(2,length(t)-1);         % [mm/ms^2]

% Allocate space
upl_b_store=zeros(1,length(t)-1);        % [m]
R_store=zeros(2,length(t)-1);
Ir=zeros(2,length(t)-1);
Im=zeros(2,length(t)-1);
Ek=zeros(2,length(t)-1);
Wi=zeros(2,length(t)-1);
We=zeros(2,length(t)-1);


% Initial conditions for the system
u0=[0; 0];               u(:,1)=u0;
v0=[v0_1; 0];            v(:,1)=v0;
a0=inv(M)*(f-Kel*u0);    a(:,1)=a0;

% Displacement for timestep n=-1.
uminus1=u0-h*v0+(h^2)*a0/2;

%% Timestep n=0
% Generates n=1

% Relative displacement between the beam and weight
du=u(1,1)-u(2,1);

% Plastic displacement for the weight
if du>uel_w && du>max(u(1,:)-u(2,:))
    deltaupl_w=du-max(uel_w,max(u(1,:)-u(2,:)));
else
    deltaupl_w=0;
end
```

```matlab
upl_w=upl_w+deltaupl_w;

% Resistance for the weight
if du<0 || upl_w>uRd_w
    R_w=0;
else
R_w=max(0,kel_w*(du-upl_w));
end
R_store(1,1)=R_w;

% Stiffness for the weight
if du==0
    ks_w=kel_w;
elseif upl_w>uRd_w
    ks_w=0;
else
    ks_w=R_w/du;
end

% Plastic displacement for the beam
if u(2,1)>uel_b && (u(2,1)-uel_b)>upl_b        % Compression plastic
    deltaupl_b=u(2,1)-(uel_b+upl_b);
elseif u(2,1)<-uel_b+upl_b                      % Tension plastic
    deltaupl_b=-abs(u(2,1)+uel_b-upl_b);
else
    deltaupl_b=0;
end
upl_b=upl_b+deltaupl_b;

% Resistance for the beam
R_b=kel_b*(u(2,1)-upl_b);
R_store(2,1)=R_b;

% Stiffness for the beam
if u(2,1)==0
    ks_b=kel_b;
elseif upl_b>uRd_b
    ks_b=0;
else
    ks_b=R_b/u(2,1);
end

% New stiffness matrix
Ks=[ks_w -ks_w; -ks_w ks_w+ks_b];


upl_b_store(:,2)=upl_b;



% Calculate u(n=1) and a(n=1)
u(:,2)=inv(M/(h^2))*(f-(Ks-2*M/(h^2))*u(:,1)-(M/(h^2))*uminus1);
a(:,2)=inv(M)*(f-Ks*u(:,2));

%% Timestepping n=1-->
% Generates n=2 -->

for i=2:length(t)-1

% Relative displacement between the beam and weight
```

```matlab
du=u(1,i)-u(2,i);

% Plastic displacement for the weight
if du>uel_w && du>max(u(1,1:i-1)-u(2,1:i-1))
    deltaupl_w=du-max(uel_w,max(u(1,1:i-1)-u(2,1:i-1)));
else
    deltaupl_w=0;
end
upl_w=upl_w+deltaupl_w;

% Resistance for the weight
if du<0 || upl_w>uRd_w
    R_w=0;
else
R_w=max(0,kel_w*(du-upl_w));
end
R_store(1,i)=R_w;

% Stiffness for the weight
if du==0
    ks_w=kel_w;
elseif upl_w>uRd_w
    ks_w=0;
else
    ks_w=R_w/du;
end

% Plastic displacement for the beam
if u(2,i)>uel_b && (u(2,i)-uel_b)>upl_b          % Compression plastic
    deltaupl_b=u(2,i)-(uel_b+upl_b);
elseif u(2,i)<-uel_b+upl_b                       % Tension plastic
    deltaupl_b=-abs(u(2,i)+uel_b-upl_b);
else
    deltaupl_b=0;
end
upl_b=upl_b+deltaupl_b;

% Resistance for the beam
R_b=kel_b*(u(2,i)-upl_b);
R_store(2,i)=R_b;

% Stiffness for the beam
if u(2,i)==0
    ks_b=kel_b;
elseif upl_b>uRd_b
    ks_b=0;
else
    ks_b=R_b/u(2,i);
end

% New stiffness matrix
Ks=[ks_w -ks_w; -ks_w ks_w+ks_b];

upl_b_store(:,i)=upl_b;

% Calculation of u(n+1), v(n) and a(n)
u(:,i+1)=inv(M/h^2)*(f-(Ks-2*M/h^2)*u(:,i)-(M/h^2)*u(:,i-1));
v(:,i)=(u(:,i+1)-u(:,i-1))/(2*h);
a(:,i)=(u(:,i+1)-2*u(:,i)+u(:,i-1))/(h^2);
```

```matlab
% Calculation of impulse
% I=Integral av F över t
Ir(1,i)=Ir(1,i-1)+(R_store(1,i)+R_store(1,i-1))*h/2;
% I=Integral av F över t
Ir(2,i)=Ir(2,i-1)+(R_store(2,i)+R_store(2,i-1))*h/2;
% I=mv
Im(2,i)=M(2,2)*v(2,i);
% I=mv
Im(1,i)=M(1,1)*v(1,i);

% Calculation of work and kinetic energy
Wi(1,i)=Wi(1,i-1)+(R_store(1,i)+R_store(1,i-1))/2*(u(1,i)-u(1,i-1));
Wi(2,i)=Wi(2,i-1)+(R_store(2,i)+R_store(2,i-1))/2*(u(2,i)-u(2,i-1));
We(1,i)=0;                                            % No force
We(2,i)=We(2,i-1)+(R_store(1,i)+R_store(1,i-1))/2*(u(2,i)-u(2,i-1));
Ek(1,i)=(M(1,1)*v(1,i)^2)/2;                          % E=mv^2/2
Ek(2,i)=(M(2,2)*v(2,i)^2)/2;                          % E=mv^2/2
end


%% Plots
% Displacement of the weight and the beam
figure
hold on
title('Displacement')
xlabel('Time [ms]')
ylabel('Displacement [mm]')
plot(t,u(1,:))
plot(t,u(2,:))
legend('Drop weight','Beam')

% Velocity of the weight and the beam
figure
hold on
title('Velocity')
xlabel('Time [ms]')
ylabel('Velocity [m/s]')
plot(t(1:(length(t)-1)),v(1,:))
plot(t(1:(length(t)-1)),v(2,:))
legend('Drop weight','Beam')

% Acceleration of the weight and the beam
figure
hold on
title('Acceleration')
xlabel('Time [ms]')
ylabel('Acceleration [mm/ms^2]')
plot(t(1:(length(t)-1)),a(1,:))
plot(t(1:(length(t)-1)),a(2,:))
legend('Drop weight','Beam')

% Resistance of the weight and the beam
figure
hold on
title('Resistance')
xlabel('Time [ms]')
ylabel('Resistance [N]')
```

```matlab
plot(t(1:(length(t)-1)),R_store(1,:)/1000)
plot(t(1:(length(t)-1)),R_store(2,:)/1000)
legend('R_1','R_2')

% Impulse on the weight
figure
hold on
title('Impulse on the drop weight')
xlabel('Time [ms]')
ylabel('Impulse [kNs]')
plot(t(1:(length(t)-1)),Ir(1,:))
plot(t(1:(length(t)-1)),Im(1,:))
legend('I(R_1)','I(m_1)')

% Impulse on the beam
figure
hold on
title('Impulse on the beam')
xlabel('Time [ms]')
ylabel('Impulse [kNs]')
plot(t(1:(length(t)-1)),Ir(2,:))
plot(t(1:(length(t)-1)),Im(2,:))
legend('I(R_2)','I(m_2)')

% Work on the drop weight
figure
hold on
title('Work on the drop weight')
xlabel('Time [ms]')
ylabel('Work [Nmm]')
plot(t(1:(length(t)-1)),Wi(1,:))
plot(t(1:(length(t)-1)),Ek(1,:))
plot(t(1:(length(t)-1)),We(1,:))
legend('Wi_1','Ek_1','We_1')

% Work on the beam
figure
hold on
title('Work on the beam')
xlabel('Time [ms]')
ylabel('Work [Nmm]')
plot(t(1:(length(t)-1)),Wi(2,:))
plot(t(1:(length(t)-1)),Ek(2,:))
plot(t(1:(length(t)-1)),We(2,:))
legend('Wi_2','Ek_2','We_2')

umax=max(u(2,:));
fprintf('The maximal displacement of the beam is %.2f mm', umax)
```

Appendix C   Mathcad calculations

Properties of the beam

Geometry

$L_b := 1000 \; mm$ $\qquad\qquad$ $c := 20 \; mm$

$h_b := 100 \; mm$ $\qquad\qquad$ $\phi_{reinf} := 6 \; mm$

$b_b := 100 \; mm$

Material properties - concrete

$f_{ck} := 28 \; MPa$ $\qquad\qquad\qquad$ Target characteristic strength

$f_{cm} := f_{ck} + 8 \; MPa = 36 \; MPa$ $\qquad\qquad$ EC 2

$f_{ctm} := 0.3 \left(\dfrac{f_{ck}}{MPa} \right)^{0.6667} \cdot MPa = 2.767 \; MPa$ $\qquad$ EC 2

$E_{cm} := 22 \left(\dfrac{f_{cm}}{10 \cdot MPa} \right)^{0.3} \cdot GPa = 32.308 \; GPa$ $\qquad$ EC 2

$E_{cm} := 32 \; GPa$ $\qquad\qquad\qquad$ Assumed in new model

$\rho_c := 0.0024 \; \dfrac{gm}{mm^3} = \left(2.4 \cdot 10^3 \right) \dfrac{kg}{m^3}$ $\qquad$ Assumed in new model

$\alpha_R := 0.81$

$\beta_R := 0.416$

Material properties - Steel

$f_{ym} := 623 \; MPa$ $\qquad\qquad$ Mean value from tests

$E_s := 196 \; GPa$ $\qquad\qquad$ Calculated from test results

$\alpha := \dfrac{E_s}{E_{cm}} = 6.125$

Moment capacity of the beam

$A_{si} := \dfrac{\phi_{reinf}^2 \cdot \pi}{4} = 28.274 \; mm^2$

$d := h_b - c = 80 \; mm$ $\qquad\qquad$ $d' := c = 20 \; mm$

$$x := \frac{f_{ym} \cdot 2 \cdot A_{si}}{\alpha_R \cdot f_{cm} \cdot b_b} = 12.082 \; \boldsymbol{mm}$$

$$M_{Rd} := \alpha_R \cdot f_{cm} \cdot b_b \cdot x \cdot (d - \beta_R \cdot x) = 2.641 \; \boldsymbol{kN \cdot m}$$

Resistance limit for the beam

$$R_b := \frac{4 \, M_{Rd}}{L_b} = 10.565 \; \boldsymbol{kN}$$

Reduced resistance limit for the beam, with regard to self-weigth

$$g_b := \rho_c \cdot g \cdot b_b \cdot h_b = 0.235 \; \frac{\boldsymbol{N}}{\boldsymbol{mm}}$$

$$R_{b.red} := R_b - \frac{g_b \cdot L_b}{2} = 10.448 \; \boldsymbol{kN} \qquad\qquad \frac{g_b \cdot L_b}{2} = 117.68 \; \boldsymbol{N}$$

Plastic limit for the equivalent concrete

$$W_{el} := \frac{b_b \cdot h_b^{\,2}}{6} = \left(1.667 \cdot 10^5\right) \; \boldsymbol{mm}^3$$

$$M_{Rd.red} := M_{Rd} - \frac{g_b \cdot L_b^{\,2}}{8} = 2.612 \; \boldsymbol{kN \cdot m}$$

$$f_{y.red} := \frac{M_{Rd.red}}{W_{el}} = 15.671 \; \boldsymbol{MPa}$$

Equivalent elastic modulus for the equivalent concrete

$$I_I := \frac{b_b \cdot h_b^{\,3}}{12} = \left(8.333 \cdot 10^6\right) \; \boldsymbol{mm}^4$$

$$x_{II} := -\frac{\alpha \cdot 2 \cdot A_{si}}{b_b} + \sqrt{\left(\frac{\alpha \cdot 2 \cdot A_{si}}{b_b}\right)^2 + \frac{2 \cdot \alpha \cdot 2 \cdot A_{si} \cdot d}{b_b}} = 20.331 \; \boldsymbol{mm}$$

$$I_{II} := \frac{b_b \cdot x_{II}^{\,3}}{3} + \alpha \cdot 2 \cdot A_{si} \cdot (d - x_{II})^2 = \left(1.513 \cdot 10^6\right) \; \boldsymbol{mm}^4$$

$$E_{eq} := E_{cm} \cdot \frac{I_{II}}{I_I} = 5.811 \; \boldsymbol{GPa}$$

Stiffness of the beam for the 2DOF model

$$k_{el\_b} := \frac{48 \cdot E_{cm} \cdot I_{II}}{L_b^{\,3}} = \left(2.324 \cdot 10^6\right) \; \frac{\boldsymbol{N}}{\boldsymbol{m}}$$

Fracture energy and crack width

The fracture energy was determined in Jönsson and Stenseke (2018) and calculated according to the CEB-FIP 2010 model code. From those values, a rounded number is chosen as input for the model.

$$G_F := 137.14 \; \frac{N}{m}$$ Measured 2018

$$G_{Fcode} := 73 \cdot \left(\frac{f_{cm}}{MPa} \right)^{0.18} = 139.142$$ Calculated

$$G_F := 140 \; \frac{N}{m}$$ Assumed in new model

$$f_{ctm} = 2.767 \; MPa$$ Calculated

$$f_{ctm} := 2.8 \; MPa$$ Assumed in new model

$$w_f := \frac{4.444 \cdot G_F}{f_{ctm}} = 0.222 \; mm$$

$$w_{fTetra} := 0.56 \cdot w_f = 0.124 \; mm$$

If linear tensile damage formulation is used:

$$w_{flinear} := \frac{2 \cdot G_F}{f_{ctm}} = 0.1 \; mm$$

$$w_{fTetralinear} := 0.56 \cdot w_{flinear} = 0.056 \; mm$$

Equvialent element length

$$V_{beam} := L_b \cdot h_b \cdot b_b = \left(1 \cdot 10^7 \right) \; mm^3$$

$$n_{el} := 896914$$ From the LS-DYNA model

$$l_{el.eq} := \sqrt[3]{\frac{V_{beam}}{n_{el}}} = 2.234 \; mm$$

$$\varepsilon_{crack} := \frac{w_f}{l_{el.eq}} = 0.099$$

Bond-slip

Calculation of the maximum bond stress for the bond-slip relationship according to the CEB-FIP model code 2010 assuming good bond conditions.

$$\tau_{max} := 2.5 \cdot \sqrt{\frac{f_{cm}}{MPa}} \cdot MPa = 15 \ MPa \qquad\qquad s_1 := 1.0 \ mm$$

Eccentricity factor

$$f_{bc} := 1.16 \cdot f_{cm} = 41.76 \ MPa$$

$$\varepsilon := \frac{f_{ctm} \cdot \left(f_{bc}^{\ 2} - f_{cm}^{\ 2}\right)}{f_{bc} \cdot \left(f_{cm}^{\ 2} - f_{ctm}^{\ 2}\right)} = 0.023$$

$$ECC := \frac{1 + \varepsilon}{2 - \varepsilon} = 0.518$$

Properties of the weight

$$E_w := 205 \ GPa$$

$$r_w := 40 \ mm$$

$$h_w := 258 \ mm$$

$$A_w := \pi \cdot r_w^{\ 2} = \left(5.027 \cdot 10^3\right) \ mm^2$$

Stiffness of the weight for the 2DOF model

$$k_{el\_w} := \frac{E_w \cdot A_w}{h_w} = \left(3.994 \cdot 10^9\right) \frac{N}{m}$$

Appendix D   Evaluation of Contact Theory

A more thorough way of treating the interaction between the drop weight and the beam is to determine the contact stiffness using contact mechanics. By using one method based on Hertz contact theory, described by Fujikake *et al.* (2006), many parameters are taken in consideration to calculate the stiffness for the interaction between two objects. The equations used in this section are applicable for calculating the stiffness of the interaction between a flat and a rounded surface. The roundness of the surface and material parameters of both materials are considered. In this study an evaluation was made of the influence on the displacement for this more advanced way of calculating the stiffness compared to the more simplified way, described in Section 5.2.2. The contact law describes the relation between the impact force, F, and local deformation at the impact zone, δ, as:

$$F = k \cdot \delta^{3/2} \tag{D.1}$$

where k is a stiffness depending on the Young's modulus, E, and Poisson's ratio, ν, for body 1 and 2 as well as the radius of the rounded surface, r_1. It is calculated as:

$$k = \frac{4\sqrt{r_1}}{3} \left[\frac{1 - \nu_1^2}{E_1} + \frac{1 - \nu_2^2}{E_2} \right]^{-1} \tag{D.2}$$

The force-displacement relation is nonlinear, but in this project, the new stiffness of the interaction, $k_{w,Hertz}$, was calculated by assuming a linear relationship at a force corresponding to the resistance of 50 kN, see Figure D-1.
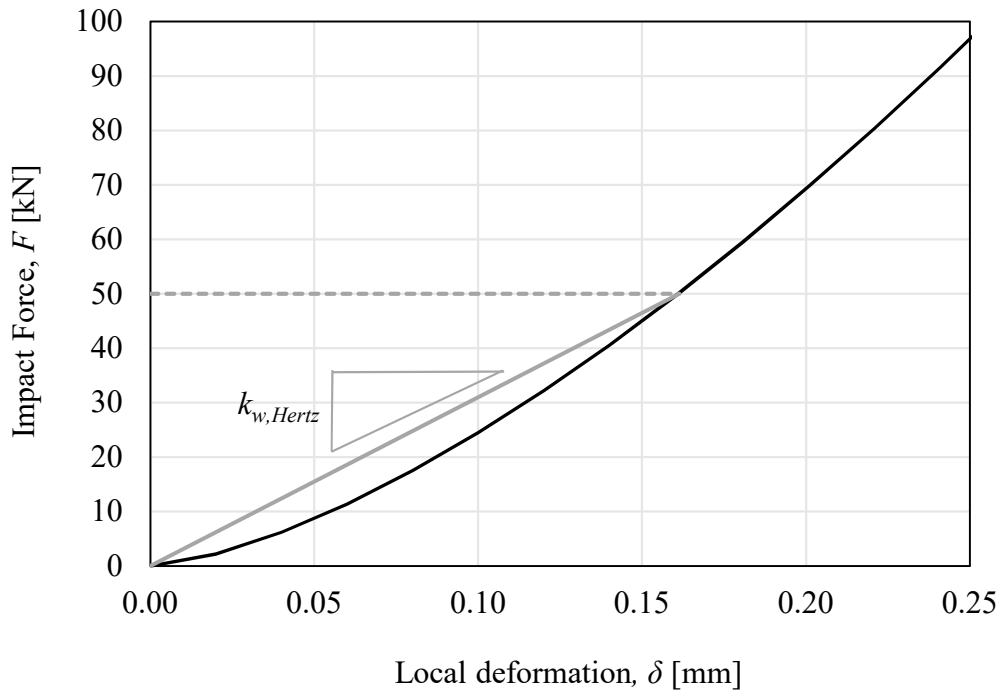
Figure D-1   Relation between impact force and local deformation according to Hertz contact theory.

The resulting stiffness of the spring representing the interaction calculated using this method is presented in Table D-1 together with the original stiffness of the interaction and the beam.

Table D-1 *Comparison of the stiffness of the spring representing the interaction calculated using different methods and the stiffness of the spring representing the beam.*

	Stiffness [N/m]
Interaction Hertz, $k_{w,Hertz}$	$3.1 \cdot 10^8$
Interaction simplified, k_w	$4.0 \cdot 10^9$
Beam	$2.4 \cdot 10^6$

When the new stiffness is calculated in this way, the difference on the force-displacement is negligible, see Figure D-2.
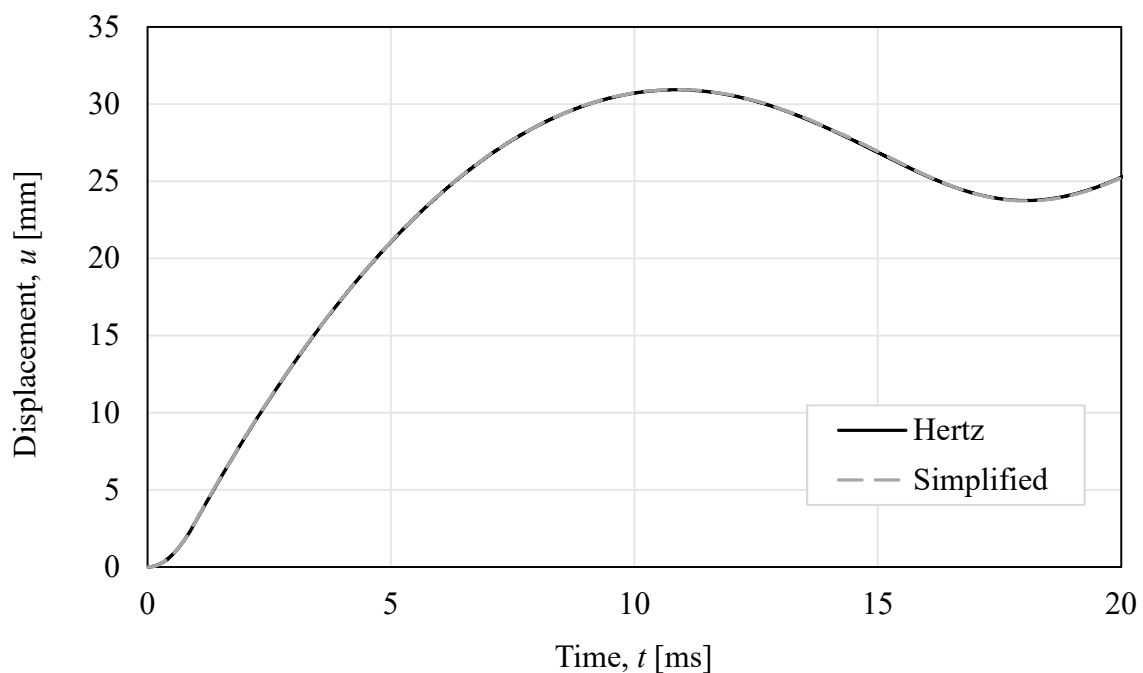
Figure D-2 *Displacement in the elasto-plastic case using the simplified stiffness and stiffness according to Hertz contact theory.*

Since the difference in displacement was very small it was of interest to see if the difference in displacement would be larger between the two ways of modelling the stiffness if the response of the interaction between the weight and the beam were elastic. The result is shown in Figure D-3 and the effect was still very small. This is due to that the stiffness for the interaction was still much higher than the stiffness of the beam and therefore the change had no significant influence.

CHALMERS, *Architecture and Civil Engineering*, Master's Thesis, ACX30-18-36
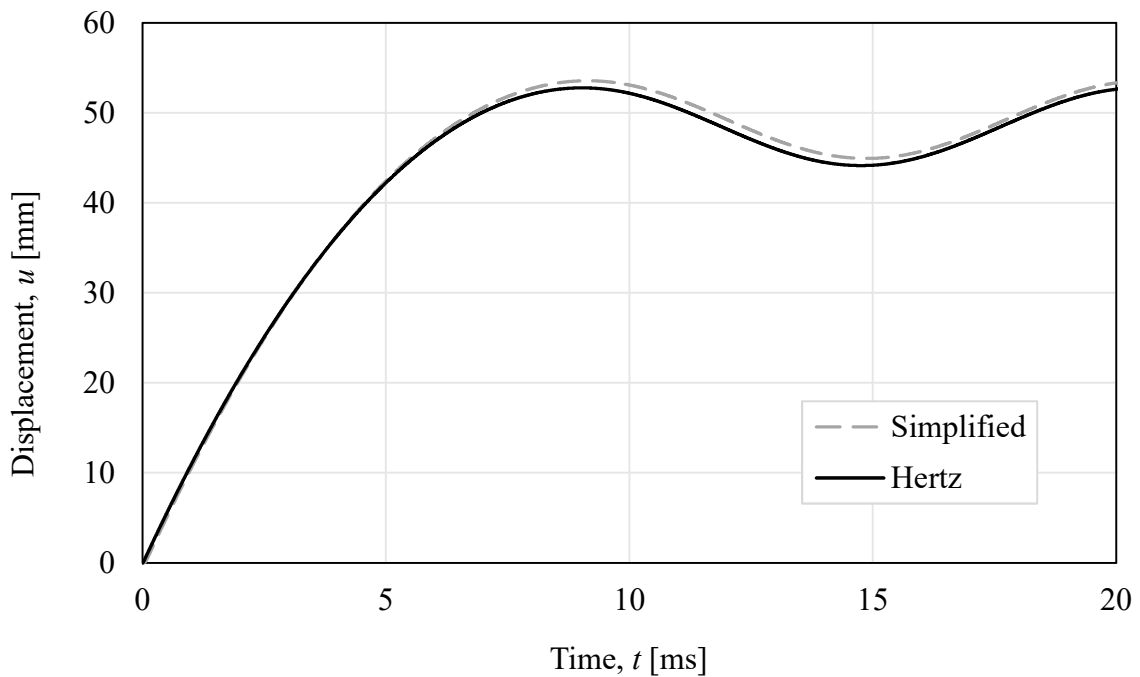
Figure D-3   Displacement for an elastic spring using the simplified stiffness and stiffness according to Hertz contact theory.

From this short evaluation it can be seen that the influence of the way of calculating the stiffness is small and therefore, the simplified expression has been used in this study. The use of Hertz contact law could be more thoroughly evaluated in a future study.

Appendix E   Compressive damage in LS-DYNA

In some load cases there were convergence issues in LS-DYNA due to local compressive failure of the concrete. To avoid this, the compressive damage variable, ε_{fc}, explained in Section 6.5.1, was increased. An evaluation was made of how the results were influenced by this modification. In the evaluation, the values presented in Table E-1 were investigated.

Table E-1   Evaluated values of the compressive damage variable.

Standard value, ε_{fc} [-]	0.001
Evaluated values, ε_{fc} [-]	0.002
	0.005
	0.010

Three different load cases that converged using the original value were investigated, they are presented in Table E-2.

Table E-2   The different load cases evaluated with regard to compressive damage variable.

	Mass of drop-weight, m [kg]	Drop height, h [m]
Standard case	10	5
Load case 1	20	5
Load case 2	10	2.5

In Figure E-1, the time-displacement curves for the different load cases with different values of the compressive damage variable can be seen.
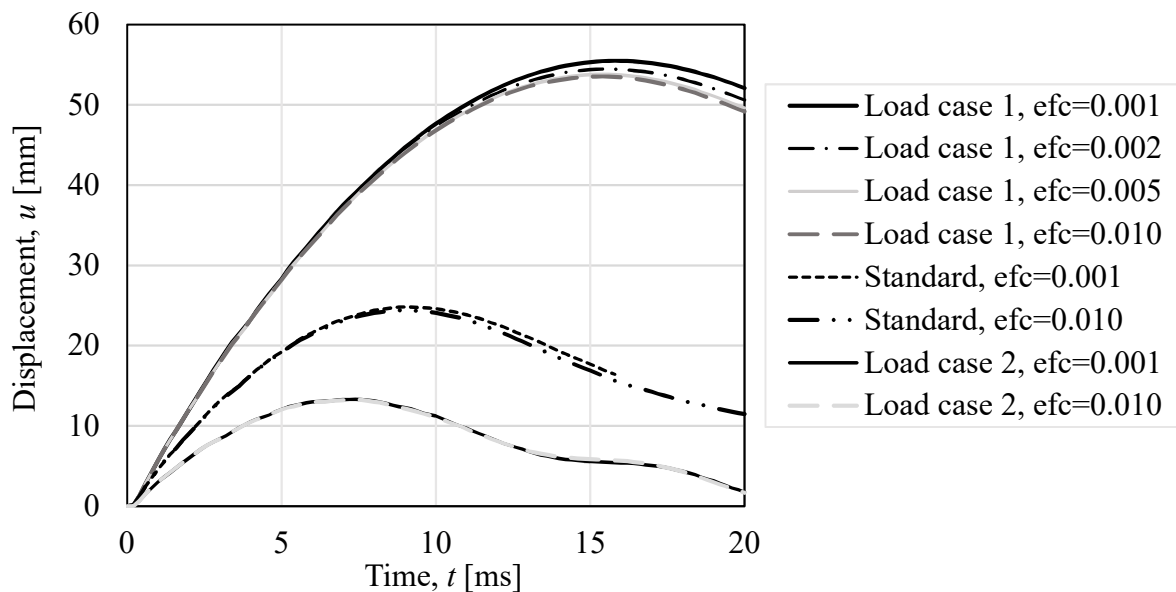
Figure E-1   Displacements for three different load cases using different values of the compressive damage variable.

The displacement was decreased when the damage variable was increased. This is reasonable since the larger value of the damage variable gives a more ductile behaviour of concrete in compression and thereby a higher capacity of the compressive zone. As shown in the graph, the difference was larger for Load case 1 with larger displacements. For the standard case and Load case 2, the differences were very small even when the damage variable was increased by a factor of ten. Therefore, no other values were investigated for these two cases. For Load case 1, the difference for the increase of ten times was more noticeable, and therefore an increase of two and five times were performed as well. To further investigate the influence of the compressive damage variable in this case, the crack patterns are compared in Table E-3.

Table E-3   *Crack patterns for Load case 1 using different values of the compressive damage variable.*

ε_{fc}	Crack pattern
0.001, standard	
0.002	
0.005	
0.010	
Principle strain [%]	0 0.99 1.98 2.97 3.96 4.95 5.94 6.93 7.92 8.91 9.9
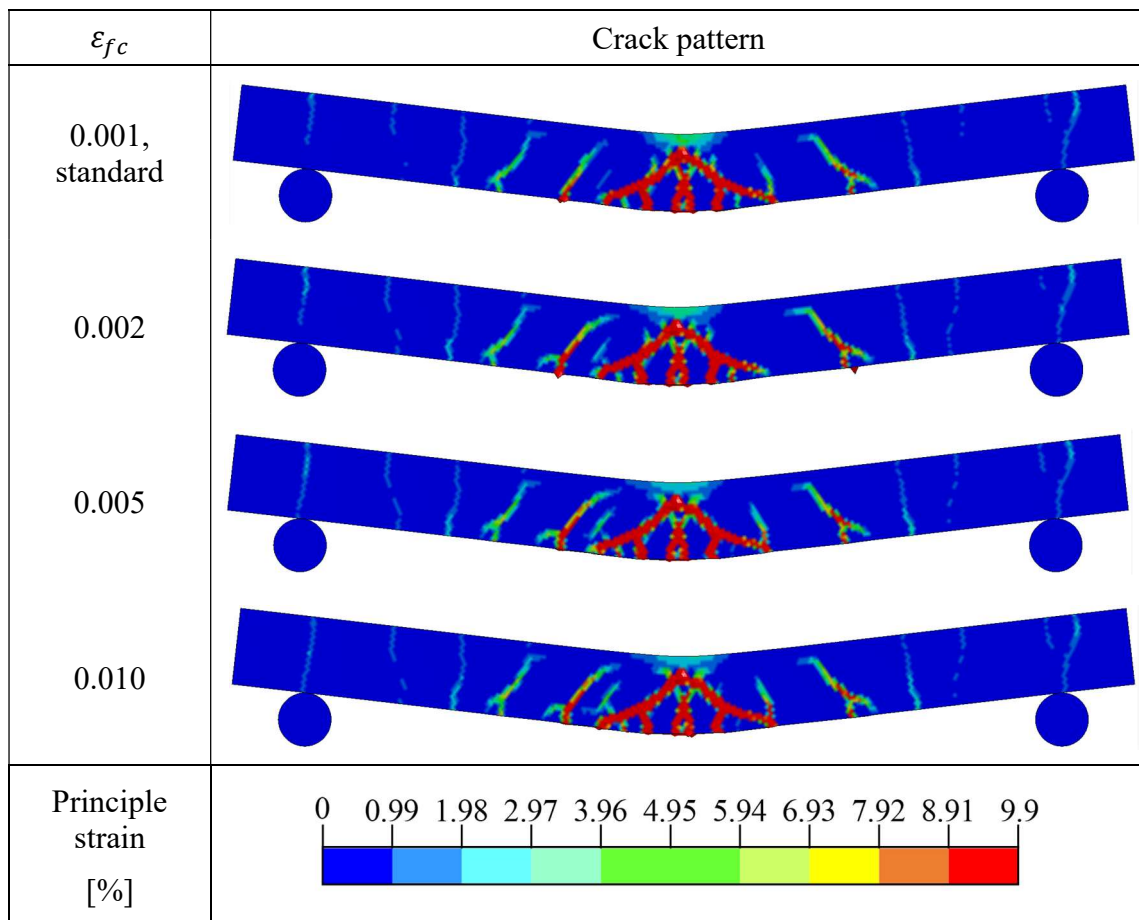
The crack patterns are very similar but it can be seen that there is a difference in the compressive zone. Since this part of the strain pattern was not of interest in this study, and the differences in the more relevant parts were considered negligible, increasing the value of the compressive damage variable in the cases with convergence issues was considered to be acceptable.

A final evaluation of two cases where the value of the compressive damage variable needed to be changed was made to confirm that the modification was applicable. In Figure E-2 the time-displacement curves for these cases are presented.
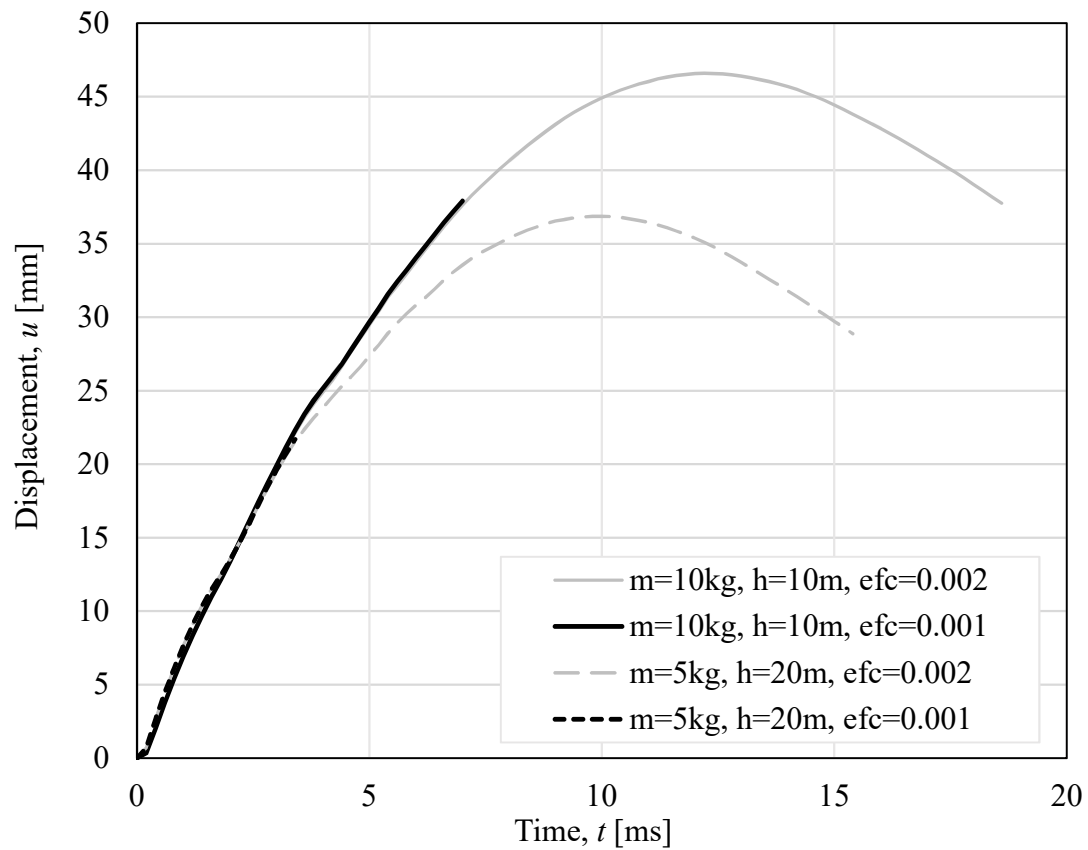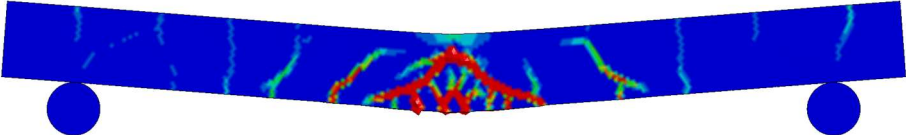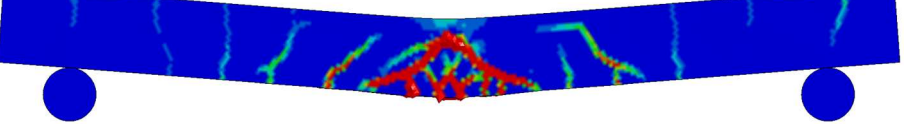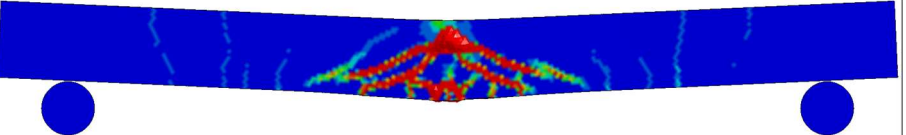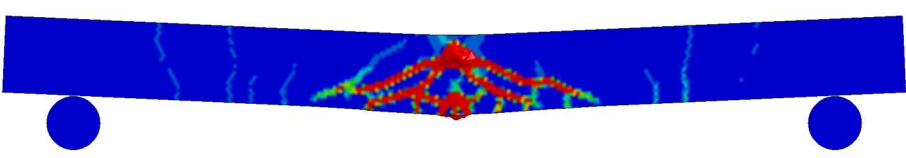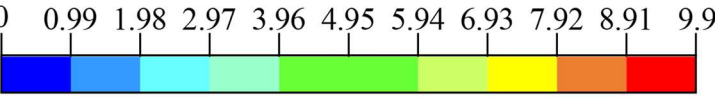
Figure E-2   Displacement for two load cases where convergence issues arose using the standard value of the compressive damage variable.

It can be seen that the time-displacement curves using different values of the compressive damage variable showed a similar behaviour until convergence issues arose. The strain patterns from the latest timesteps possible are compared to verify that there were no major differences, see Table E-4.

Table E-4   *Crack pattern for two cases just before convergence issues arose compared with strain pattern for the same timestep with a higher compressive damage variable.*

Load case	Crack pattern
m = 10 kg, h = 10 m, efc = 0.001	
m = 10 kg, h = 10 m, efc = 0.002	
m = 5 kg, h = 20 m, efc = 0.001	
m = 5 kg, h = 20 m, efc = 0.002	
Principle strain [%]	0 0.99 1.98 2.97 3.96 4.95 5.94 6.93 7.92 8.91 9.9

The conclusion from this evaluation was that the compressive damage variable can be changed to a larger value when needed. When that is done, the used value should be presented.

Appendix F   Results from parametric study in 2DOF and Abaqus

F.1   Input values for the parametric study

The input values for the nine different beams studied in the parametric study using 2DOF and Abaqus are presented in Table F-1. The descriptions of the studied beams are presented in Table F-2.

Table F-1   Input values for the parameters of the beam that were varied in the 2DOF model and Abaqus model.

	2DOF		Abaqus	
Beam	k_b [N/m]	$R_{m,b}$ [kN]	E_{eq} [GPa]	$f_{y.red}$ [MPa]
1	$1.72 \cdot 10^6$	7.37	4.30	11.05
2	$2.32 \cdot 10^6$	10.45	5.80	15.67
3	$3.66 \cdot 10^6$	17.69	9.10	26.53
4	$2.59 \cdot 10^6$	10.68	3.20	8.01
5	$13.33 \cdot 10^6$	24.42	4.20	9.16
6	$0.21 \cdot 10^6$	3.51	4.30	10.53
7	$0.29 \cdot 10^6$	5.05	5.80	15.14
8	$0.46 \cdot 10^6$	8.67	9.10	26.00
9	$0.50 \cdot 10^6$	9.62	10.00	28.87

Table F-2   Description of the beams studied in the parametric studies.

Beam	Width, b [m] 0.1	0.2	Height, h [m] 0.1	0.2	Length, L [m] 1.0	2.0	Reinforcement 2φ5	2φ6	2φ8	4φ6
1	●		●		●		●			
2	●		●		●			●		
3	●		●		●				●	
4		●	●		●			●		
5	●			●	●			●		
6	●		●			●	●			
7	●		●			●		●		
8	●		●			●			●	
9	●		●			●				●

F.2 Time-displacement curves from 2DOF and Abaqus

The time-displacement curves from 2DOF and Abaqus for all the load cases for each beam are presented below. In Figure F-1 the results for Beam 1 are presented.
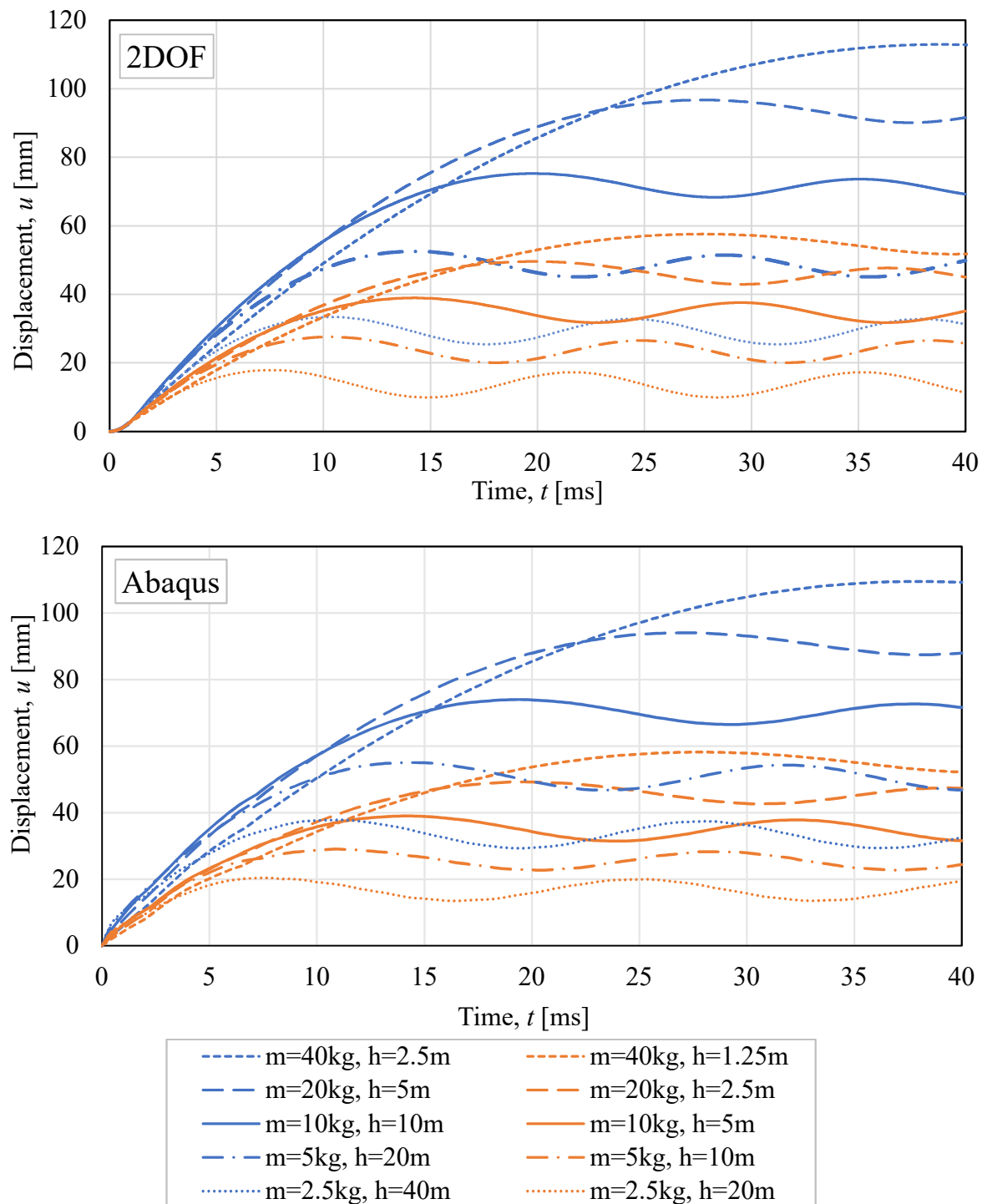
Figure F-1 Time-displacement curves for all load cases from 2DOF and Abaqus for Beam 1.

CHALMERS, *Architecture and Civil Engineering*, Master's Thesis, ACX30-18-36

In Figure F-2, the results for Beam 2 are presented.
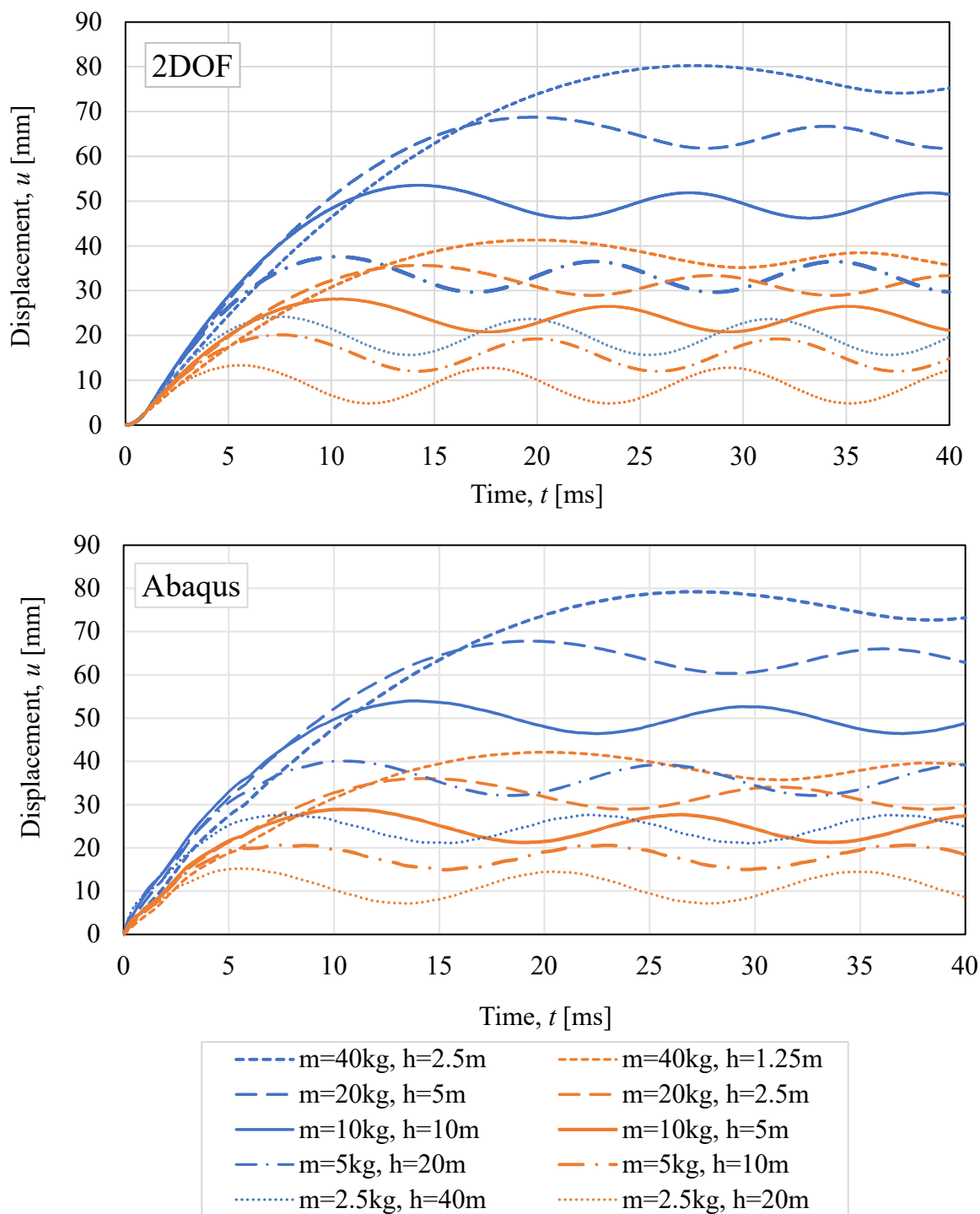
Figure F-2   *Time-displacement curves for all load cases from 2DOF and Abaqus for Beam 2.*

In Figure F-3, the results for Beam 3 are presented.
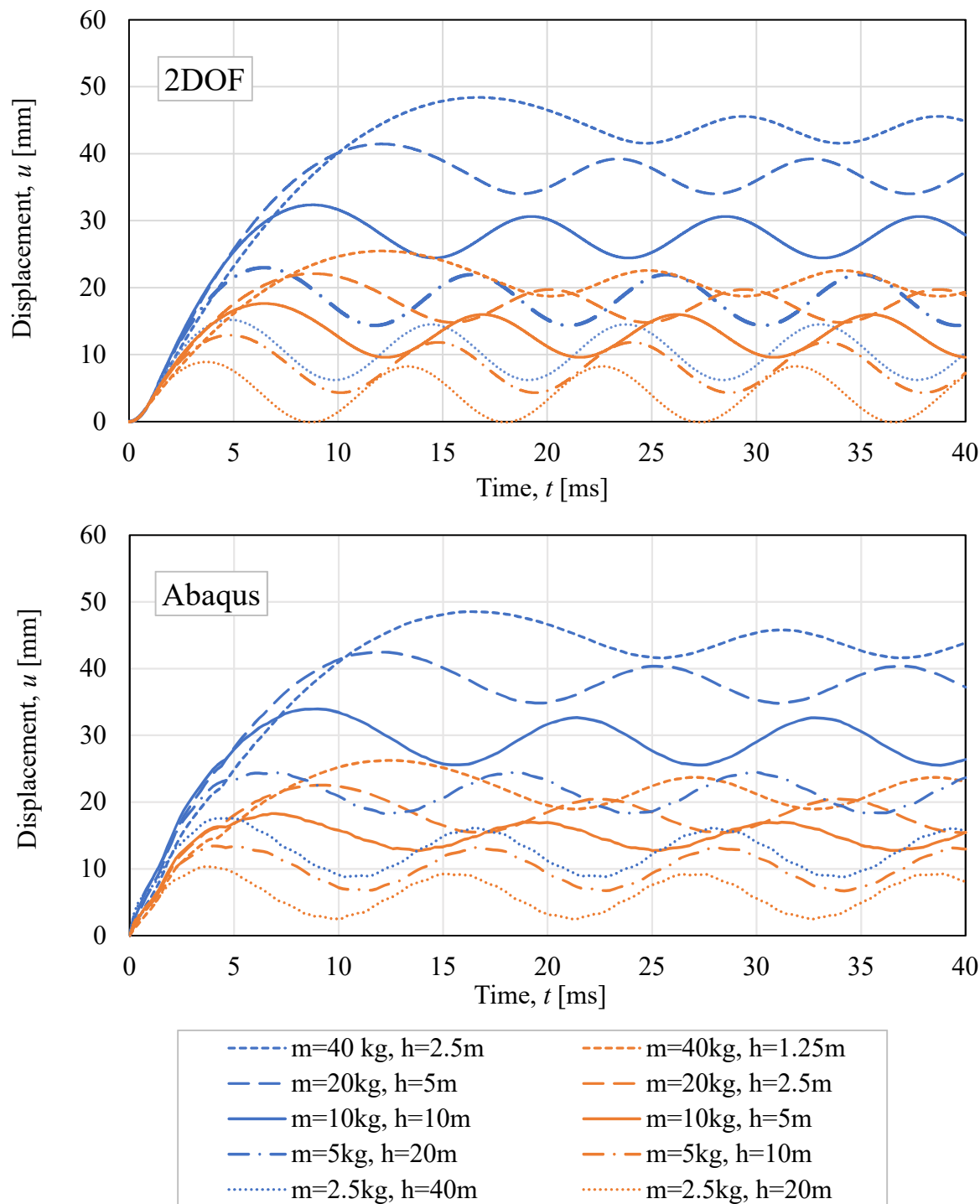
Figure F-3   *Time-displacement curves for all load cases from 2DOF and Abaqus for Beam 3.*

In Figure F-4 the results for Beam 4 are presented.
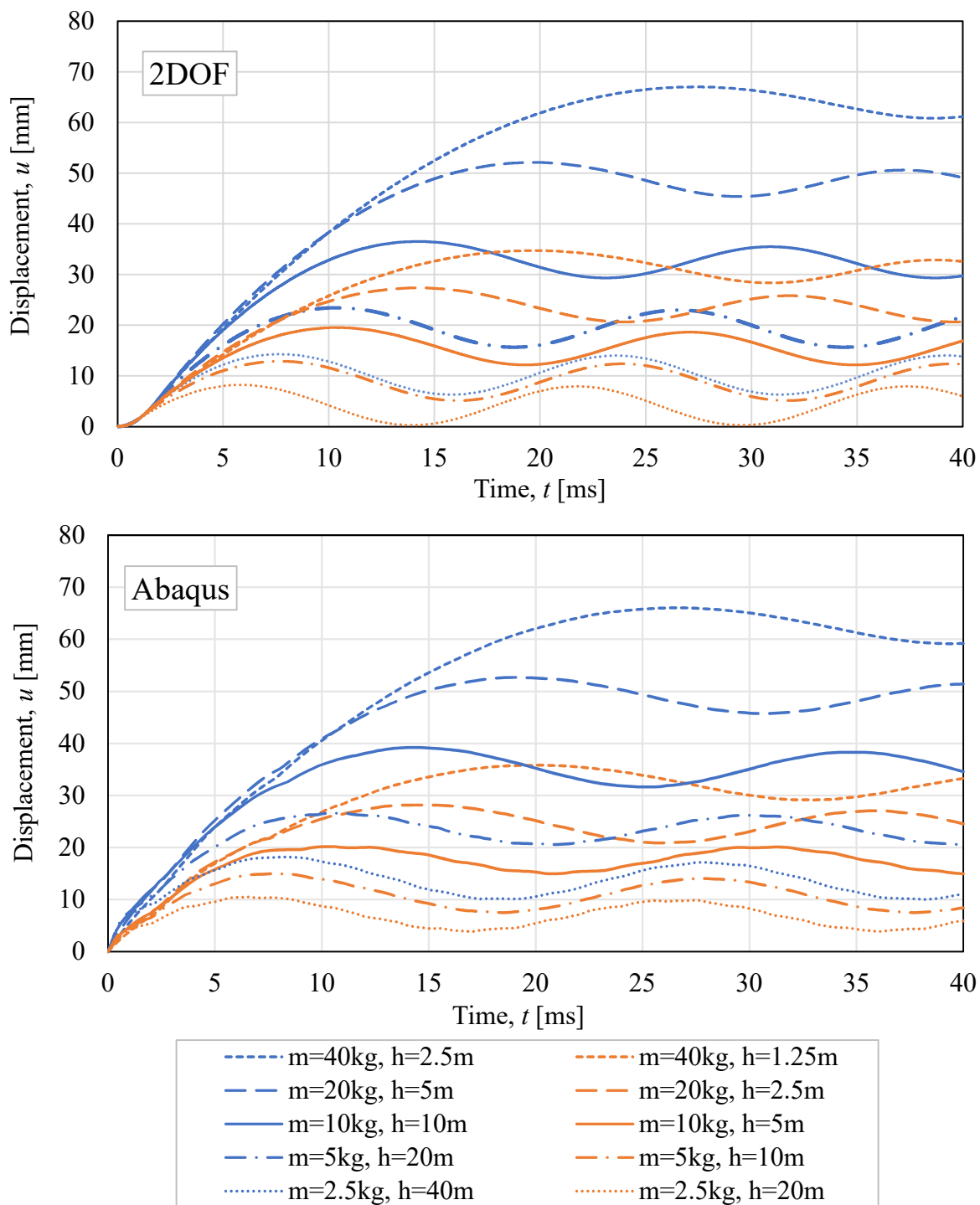
Figure F-4   Time-displacement curves for all load cases from 2DOF and Abaqus for Beam 4.

In Figure F-5, the results for Beam 5 are presented.
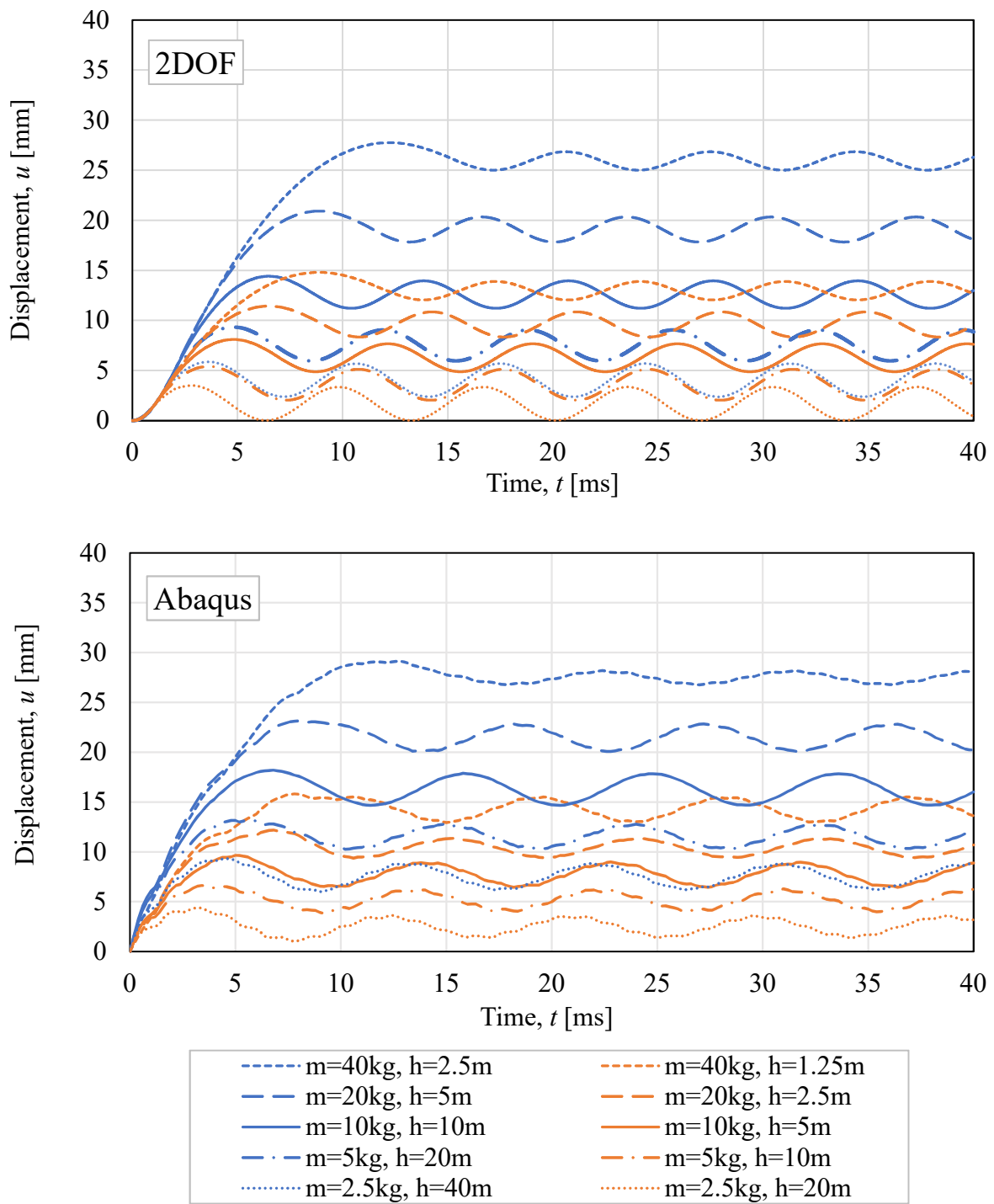
Figure F-5   *Time-displacement curves for all load cases from 2DOF and Abaqus for Beam 5.*

In Figure F-6, the results for Beam 6 are presented.
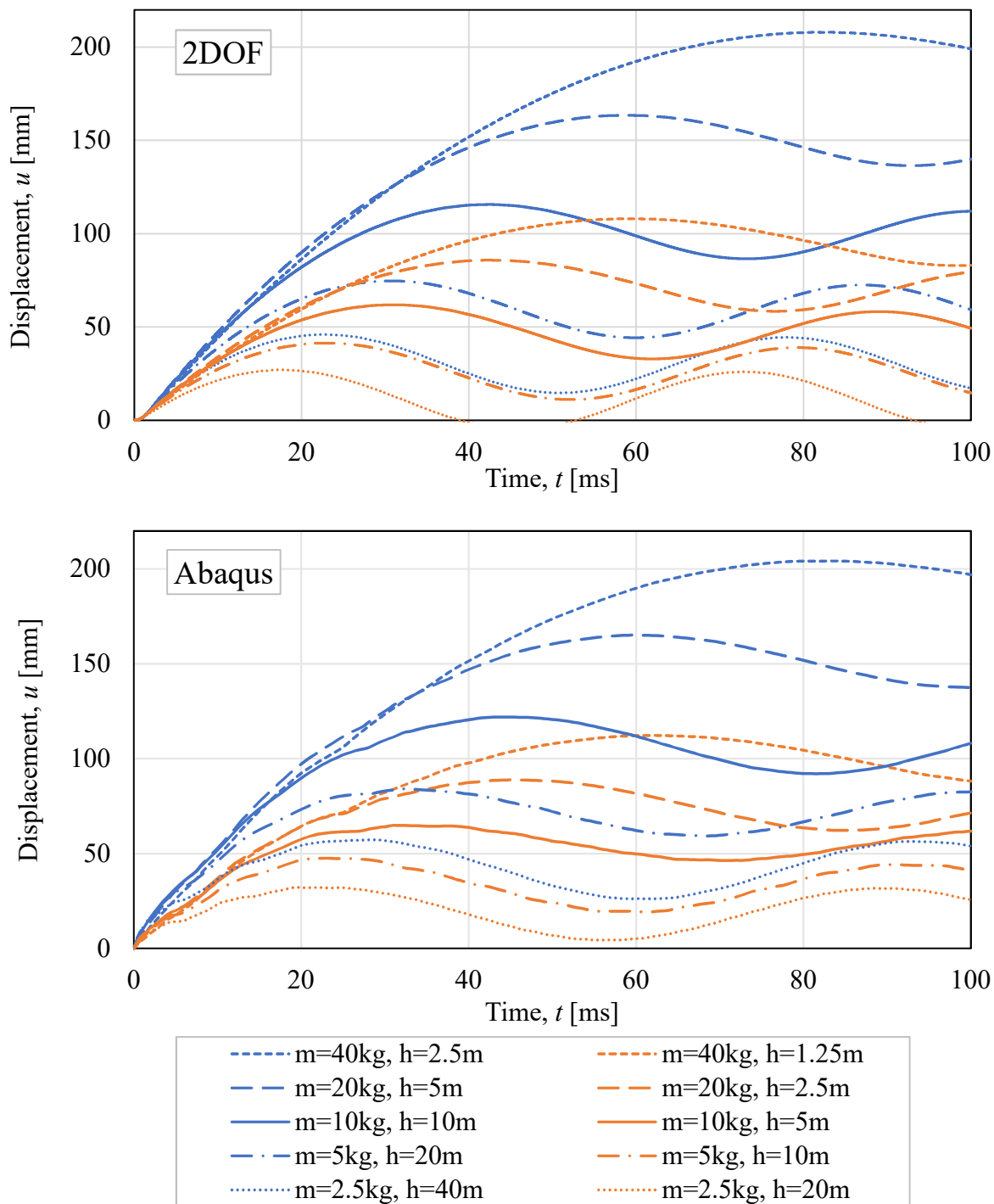
Figure F-6   *Time-displacement curves for all load cases from 2DOF and Abaqus for Beam 6.*

In Figure F-7, the results for Beam 7 are presented.
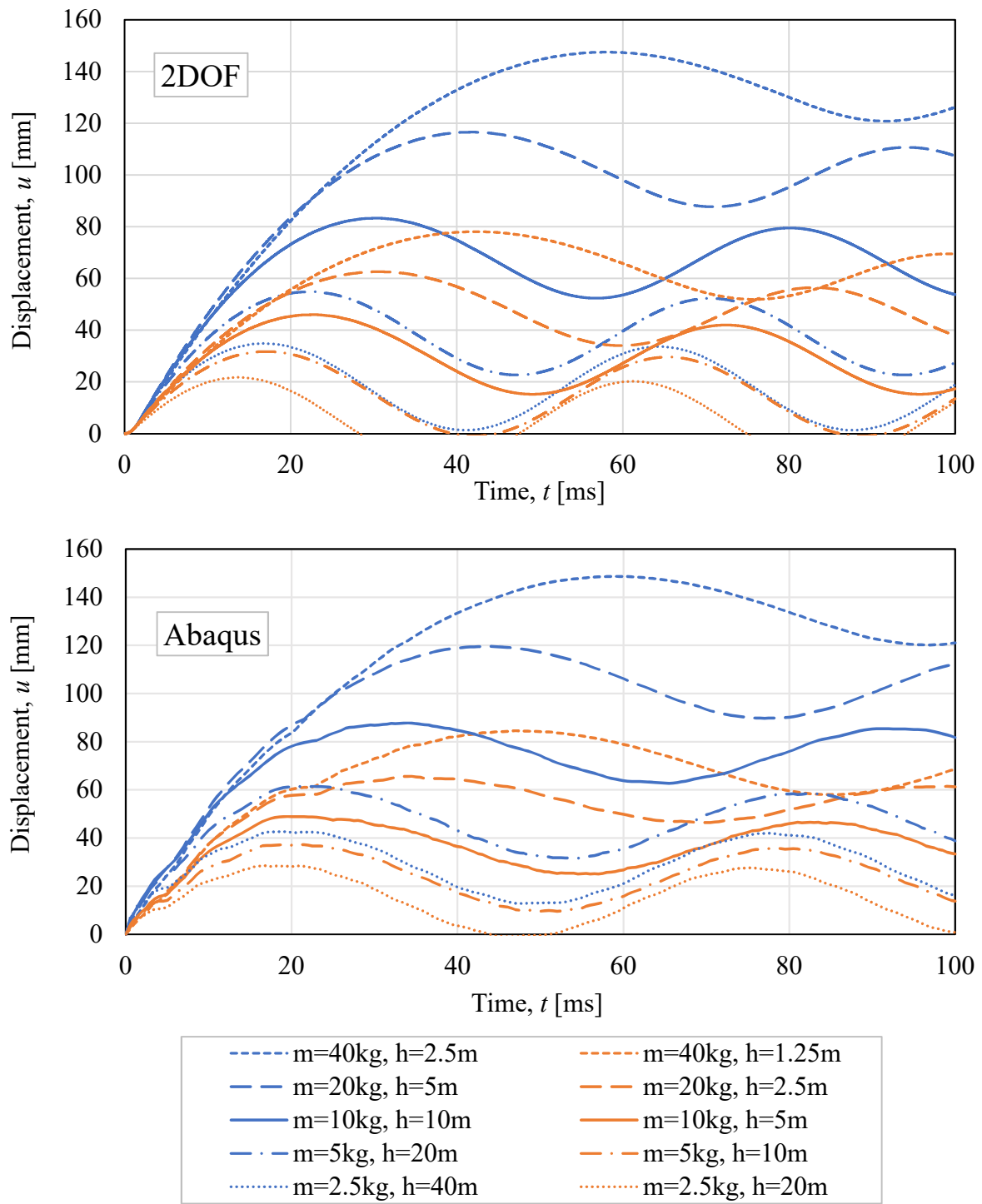
Figure F-7   Time-displacement curves for all load cases from 2DOF and Abaqus for Beam 7.

In Figure F-8, the results for Beam 8 are presented.
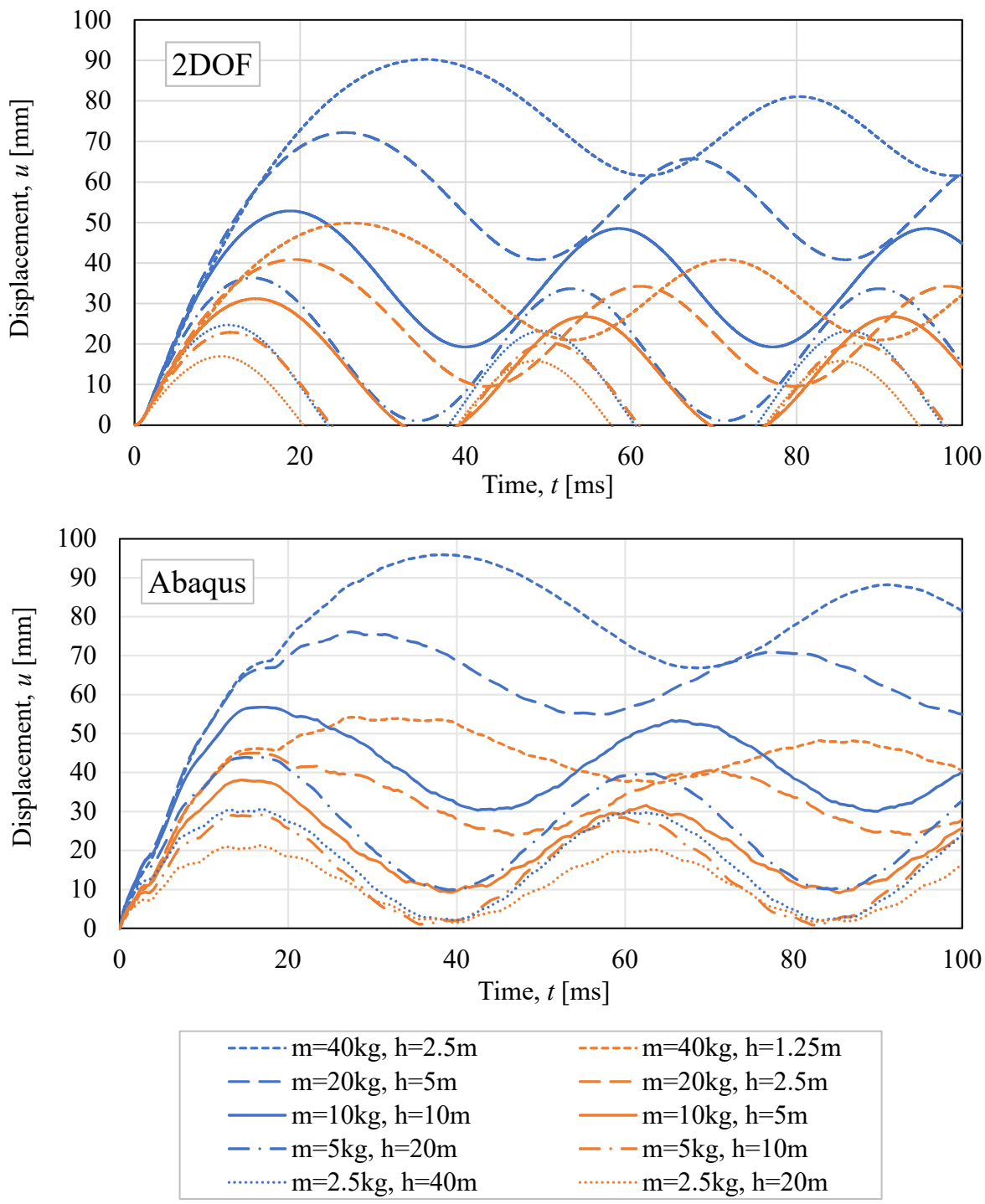
Figure F-8   *Time-displacement curves for all load cases from 2DOF and Abaqus for Beam 8.*

In Figure F-9, the results for Beam 9 are presented.
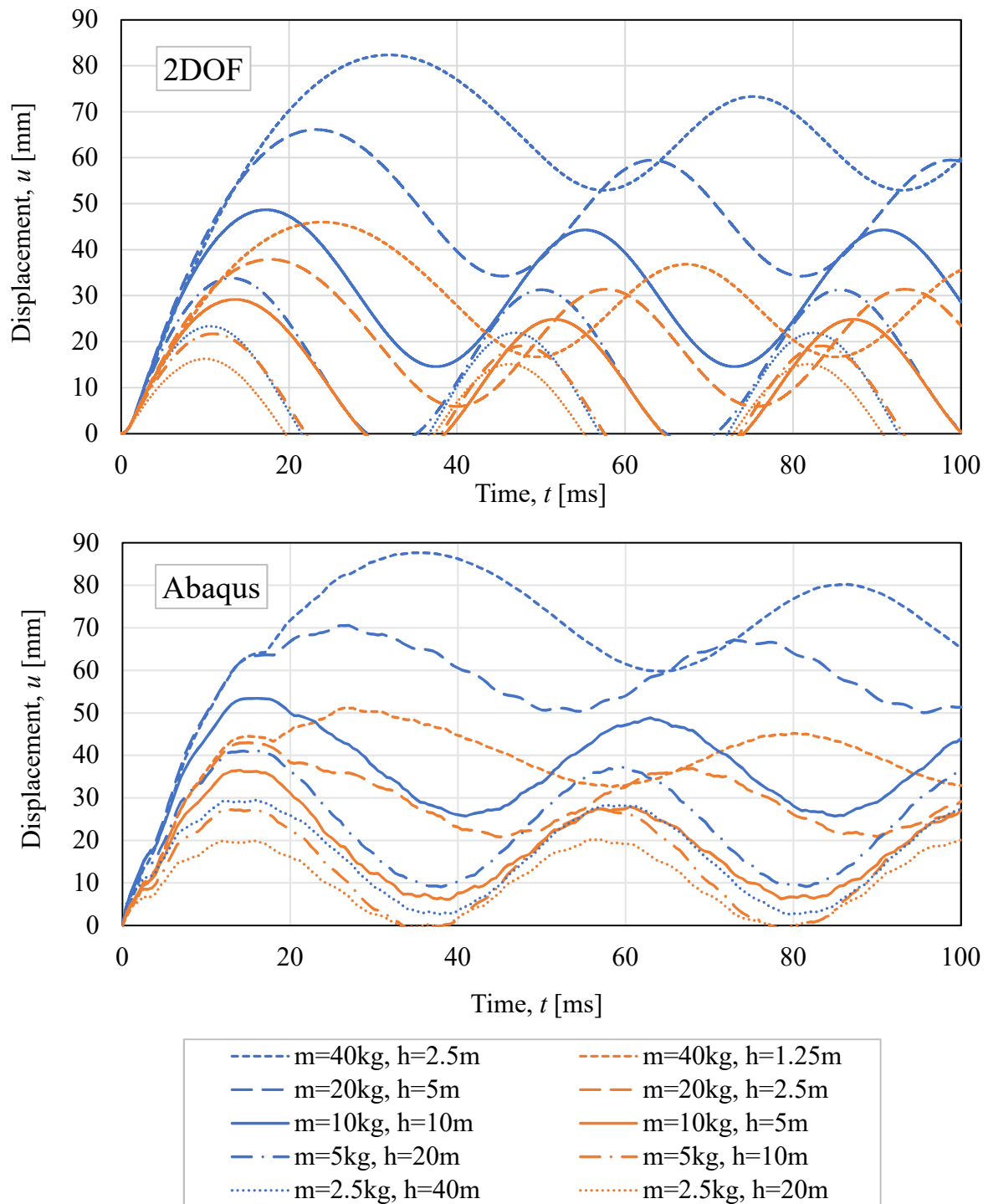
Figure F-9   *Time-displacement curves for all load cases from 2DOF and Abaqus for Beam 9.*

    CHALMERS, *Architecture and Civil Engineering*, Master's Thesis, ACX30-18-36

F.3 Displacement and energy ratios

The transferred energy for the hand calculation is calculated according to equation (F.1).

$$W_y = \frac{m_w}{m_w + m_b} E_{k,0} \tag{F.1}$$

For the displacement, equations (F.2), (F.3) and (F.4) are used.

$$W_y = W_i \tag{F.2}$$

$$u_{el-pl.el} = \frac{R_m}{k} \tag{F.3}$$

$$u_{tot} = \begin{cases} \dfrac{2\,W_i}{R_m} & if \quad \dfrac{R_m u_{el-pl.el}}{2} \geq W_i \\[3mm] \dfrac{W_i}{R_m} + \dfrac{u_{el-pl.el}}{2} & if \quad \dfrac{R_m u_{el-pl.el}}{2} < W_i \end{cases} \tag{F.4}$$

To obtain the transferred energy for Abaqus and 2DOF the following equations are used where the total displacement, u_{tot}, is the displacement obtained from the analysis.

$$u_{el-pl.el} = \frac{R_m}{k} \tag{F.5}$$

$$W_i = \begin{cases} \dfrac{k\,u_{tot}^2}{2} & if \quad u_{el-pl.el} \geq u_{tot} \\[3mm] \dfrac{R_m}{2}(u_{el-pl.el} + 2(u_{tot} - u_{el-pl.el})) & if \quad u_{el-pl.el} < u_{tot} \end{cases} \tag{F.6}$$

$$W_i = W_y \tag{F.7}$$

Table F-3   *Displacements and comparison of displacements and transferred energy from all load cases in Abaqus and hand calculations compared to 2DOF for Beam 1.*

Load case	m [kg]	h [m]	Displacement, u [m]			η_u [−]		η_{W_y} [−]	
			2DOF	Abaqus	Calc.	Abaqus	Calc.	Abaqus	Calc.
A	40	1.25	57.6	58.2	57.6	1.01	1.00	1.01	1.00
B	20	2.5	49.6	49.2	49.7	0.99	1.00	0.99	1.00
C	10	5	39.0	39.0	39.1	1.00	1.00	1.00	1.00
D	5	10	27.6	29.0	27.7	1.05	1.01	1.06	1.01
E	2.5	20	17.9	20.4	18.0	1.14	1.01	1.16	1.01
F	40	2.5	112.9	109.5	113.1	0.97	1.00	0.97	1.00
G	20	5	96.7	94.1	97.2	0.97	1.01	0.97	1.01
H	10	10	75.2	74.0	76.1	0.98	1.01	0.98	1.01
I	5	20	52.6	55.0	53.3	1.05	1.01	1.05	1.02
J	2.5	40	33.4	37.8	33.8	1.13	1.01	1.14	1.01

Table F- 4   *Displacements and comparison of displacements and transferred energy from all load cases in Abaqus and hand calculations compared to 2DOF for Beam 2.*

Load case	m [kg]	h [m]	Displacement, u [m]			η_u [−]		η_{W_y} [−]	
			2DOF	Abaqus	Calc.	Abaqus	Calc.	Abaqus	Calc.
A	40	1.25	41.3	42.1	41.4	1.02	1.00	1.02	1.00
B	20	2.5	35.7	36.0	35.8	1.01	1.00	1.01	1.00
C	10	5	28.1	28.9	28.3	1.03	1.01	1.03	1.01
D	5	10	20.1	20.7	20.3	1.03	1.01	1.03	1.01
E	2.5	20	13.3	15.2	13.4	1.14	1.01	1.17	1.01
F	40	2.5	80.3	79.2	80.5	0.99	1.00	0.99	1.00
G	20	5	68.8	67.8	69.3	0.99	1.01	0.99	1.01
H	10	10	53.5	54.0	54.4	1.01	1.02	1.01	1.02
I	5	20	37.6	40.1	38.4	1.07	1.02	1.07	1.02
J	2.5	40	24.2	27.7	24.6	1.15	1.02	1.16	1.02

Table F-5   *Displacements and comparison of displacements and transferred energy from all load cases in Abaqus and hand calculations compared to 2DOF for Beam 3.*

Load case	m [kg]	h [m]	Displacement, u [m] 2DOF	Abaqus	Calc.	η_u [$-$] Abaqus	Calc.	η_{W_y} [$-$] Abaqus	Calc.
A	40	1.25	25.5	26.2	25.5	1.03	1.00	1.03	1.00
B	20	2.5	22.1	22.5	22.2	1.02	1.01	1.02	1.01
C	10	5	17.6	18.3	17.8	1.04	1.01	1.04	1.01
D	5	10	12.9	13.4	13.1	1.04	1.01	1.05	1.02
E	2.5	20	8.9	10.3	9.0	1.16	1.01	1.22	1.02
F	40	2.5	48.4	48.5	48.6	1.00	1.00	1.00	1.01
G	20	5	41.5	42.5	42.0	1.02	1.01	1.03	1.01
H	10	10	32.4	33.9	33.2	1.05	1.03	1.05	1.03
I	5	20	23.0	24.5	23.7	1.06	1.03	1.07	1.04
J	2.5	40	15.2	17.6	15.6	1.16	1.03	1.19	1.03

Table F-6   *Displacements and comparison of displacements and transferred energy from all load cases in Abaqus and hand calculations compared to 2DOF for Beam 4.*

Load case	m [kg]	h [m]	Displacement, u [m] 2DOF	Abaqus	Calc.	η_u [$-$] Abaqus	Calc.	η_{W_y} [$-$] Abaqus	Calc.
A	40	1.25	34.7	35.8	34.9	1.03	1.00	1.03	1.00
B	20	2.5	27.4	28.2	27.6	1.03	1.01	1.03	1.01
C	10	5	19.5	20.2	19.7	1.03	1.01	1.04	1.01
D	5	10	12.9	15.0	13.0	1.16	1.01	1.19	1.01
E	2.5	20	8.2	10.5	8.3	1.28	1.01	1.37	1.01
F	40	2.5	67.0	66.0	67.6	0.99	1.01	0.98	1.01
G	20	5	52.1	52.7	53.1	1.01	1.02	1.01	1.02
H	10	10	36.5	39.2	37.4	1.07	1.02	1.08	1.02
I	5	20	23.4	26.6	23.9	1.14	1.02	1.15	1.02
J	2.5	40	14.3	18.2	14.5	1.27	1.01	1.32	1.02

Table F-7   *Displacements and comparison of displacements and transferred energy from all load cases in Abaqus and hand calculations compared to 2DOF for Beam 5.*

Load case	m [kg]	h [m]	Displacement, u [m]			η_u [−]		η_{W_y} [−]	
			2DOF	Abaqus	Calc.	Abaqus	Calc.	Abaqus	Calc.
A	40	1.25	14.80	15.81	15.26	1.07	1.03	1.07	1.03
B	20	2.5	11.43	12.18	12.07	1.07	1.06	1.07	1.06
C	10	5	8.11	9.65	8.64	1.19	1.07	1.22	1.07
D	5	10	5.41	6.63	5.70	1.22	1.05	1.27	1.06
E	2.5	20	3.52	4.39	3.63	1.25	1.03	1.33	1.04
F	40	2.5	27.76	29.13	29.61	1.05	1.07	1.05	1.07
G	20	5	20.91	23.14	23.23	1.11	1.11	1.11	1.12
H	10	10	14.42	18.20	16.37	1.26	1.14	1.28	1.14
I	5	20	9.34	13.15	10.48	1.41	1.12	1.45	1.13
J	2.5	40	5.87	9.31	6.34	1.59	1.08	1.69	1.09

Table F-8   *Displacements and comparison of displacements and transferred energy from all load cases in Abaqus and hand calculations compared to 2DOF for Beam 6.*

Load case	m [kg]	h [m]	Displacement, u [m]			η_u [−]		η_{W_y} [−]	
			2DOF	Abaqus	Calc.	Abaqus	Calc.	Abaqus	Calc.
A	40	1.25	108.02	112.28	108.04	1.04	1.00	1.04	1.00
B	20	2.5	85.80	88.89	85.85	1.04	1.00	1.04	1.00
C	10	5	61.89	64.93	61.95	1.05	1.00	1.06	1.00
D	5	10	41.37	47.58	41.46	1.15	1.00	1.19	1.00
E	2.5	20	27.01	32.17	27.07	1.19	1.00	1.27	1.00
F	40	2.5	207.92	204.19	207.92	0.98	1.00	0.98	1.00
G	20	5	163.46	165.11	163.53	1.01	1.00	1.01	1.00
H	10	10	115.62	121.95	115.73	1.05	1.00	1.06	1.00
I	5	20	74.70	84.20	74.75	1.13	1.00	1.14	1.00
J	2.5	40	45.91	57.23	45.96	1.25	1.00	1.30	1.00

Table F-9   *Displacements and comparison of displacements and transferred energy from all load cases in Abaqus and hand calculations compared to 2DOF for Beam 7.*

Load case	m [kg]	h [m]	Displacement, u [m]			η_u [−]		η_{W_y} [−]	
			2DOF	Abaqus	Calc.	Abaqus	Calc.	Abaqus	Calc.
A	40	1.25	78.1	84.5	78.1	1.08	1.00	1.09	1.00
B	20	2.5	62.6	65.6	62.7	1.05	1.00	1.06	1.00
C	10	5	46.0	48.9	46.1	1.06	1.00	1.08	1.00
D	5	10	31.7	37.2	31.8	1.17	1.00	1.24	1.00
E	2.5	20	21.8	28.5	21.8	1.31	1.00	1.51	1.00
F	40	2.5	147.5	148.6	147.5	1.01	1.00	1.01	1.00
G	20	5	116.5	119.5	116.7	1.03	1.00	1.03	1.00
H	10	10	83.3	87.8	83.4	1.05	1.00	1.06	1.00
I	5	20	54.9	61.4	55.0	1.12	1.00	1.14	1.00
J	2.5	40	34.9	42.6	35.0	1.22	1.00	1.30	1.00

Table F-10   *Displacements and comparison of displacements and transferred energy from all load cases in Abaqus and hand calculations compared to 2DOF for Beam 8.*

Load case	m [kg]	h [m]	Displacement, u [m]			η_u [−]		η_{W_y} [−]	
			2DOF	Abaqus	Calc.	Abaqus	Calc.	Abaqus	Calc.
A	40	1.25	49.9	54.2	49.9	1.09	1.00	1.11	1.00
B	20	2.5	40.9	45.0	40.9	1.10	1.00	1.13	1.00
C	10	5	31.2	38.1	31.2	1.22	1.00	1.32	1.00
D	5	10	22.9	29.1	23.0	1.27	1.00	1.46	1.01
E	2.5	20	17.0	21.4	15.3	1.26	0.90	1.56	1.01
F	40	2.5	90.3	95.9	90.3	1.06	1.00	1.07	1.00
G	20	5	72.2	76.1	72.4	1.05	1.00	1.06	1.00
H	10	10	52.8	56.8	53.0	1.07	1.00	1.09	1.00
I	5	20	36.3	43.9	36.4	1.21	1.00	1.28	1.00
J	2.5	40	24.7	30.7	24.8	1.24	1.00	1.39	1.00

Table F-11   Displacements and comparison of displacements and transferred energy from all load cases in Abaqus and hand calculations compared to 2DOF for Beam 9.

Load case	m [kg]	h [m]	Displacement, u [m]			η_u [−]		η_{W_y} [−]	
			2DOF	Abaqus	Calc.	Abaqus	Calc.	Abaqus	Calc.
A	40	1.25	46.0	51.2	46.0	1.11	1.00	1.14	1.00
B	20	2.5	37.9	43.0	38.0	1.13	1.00	1.18	1.00
C	10	5	29.2	36.5	29.2	1.25	1.00	1.38	1.00
D	5	10	21.7	27.5	21.8	1.27	1.00	1.48	1.01
E	2.5	20	16.2	20.3	13.8	1.25	0.85	1.55	1.01
F	40	2.5	82.4	87.6	82.5	1.06	1.00	1.07	1.00
G	20	5	66.1	70.6	66.3	1.07	1.00	1.08	1.00
H	10	10	48.7	53.4	48.8	1.10	1.00	1.12	1.00
I	5	20	33.8	41.0	33.9	1.21	1.00	1.30	1.00
J	2.5	40	23.3	29.5	23.4	1.26	1.00	1.45	1.00

Appendix G Results from parametric study in LS-DYNA

G.1 Time-displacement curves from LS-DYNA
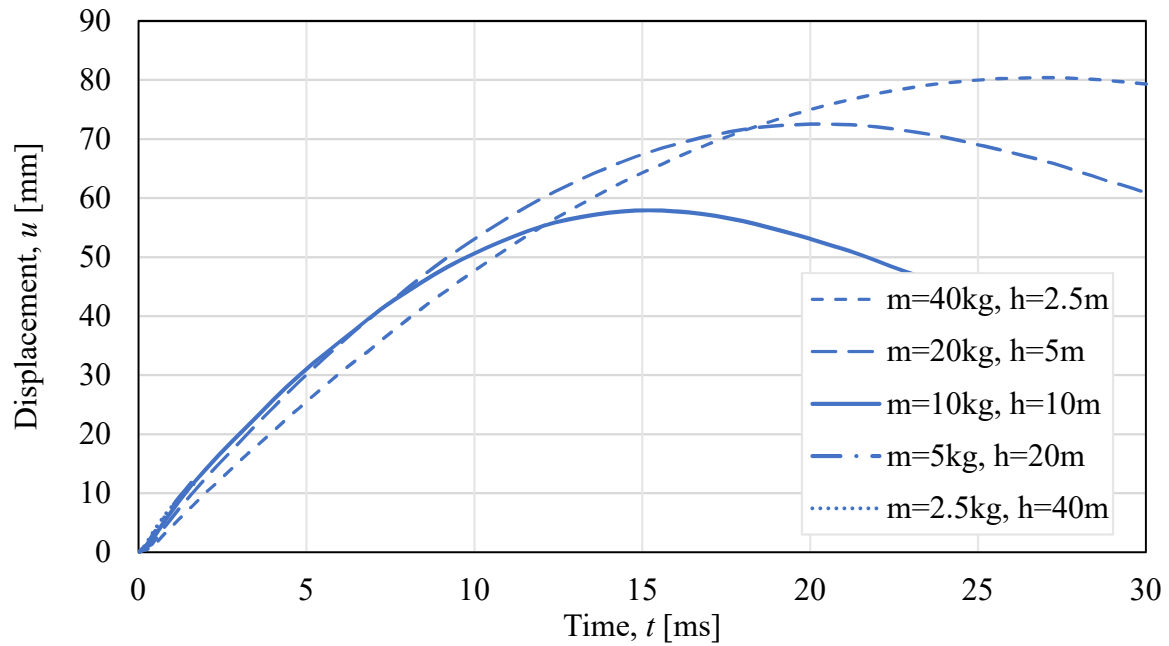
Figure G-1   Time-displacement curves for all load cases for Beam 2, note that the results for two load cases end at around 2 ms.
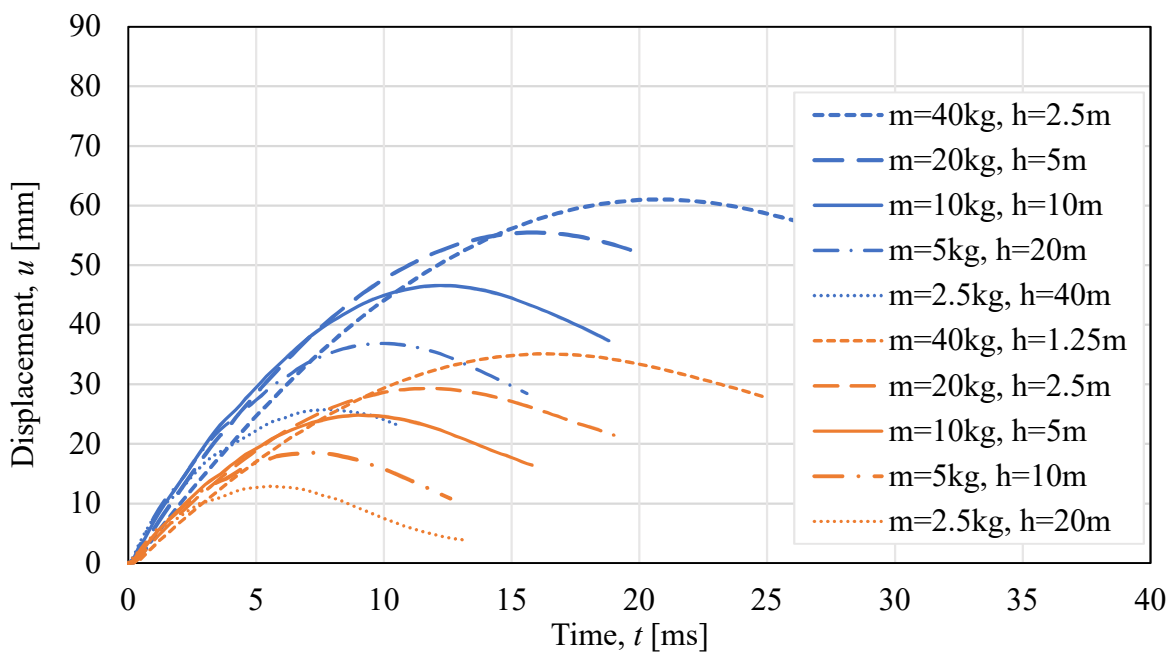
Figure G-2   Time-displacement curves for all load cases for Beam 2.
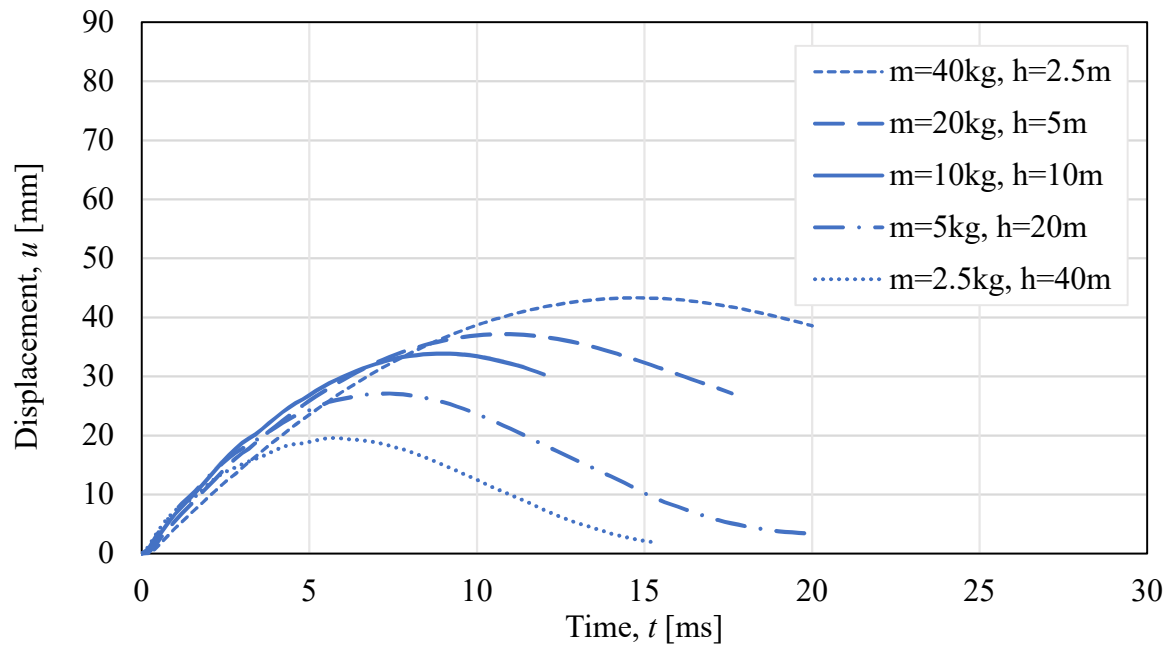
Figure G-3   *Time-displacement curves for all load cases for Beam 3.*

G.2 Crack patterns from LS-DYNA

Table G-1 *Crack patterns at the time of maximum displacement for load cases F-J for Beam 1.*

Load case	Crack pattern
F (40 kg, 2.5 m)	
G (20 kg, 5 m)	
H (10 kg, 10 m)	
I (5 kg, 20 m)	-
J (2.5 kg, 40 m)	-
Principle strain [%]	0 0.99 1.98 2.97 3.96 4.95 5.94 6.93 7.92 8.91 9.9
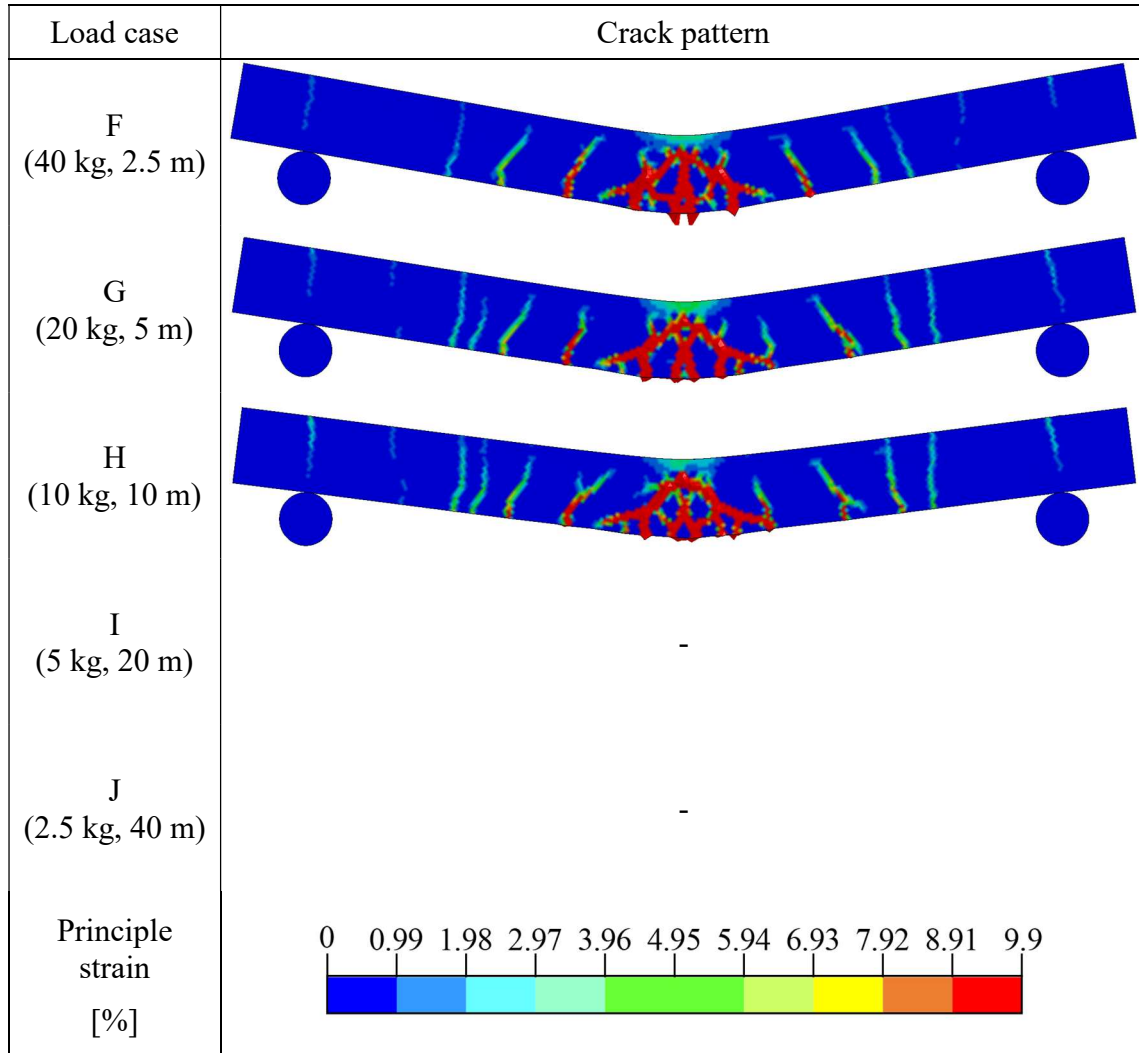
Table G-2   Crack patterns at the time of maximum displacement for load cases A-E for Beam 2.

Load case	Crack pattern
A (40 kg, 1.25 m)	
B (20 kg, 2.5 m)	
C (10 kg, 5 m)	
D (5 kg, 10 m)	
E (2.5 kg, 20 m)	
Principle strain [%]	0 0.99 1.98 2.97 3.96 4.95 5.94 6.93 7.92 8.91 9.9
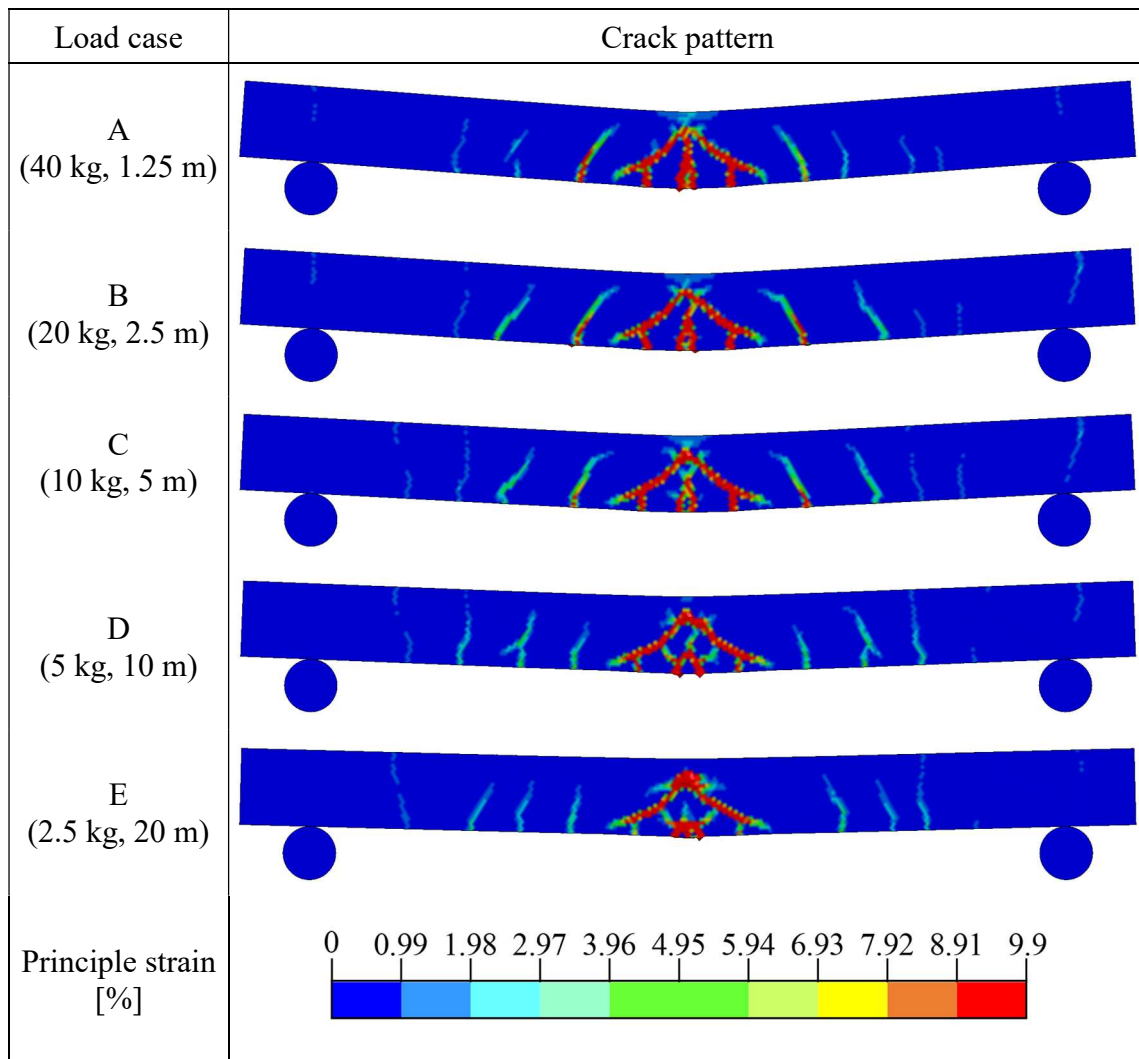
Table G-3   *Crack patterns at the time of maximum displacement for load cases F-J for Beam 2.*

Load case	Crack pattern
F (40 kg, 2.5 m)	
G (20 kg, 5 m)	
H (10 kg, 10 m)	
I (5 kg, 20 m)	
J (2.5 kg, 40 m)	
Principle strain [%]	0 0.99 1.98 2.97 3.96 4.95 5.94 6.93 7.92 8.91 9.9
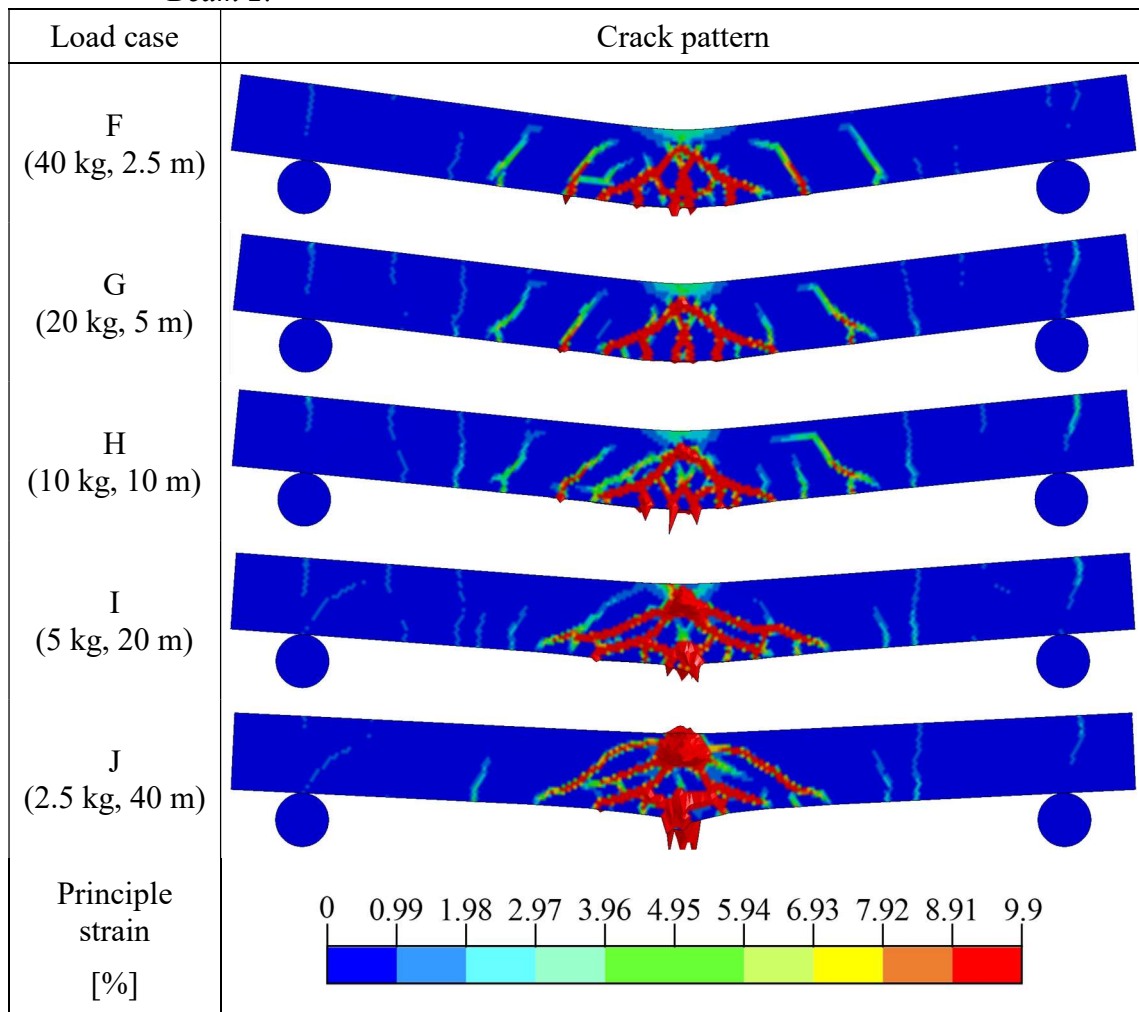
Table G- 4   *Crack patterns at the time of maximum displacement for load cases F-J for*
             Beam 3.

Load case	Crack pattern
F (40 kg, 2.5 m)	
G (20 kg, 5 m)	
H (10 kg, 10 m)	
I (5 kg, 20 m)	
J (2.5 kg, 40 m)	
Principle strain [%]	0 0.99 1.98 2.97 3.96 4.95 5.94 6.93 7.92 8.91 9.9

CHALMERS, *Architecture and Civil Engineering*, Master's Thesis, ACX30-18-36
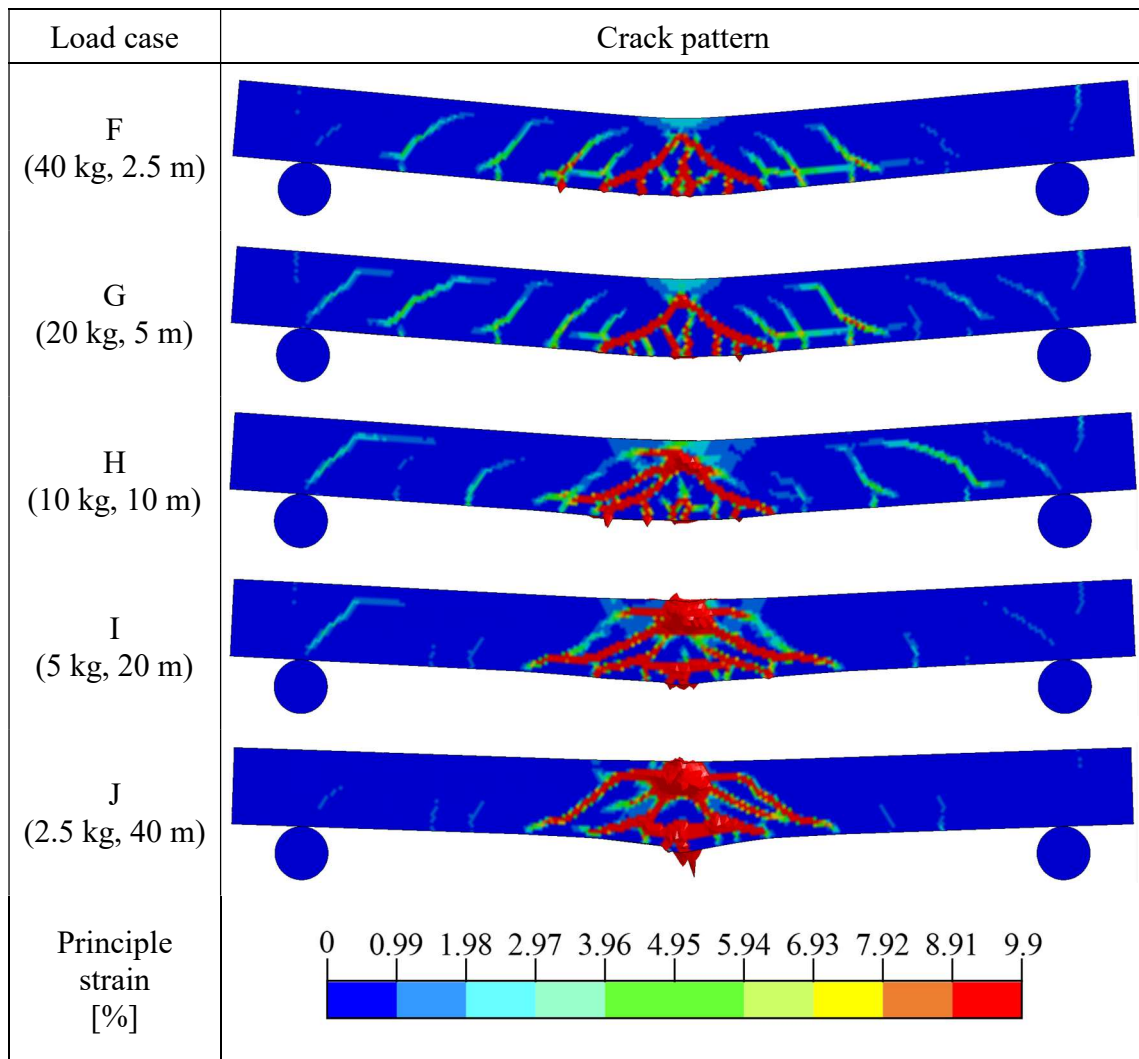
Appendix H   Abaqus script file

```
*Heading
** Job name: Explicit_2018 Model name: Dynamic - Explicit
** Generated by: Abaqus/CAE 2017
*Preprint, echo=NO, model=NO, history=NO, contact=NO
**
** PARTS
**
*Part, name=Beam
*End Part
**
**
** ASSEMBLY
**
*Assembly, name=Assembly
**
*Instance, name=Beam-1, part=Beam
*Node
      1,         -500.,          0.
      2,            0.,          0.
      3,          500.,          0.
      4,         -490.,          0.
      5,         -480.,          0.
      …
    100,          480.,          0.
    101,          490.,          0.
*Element, type=B21
 1,  1,  4
 2,  4,  5
 3,  5,  6
 …
 99, 100, 101
100, 101,   3
*Nset, nset=Set-1, generate
   1, 101,    1
*Elset, elset=Set-1, generate
   1, 100,    1
*Nset, nset=Set-2, generate
   1, 101,    1
*Elset, elset=Set-2, generate
   1, 100,    1
** Section: Beam  Profile: Beam profile
*Beam     Section,     elset=Set-1,     material="Equivalent     concrete",
temperature=GRADIENTS, section=RECT
100., 100.
0.,0.,-1.
3
*End Instance
**
*Node
      1,            0.,          200.,           0.
*Nset, nset="Attachment Points-1-Set-1"
 1,
*Nset, nset=Set-1, instance=Beam-1
 1,
*Nset, nset=Set-2, instance=Beam-1
 3,
*Nset, nset=Set-3, instance=Beam-1
 2,
```

```
*Nset, nset=Set-4, instance=Beam-1
 1,
*Nset, nset=Set-5, instance=Beam-1
 3,
*Nset, nset=Set-12, instance=Beam-1
 1,
*Nset, nset=Set-13, instance=Beam-1
 3,
*Nset, nset=Set-14, instance=Beam-1
 1,
*Nset, nset=Set-15, instance=Beam-1
 3,
*Nset, nset=Set-18, instance=Beam-1
 2,
*Nset, nset=Set-29
 1,
*Nset, nset=Set-30
 1,
*Element, type=MASS, elset="Set-29_Point mass_"
1, 1
*Mass, elset="Set-29_Point mass_"
10000.,
*Spring, elset=Spring-spring, nonlinear

-3.99e+09, -1000
0, 0
0.1, 1000
*Element, type=SpringA, elset=Spring-spring
2, 1, Beam-1.2
*End Assembly
**
** MATERIALS
**
*Material, name="Equivalent concrete"
*Density
 0.0024,
*Elastic
5800., 0.2
*Plastic
 15.67,0.
 15.68,1.
**
** BOUNDARY CONDITIONS
**
** Name: Left Type: Displacement/Rotation
*Boundary
Set-14, 1, 1
Set-14, 2, 2
** Name: Right Type: Displacement/Rotation
*Boundary
Set-15, 2, 2
**
** PREDEFINED FIELDS
**
** Name: Initial velocity   Type: Velocity
*Initial Conditions, type=VELOCITY
Set-30, 1, 0.
Set-30, 2, -9.9
** ----------------------------------------------------------------
**
** STEP: Dynamic explicit
```

```
**
*Step, name="Dynamic explicit", nlgeom=YES
*Dynamic, Explicit, direct user control
0.002, 40.
*Bulk Viscosity
0.06, 1.2
**
** OUTPUT REQUESTS
**
*Restart, write, number interval=1, time marks=NO
**
** FIELD OUTPUT: F-Output-1
**
*Output, field, number interval=200
*Node Output
A, RF, RM, RT, U, V
*Element Output, directions=YES
E, MISES, S, SF
**
** HISTORY OUTPUT: H-Output-1
**
*Output, history
*Energy Output
ALLAE, ALLCD, ALLCW, ALLDC, ALLDMD, ALLFD, ALLIE, ALLKE, ALLMW, ALLPD,
ALLPW, ALLSE, ALLVD, ALLWK, ETOTAL
*End Step
```

Appendix I   LS-DYNA script file

```
$# LS-DYNA Keyword file created by LS-PrePost(R) V4.5.4 - 07Nov2017
$# Created on Apr-11-2018 (08:48:51)
*KEYWORD
*TITLE
$#                                                                        title
LS-DYNA keyword deck by LS-PrePost
*CONTROL_TERMINATION
$#   endtim    endcyc     dtmin    endeng    endmas     nosol
       20.0         0       0.0      0.01.000000E8         0
*DATABASE_ELOUT
$#       dt    binary      lcur     ioopt   option1   option2   option3   option4
        0.1         3         0         1         0         0         0         0
*DATABASE_GLSTAT
$#       dt    binary      lcur     ioopt
        0.1         3         0         1
*DATABASE_MATSUM
$#       dt    binary      lcur     ioopt
        0.1         3         0         1
*DATABASE_NCFORC
$#       dt    binary      lcur     ioopt
        0.5         3         0         1
*DATABASE_NODFOR
$#       dt    binary      lcur     ioopt
        0.5         3         0         1
*DATABASE_NODOUT
$#       dt    binary      lcur     ioopt   option1   option2
        0.5         3         0         1       0.0         0
*DATABASE_RCFORC
$#       dt    binary      lcur     ioopt
        0.1         0         0         1
*DATABASE_BINARY_D3PLOT
$#       dt      lcdt      beam     npltc    psetid
        0.2         0         0         0         0
$#    ioopt
          0
*DATABASE_EXTENT_BINARY
$#    neiph     neips    maxint    strflg    sigflg    epsflg    rltflg    engflg
          5         0         0         1         1         1         1         1
$#   cmpflg    ieverp    beamip     dcomp      shge     stssz    n3thdt   ialemat
          0         0         1         1         1         1         2         1
$#  nintsld   pkp_sen      sclp     hydro     msscl     therm    intout    nodout
          0         0       1.0         0         0         0
$#     dtdt    resplt     neipb     quadr     cubic
          0         0         0         0         0
*BOUNDARY_SPC_SET_ID
$#       id                                                               heading
         1BC left vertical
$#     nsid       cid      dofx      dofy      dofz     dofrx     dofry     dofrz
          1         0         0         0         1         0         0         0
*SET_NODE_LIST_TITLE
BC Left vertical
$#      sid       da1       da2       da3       da4    solver
          1       0.0       0.0       0.0       0.0MECH
$#     nid1      nid2      nid3      nid4      nid5      nid6      nid7      nid8
      10299     10300     10342     10343     11178     11179     11180     11181
      11182     11183     11184     11185     11186     11187     11188     11189
      11190     11191     11192     11193     11194     11195     11196     11197
      11198     11199     11200     11201     11202     11203     11204     11205
      11206     11207     11208     11209     11210     11211     11212     11213
      11214     11215     11216     11217         0         0         0         0
*BOUNDARY_SPC_SET_ID
$#       id                                                               heading
         2BC left horizonal
$#     nsid       cid      dofx      dofy      dofz     dofrx     dofry     dofrz
```

```
             2             0             1             1             0             0             0             0
*SET_NODE_LIST_TITLE
BC Left horizontal
$#      sid        da1        da2        da3        da4     solver
          2        0.0        0.0        0.0        0.0MECH
$#     nid1       nid2       nid3       nid4       nid5       nid6       nid7       nid8
      10288      10331      10958      10959      10960      10961      10962      10963
      10964      10965      10966      10967      10968      10969      10970      10971
      10972      10973      10974      10975      10976      10977          0          0
*BOUNDARY_SPC_SET_ID
$#       id                                                                      heading
          3BC right vertical
$#     nsid        cid       dofx       dofy       dofz      dofrx      dofry      dofrz
          3          0          0          0          1          0          0          0
*SET_NODE_LIST_TITLE
BC Right vertical
$#      sid        da1        da2        da3        da4     solver
          3        0.0        0.0        0.0        0.0MECH
$#     nid1       nid2       nid3       nid4       nid5       nid6       nid7       nid8
      15381      15382      15424      15425      15886      15887      15888      15889
      15890      15891      15892      15893      15894      15895      15896      15897
      15898      15899      15900      15901      15902      15903      15904      15905
      15906      15907      15908      15909      15910      15911      15912      15913
      15914      15915      15916      15917      15918      15919      15920      15921
      15922      15923      15924      15925          0          0          0          0
*BOUNDARY_SPC_SET_ID
$#       id                                                                      heading
          4BC right horizontal
$#     nsid        cid       dofx       dofy       dofz      dofrx      dofry      dofrz
          4          0          1          1          0          0          0          0
*SET_NODE_LIST_TITLE
BC Right horizontal
$#      sid        da1        da2        da3        da4     solver
          4        0.0        0.0        0.0        0.0MECH
$#     nid1       nid2       nid3       nid4       nid5       nid6       nid7       nid8
      15392      15435      16106      16107      16108      16109      16110      16111
      16112      16113      16114      16115      16116      16117      16118      16119
      16120      16121      16122      16123      16124      16125          0          0
*CONTACT_AUTOMATIC_SURFACE_TO_SURFACE_ID
$#      cid                                                                        title
          1Contact-Weight-beam
$#     ssid       msid      sstyp      mstyp     sboxid     mboxid        spr        mpr
          3          8          3          3          0          0          0          0
$#       fs         fd         dc         vc        vdc     penchk         bt         dt
        0.0        0.0        0.0        0.0        0.0          0       0.011.00000E20
$#      sfs        sfm        sst        mst       sfst       sfmt        fsf        vsf
        1.0        1.0        0.0        0.0        1.0        1.0        1.0        1.0
*CONTACT_AUTOMATIC_SURFACE_TO_SURFACE_ID
$#      cid                                                                        title
          2Contact-left support-beam
$#     ssid       msid      sstyp      mstyp     sboxid     mboxid        spr        mpr
          1          8          3          3          0          0          0          0
$#       fs         fd         dc         vc        vdc     penchk         bt         dt
        0.0        0.0        0.0        0.0        0.0          0       0.011.00000E20
$#      sfs        sfm        sst        mst       sfst       sfmt        fsf        vsf
        1.0        1.0        0.0        0.0        1.0        1.0        1.0        1.0
*CONTACT_AUTOMATIC_SURFACE_TO_SURFACE_ID
$#      cid                                                                        title
          3Contact-right support-beam
$#     ssid       msid      sstyp      mstyp     sboxid     mboxid        spr        mpr
          2          8          3          3          0          0          0          0
$#       fs         fd         dc         vc        vdc     penchk         bt         dt
        0.0        0.0        0.0        0.0        0.0          0       0.011.00000E20
$#      sfs        sfm        sst        mst       sfst       sfmt        fsf        vsf
        1.0        1.0        0.0        0.0        1.0        1.0        1.0        1.0
*PART
$#                                                                                  title
Left support
```

```
$#       pid      secid        mid      eosid       hgid       grav     adpopt       tmid
           1          2          1          0          0          0          0          0
*SECTION_SOLID_TITLE
Support
$#     secid     elform        aet
           2          1          0
*MAT_ELASTIC_TITLE
Weight and supports
$#       mid         ro          e         pr         da         db   not used
           1   0.007753   200000.0        0.3        0.0        0.0          0
*PART
$#                                                                            title
Right support
$#       pid      secid        mid      eosid       hgid       grav     adpopt       tmid
           2          2          1          0          0          0          0          0
*PART
$#                                                                            title
Weight
$#       pid      secid        mid      eosid       hgid       grav     adpopt       tmid
           3          3          1          0          0          0          0          0
*SECTION_SOLID_TITLE
Weight
$#     secid     elform        aet
           3          1          0
*PART
$#                                                                            title
Reinforcement, top-front
$#       pid      secid        mid      eosid       hgid       grav     adpopt       tmid
           4          1          5          0          0          0          0          0
*SECTION_BEAM_TITLE
Reinforcment
$#     secid     elform       shrf    qr/irid        cst      scoor        nsm
           1          1        1.0          1          1        0.0        0.0
$#       ts1        ts2        tt1        tt2      nsloc      ntloc
           6.0        6.0        0.0        0.0        0.0        0.0
*MAT_PIECEWISE_LINEAR_PLASTICITY_TITLE
Multi-linear reinforcment
$#       mid         ro          e         pr       sigy       etan       fail       tdel
           5     0.0078   196000.0        0.3        0.0        0.01.00000E21        0.0
$#         c          p       lcss       lcsr         vp
           0.0        0.0          0          0        0.0
$#      eps1       eps2       eps3       eps4       eps5       eps6       eps7       eps8
           0.0     0.0016     0.0036     0.0128     0.0272      0.048      0.075       0.11
$#       es1        es2        es3        es4        es5        es6        es7        es8
         420.0      500.0      520.0      560.0      590.0      610.0      620.0      623.0
*PART
$#                                                                            title
Reinforcement, top-back
$#       pid      secid        mid      eosid       hgid       grav     adpopt       tmid
           5          1          5          0          0          0          0          0
*PART
$#                                                                            title
Reinforcement, bottom-front
$#       pid      secid        mid      eosid       hgid       grav     adpopt       tmid
           6          1          5          0          0          0          0          0
*PART
$#                                                                            title
Reinforcement, bottom-back
$#       pid      secid        mid      eosid       hgid       grav     adpopt       tmid
           7          1          5          0          0          0          0          0
*PART
$#                                                                            title
Beam
$#       pid      secid        mid      eosid       hgid       grav     adpopt       tmid
           8          4          3          0          0          0          0          0
*SECTION_SOLID_TITLE
Concrete
```

```
$#    secid     elform       aet
         4         10          0
*MAT_CONCRETE_DAMAGE_PLASTIC_MODEL_TITLE
Beam Concrete-CDPM2
$#     mid         ro          e          pr        ecc        qh0         ft         fc
         3     0.0024    32000.0         0.2      0.518        0.3        2.8       36.0
$#      hp         ah         bh          ch         dh         as         df        fc0
      0.01       0.08      0.003    2.01.00000E-6       15.0       0.85        0.0
$#    type         bs         wf         wf1        ft1     strflg    failflg        efc
       1.0        1.0      0.124         0.0        0.0        0.0        0.0      0.001
*MAT_PLASTIC_KINEMATIC_TITLE
Reinforcment
$#     mid         ro          e          pr       sigy       etan       beta
         2    0.00785   200000.0         0.3      609.8      584.0        0.0
$#     src        srp         fs          vp
       0.0        0.0        0.0         0.0
*MAT_ELASTIC_TITLE
Beam elastic concrete
$#     mid         ro          e          pr         da         db   not used
         4     0.0024     3470.0         0.2        0.0        0.0          0
*INITIAL_VELOCITY_GENERATION
$#nsid/pid       styp      omega          vx         vy         vz      ivatn       icid
         3          2        0.0         0.0        0.0       -9.9          0          0
$#      xc         yc         zc          nx         ny         nz      phase     irigid
       0.0        0.0        0.0         0.0        0.0        0.0          0          0
*CONSTRAINED_BEAM_IN_SOLID_ID
$#  coupid                                                                       title
         1reinforcmenttop-front
$#   slave     master      sstyp       mstyp                             ncoup       cdir
         4          8          1           1          0          0          0          1
$#   start        end      axfor
       0.0        0.0          0          -1
*CONSTRAINED_BEAM_IN_SOLID_ID
$#  coupid                                                                       title
         2reinforcmenttop-back
$#   slave     master      sstyp       mstyp                             ncoup       cdir
         5          8          1           1          0          0          0          1
$#   start        end      axfor
       0.0        0.0          0          -1
*CONSTRAINED_BEAM_IN_SOLID_ID
$#  coupid                                                                       title
         3reinforcmentbottom-front
$#   slave     master      sstyp       mstyp                             ncoup       cdir
         6          8          1           1          0          0          0          1
$#   start        end      axfor
       0.0        0.0          0          -1
*CONSTRAINED_BEAM_IN_SOLID_ID
$#  coupid                                                                       title
         4reinforcmentbottom-back
$#   slave     master      sstyp       mstyp                             ncoup       cdir
         7          8          1           1          0          0          0          1
$#   start        end      axfor
       0.0        0.0          0          -1
*ELEMENT_SOLID
$#   eid        pid         n1         n2         n3         n4         n5         n6         n7         n8
   13000          1      10595      10643      13938      12838      10596      10596      12378      12378
   13001          1      12838      13938      13939      12839      12378      12378      12379      12379
   13002          1      12839      13939      13940      12840      12379      12379      12380      12380
   13003          1      12840      13940      13941      12841      12380      12380      12381      12381
…
35177          7      36212      36214      36215          0          0          0          0          2
   35178          7      36214      36216      36217          0          0          0          0          2
   35179          7      36216      36218      36219          0          0          0          0          2
   35180          7      36218      36220      36221          0          0          0          0          2
*NODE
$#  nid                  x                  y                  z         tc         rc
         1                0.0             -590.0              -35.0          0          0
         2              100.0             -500.0                0.0          0          0
```

```
       3               0.0          -500.0   1.672415e-015        0        0
       4             100.0          -504.981  -0.3562494          0        0
…
196208          26.37588      -453.5173          41.99794         0        0
  196209        71.48462      -417.763           63.55512         0        0
  196210        73.74369      -177.108           35.98502         0        0
  196211        73.39993      -135.9213          35.75033         0        0
*DEFINE_FUNCTION
$#     fid                                                              heading
        1Bond-slip between reinforcement and concrete
$#                                                                     function
float force(float slip,float leng)
{
float force,pi,d,area,shear,pf,s1,s2,s3,tmax,tf;
pi = 3.1415926;
d = 6;
s1 = 1.0;
tmax = 15;
area = pi*d*leng;
if(slip < s1) {
shear = tmax*(slip/s1)**0.4;
} else{
shear = tmax;
}

force = shear*area;
return force;
}
*END
```